ISBN 978-82-326-2434-8 (printed version)
ISBN 978-82-326-2435-5 (electronic version)
ISSN 1503-8181

Doctoral theses at NTNU, 2017:181

Christopher Andrew Dirdal

Metamaterial effective parameters

NTNU
Norwegian University of
Science and Technology
Faculty of Information Technology and Electrical
Engineering
Department of Electronic Systems

NTNU
Norwegian University of
Science and Technology

Doctoral Thesis
Christopher Andrew Dirdal
Doctoral theses at NTNU, 2017:181
NTNU

NTNU
Norwegian University of
Science and Technology

Christopher Andrew Dirdal

Metamaterial effective parameters

Thesis for the degree of Philosophiae Doctor

Oslo, June 2017

Norwegian University of Science and Technology
Faculty of Information Technology and Electrical Engineering
Department of Electronic Systems

NTNU
Norwegian University of
Science and Technology

NTNU
Norwegian University of Science and Technology

Thesis for the degree of Philosophiae Doctor

Faculty of Information Technology and Electrical Engineering
Department of Electronic Systems

ISBN 978-82-326-2434-8 (printed version)
ISBN 978-82-326-2435-5 (electronic version)
ISSN 1503-8181

Doctoral theses at NTNU, 2017:181

Printed by Skipnes Kommunikasjon as

Abstract

Metamaterials are a class of composite materials acting as effectively continuous media, which are capable of realizing entirely new phenomena such as *negative refraction* and *transformation optics*. They have thereby opened up for novel concepts such as the *perfect lens* and *invisibility cloaking*, which have attracted significant attention from the scientific community as well as in popular culture. The unprecedented control over field propagation offered by metamaterials naturally raises the question of what is ultimately achieveable by their use. This thesis sheds some light on this question by investigating the possibilities and limitations of the effective medium parameters ϵ and μ, the permittivity and permeability, respectively. The functional forms taken by these parameters directly determine the solutions of the macroscopic Maxwell's equations, and hence the effective field behavior.

The investigations of this thesis have followed two lines of inquiry, namely *causality considerations* and *effective medium theory*. The latter approach addresses the complexities of metamaterial structures and determines how to extract effective parameters which describe their macroscopic properties, whereas the former approach avoids getting into structural detail, but rather introduces dispersion constraints such as the *Kramers-Kronig (K.K.) relations*.

An analytical framework relying on rational functions and polar plots is introduced to evaluate the possibility of achieving negative refraction with low loss or gain in media which abide by the K.K. relations. At the same time, this thesis argues that metamaterials attain some additional freedom in relation to the standard K.K. relations owing to the fact that they cease to be effective media at relatively long wavelengths. For instance, passive arrangements of split ring cylinders can have dispersions which are only attainable in conventional media which possess gain at high frequencies. Such relaxed dispersion constraints are characterized through the formulation of generalized K.K.-relations.

Apart from leading to K.K. relations, the principle of causality can also be used to show that any causal susceptibility function χ can be expressed as a superposition of Lorentzian response functions. This may serve to generalize typical textbook treatments of dispersion, and furthermore presents a route towards dis-

persion engineering: Given the abundance of metamaterial structures which give Lorentzian-like resonances, a desired dispersion can in principle be realized in terms of its decomposition into Lorentzian functions.

Using homogenization theory for metamaterials, it is shown that the permeability function does not necessarily tend to unity at large frequencies. This result serves to explain diamagnetism in passive and causal media. This thesis also discusses the importance of higher order multipole terms in homogenization theories for metamaterials. While it is common to include polarization, magnetic dipole and perhaps electric quadrupole terms, it is shown that certain higher order terms are generally significant when second order spatially dispersive effects (e.g. magnetism) are concerned. Hence, some of the underlying assumptions regarding the non-importance of such higher order terms needs to be reconsidered when applied to metamaterials.

Acknowledgements

This thesis concludes an almost five year venture on my part, for which I hold much gratitude to colleagues, family and friends. On this note I must *sincerely* thank my supervisor Johannes Skaar for the countless hours he has generously dedicated to me and this project. He is one of those rare people who displays consistency and excellence on *both* a professional and personal level, for which he holds my highest respect and recommendation. I am grateful for our many office discussions, which have often taken surprising detours from electromagnetism to other formational topics such as family and parenthood, or advice on practical matters related to purchasing my first apartment, new car, and so on. Johannes has made a profound impression on me, and I hope to keep his friendship also in the future.

I would also like to thank the administration at the former *University Graduate Center at Kjeller (UNIK)*, now known as the *Department of Technology Systems (ITS)* at the University of Oslo, for the support they have given. In this respect, I especially thank the Head of Department Stian Løvold for his enthusiasm for prospective metamaterial projects, as well as financial support for conference participation and, in fact, the computer on which this thesis has been written. I would also like to thank my fellow PhD colleague Hans Olaf Hågenvik for many interesting discussions, as well as Haakon Aamot Haave who I had the pleasure of co-supervising on his Masters Thesis. I must also thank NTNU for this opportunity, having funded me with internal resources.

During the past years of work on this thesis, my life has seen many changes. I have become a husband, a father, and I'm quickly approaching 30. The fixed points of my life in this time of flux have been God and my dear wife Eva, both to whom I am immensely grateful. On the part of my wife, she has been an unwavering support, despite the challenges of moving to a new country, learning a new language, finishing a new degree and getting a first job – as well as becoming a mother! I must also thank my parents and my brother Johann: My father who just became fifty years old, for never letting any opportunity pass either of his sons, and my mother for always being delightfully biased in our favor.

Contents

1 Introduction **1**

2 What is a metamaterial? **5**
2.1 The big picture – Macroscopic Maxwell's equations and effective parameters . . . 5
2.2 Make your own metamaterial . . . 13
2.2.1 Negative permeability through resonance . . . 13
2.2.2 Negative permittivity through plasma response . . . 18
2.3 Transmission line metamaterials . . . 20
2.3.1 Brune synthesis of RLC impedances . . . 23
2.4 Model breakdown . . . 26

3 Making Maxwell's equations do something new **29**
3.1 Left-handed media . . . 29
3.2 Flying fish and perfect lenses . . . 34
3.3 Step-by-step guide to invisibility . . . 36
3.3.1 Step 1: Find a transform . . . 37
3.3.2 Step 2: Determine the needed effective parameters . . . 39
3.3.3 Step 3: Realize effective parameters in a metamaterial . . . 41

4 The far-reaching consequences of causality **43**
4.1 Analyticity of the response function ϵ . . . 43
4.2 Consequences of analyticity . . . 46
4.2.1 Kramers-Kronig relations . . . 46
4.2.2 Decomposition into Lorentzian functions . . . 48

5 Spatial dispersion in metamaterials **53**
5.1 Obtaining local parameters . . . 53
5.2 Homogenization of a 1d metamaterial . . . 55
5.2.1 Model . . . 55
5.2.2 Eigenvalue problems . . . 57

5.2.3 Current-driven homogenization 57
5.3 Passivity in a spatially dispersive metamaterial 60

6 Summary and future work **65**

7 Contribution in papers **69**

Papers **79**

I Negative refraction in causal media by evaluating polar paths for rational functions **81**

II Superpositions of Lorentzians as the class of causal functions **91**

III Superposing Lorentzian resonance functions towards engineering target responses **101**

IV Relaxed dispersion constraints and metamaterial effective parameters with physical meaning for all frequencies **109**

V Higher order terms in metamaterial homogenization **119**

VI Diamagnetism and the dispersion of the magnetic permeability **129**

Chapter 1

Introduction

Metamaterials are structured, composite materials which have the potential of realizing electromagnetic properties beyond those of conventional ones. The field of metamaterials has therefore generated significant interest since its emergence at the beginning of the new millennium, even crossing over into popular culture. The underlying theory of metamaterials, however, has a much older history. Following World War II and onwards, considerable research on the electromagnetic response of composite materials was conducted [1–8]. Furthermore, already in 1898 Jagadis Chunder Bose reported the use of twisted structures in a composite medium for field rotation [9], and JC Maxwell Garnett is known for having calculated the effective permittivity for metal inclusions in glass in 1904 [10], which in turn relied on the Clausius-Mossotti relation derived even earlier (1850s). With this long standing tradition in mind, why have metamaterials entered the front stage of the scientific scene only recently? One part of the answer is that the emergence of metamaterials is intricately related with the dramatic improvements the last decades have seen in micro and nano-structuring techniques, as well as in computer processing and simulation tools. Together these technologies have presented the scientific community with a new design and fabrication paradigm with unprecedented possibility of generating entirely new electromagnetic properties. Perhaps more importantly, however, was the discovery that effective media have the potential of probing uncharted areas of the ordinary classical Maxwell's equations, leading to entirely new developments such as the realization of *negative refraction* and *transformation optics*.

Sir John Pendry's proposal in 1999 to create a negative permeability $\mu < 0$ using a composite medium of small conducting split-ring cylinders [11], is often considered to be the start of the metamaterial field. In reality, negative permeability in similar structures had in fact been studied much earlier [12] and also just prior to Pendry's article [13, 14], as discussed for instance in [15]. Pendry's article is nevertheless seminal to the metamaterial field in the sense that it lead to the

discovery of composite structures which give *simultaneously* negative permittivity $\epsilon < 0$ and negative permeability $\mu < 0$ [16, 17]. This was done by David Smith et al. by combining the split-ring and wire structures, similar to those Pendry had been studying in recent years [11, 18, 19], into a single composite effective medium. Despite the fact that no natural materials are known to display $\epsilon < 0$ and $\mu < 0$ simultaneously, Soviet theoreticians had already by 1940 studied the solutions of Maxwell's equations for such parameter values. In lectures given by Leonid I. Mandelshtam at Moscow State University from the 1930s and onwards [20, 21], and later in Victor G. Veselago's paper from 1967 [22], it was shown that a medium with simultaneously negative permittitvity and permeability could sustain *negative refraction* – a phenomenon not found in natural media, where the refraction angle over an interface can be negative, and the phase velocity and energy propagation may point in opposing directions! Indeed, the phenomenon had been discussed even earlier: Waves with negative group velocity were discussed already in 1904 by Horace Lamb [23] and reportedly by Arnold Schuster the same year [15, 24]. It was however not until Smith et al. made the split-ring and wire composite a century later, using techniques of material fabrication that were unavailable to Lamb, Schuster, Mandelshtam and Veselago, that the phenomenon was verified experimentally. Such composite *materials* would soon be given the Greek prefix *meta*, which may be translated as *beyond*, in order to indicate the superior properties of *metamaterials* beyond those of natural materials.

In his paper *The Electrodynamics of Substances with Simultaneously Negative Values of* ϵ *and* μ, Veselago proposed using a slab of a negative index medium as an unconventional lens. After the re-discovery of this article by Smith et al. in the year 2000 [16], Pendry would soon realize that such an arrangement represents more than just an unconventional lens – rather it in some sense constitutes a *perfect* lens with infinite resolution [25]. Conventional lens resolution is limited to values on the order of the wavelength of radiation, in accordance with the Abbe diffraction limit, due to the rapid attenuation of the evanescent field spectrum in ordinary media. Pendry demonstrated that no such resolution limit applies to Veselago's lens arrangement, since the negative index medium acts to amplify, or restore, the evanescent field. In other words the total field is reconstructed at the image plane, and no information is lost. It should be mentioned that Pendry's analysis relied on the assumption of lossless media: In practice all passive media contain loss, and any attempt of making a perfect lens with lossy elements faces significant complications.

Things were about to become even more exciting. In 2006 the possibility to render objects *completely* invisible by using metamaterials was proposed independently by Leonhardt on the one hand (for the far field) [26] and Pendry, Schurig and Smith on the other (for the entire field) [27, 28]. The concept, known as meta-

material cloaking, relies on using anisotropic metamaterials to realize coordinate transformations where certain areas are "hidden" in the sense that no coordinates exist for those areas in the transformed coordinates. Such areas are thus unprobed by the electromagnetic fields, and therefore hidden. Partial experimental verification of this concept was given already the same year when a copper cylinder was made (almost) invisible for a narrow bandwidth of microwave frequencies [29]. Following such developments, metamaterials naturally started raising eyebrows well outside of university campuses. An internet search of "*metamaterial invisibility cloak*" today reveals a significant interest within popular media. In some sense metamaterials confront us with an illusory world where things are not entirely as they appear; where objects may be invisible and images may be false. The latter is made clear in the recent development of *metasurfaces* where optical vortexes and holographic images can be made by structuring planar surfaces [30, 31]. This is achieved by causing abrupt phase discontinuities upon reflection, or transmission through, the surfaces by use of sub-wavelength resonance structures. It is therefore perhaps not surprising that popular culture often links metamaterials with the magical cloak of the fictional character *Harry Potter* in J.K. Rowling's books. Furthermore, the theory of metamaterial invisibility relies on the theory of *differential geometry* [32] which, despite being commonplace in general relativity, is *not* a daily affair in the electromagnetic theory of media. An implication of this is that metamaterials can be used as laboratory analogies of something as otherworldly as *a black hole* [33–35] or the early universe [36]. The field of metamaterials has also surfaced on the radars, so to say, of defense research institutions, as one might expect given the prospect of making things invisible. As with the super-lens, however, there are certain practical challenges towards realizing useful invisibility cloaks with metamaterials: The effective permittivity and permeability values needed to make the invisibility cloak are often only attainable over a narrow frequency bandwidth, and there is often significant amounts of loss present. Thus an invisibility cloak that works in daylight is therefore not realistic as of yet.

The many developments seen in metamaterials indicate a significant amount of freedom in what dispersions can be realized. Exactly how great is this freedom? Can any desired dispersion be realized? The papers included in this thesis all contribute in some way to shed some light on the fundamental possibilities and limitations of metamaterial effective parameters. In this respect the concept of causality is important, because any system should abide by the principle that *no effect precedes the cause*. Paper 1 of this thesis presents a conceptual framework for evaluating the possibility of obtaining a negative refractive index in causal media while having low loss or gain. It turns out that causality also implies that a metamaterial parameter ϵ or μ can be approximated arbitrarily well as a superposition of Lorentzian response functions (Papers 2 & 3). Causality concepts

represent in a sense *global* approaches towards metamaterials, where the details of the microstructure are not considered directly. It is also necessary to take the *bottom-up* approach represented by *homogenization* theory, where the microstructure is tackled. Paper 4 considers the wavelength regime where a metamaterial structure ceases to be an effective medium; i.e. when the structural dimensions no longer are small. The fact that this occurs at longer wavelengths for a metamaterial than in molecular media has interesting consequences for the formulation of Kramers-Kronig relations for metamaterials. In particular, it is shown that metamaterials attain some degree of additional freedom relative to media obeying the standard Kramers-Kronig relations. Finally, Papers 5 & 6 consider the importance of spatial dispersion when deriving effective parameters ϵ and μ from homogenization theory. It turns out that certain higher order multipoles, which are typically negligible in ordinary media, are generally important in metamaterials. Furthermore, it turns out that spatial dispersion may explain diamagnetism in causal, passive media, in the sense that the permeability μ not necessarily tends to unity for large frequencies.

Chapter 2

What is a metamaterial?

A metamaterial is essentially an *effective medium*, and is intricately related to the process of homogenization. To get to grips with what a metamaterial is, therefore, an introduction into homogenization theory shall be given before moving on to some common metamaterial examples.

2.1 The big picture – Macroscopic Maxwell's equations and effective parameters

When considering light propagation over boundaries, such as an air-water interface, one often thinks of Snell's law relating incident and refracted rays. However, when confronted with water's discontinuous structure on the molecular level, as illustrated in Fig. 2.1, one quickly realizes that this picture is a simplification. Or rather, Snell's law describes the *effective* light behavior between two electromagnetic media each described by a refractive index $n = \sqrt{\epsilon\mu}$. Obtaining such an effective medium is the topic of *homogenization theory* – the process by which the effective macroscopic properties of the complex microscopic structure is described in terms of one or more parameters. This section considers homogenization according to Russakoff-Jackson [37, 38] and effective parameters according to the Landau-Lifshitz and Casimir formulations.

As a starting point, consider the microscopic Maxwell's equation for a non-

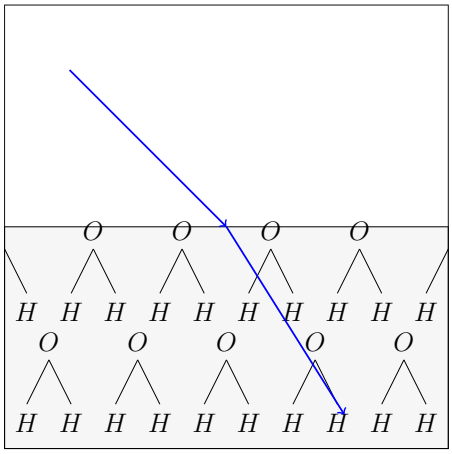

Figure 2.1: Illustration of two perspectives of an air-water interface. The *macroscopic* perspective is that of a refracted light ray obeying Snell's law between two continuous media. The *microscopic* perspective consisting of H_2O molecules, however, reveals that the interface is not clear-cut, and the medium of water is anything but continuous.

magnetic medium

$$\nabla \times \mathbf{e}(\mathbf{r}) = i\omega \mathbf{b}(\mathbf{r}), \tag{2.1a}$$

$$\nabla \times \frac{\mathbf{b}(\mathbf{r})}{\mu_0} = -i\omega\epsilon_0 \mathbf{e}(\mathbf{r}) + \mathbf{j}(\mathbf{r}) + \mathbf{j}_{\text{ext}}, \tag{2.1b}$$

$$\nabla \cdot \mathbf{e}(\mathbf{r}) = \frac{\varrho(\mathbf{r}) + \varrho_{\text{ext}}(\mathbf{r})}{\epsilon_0} \tag{2.1c}$$

$$\nabla \cdot \mathbf{b}(\mathbf{r}) = 0. \tag{2.1d}$$

In addition to the induced current and charge densities $\mathbf{j}(\mathbf{r})$ and $\varrho(\mathbf{r})$, respectively, the source current and charge densities $\mathbf{j}_{\text{ext}}(\mathbf{r})$ and $\varrho_{\text{ext}}(\mathbf{r})$, respectively, are explicitly stated. The microscopic electric and magnetic fields are represented by $\mathbf{e}(\mathbf{r})$ and $\mathbf{b}(\mathbf{r})$, respectively, and the $\mathrm{e}^{-i\omega t}$ dependence has been suppressed. The generalization to magnetic media is not very complicated, however excluding them yields more transparent equations.

If no charges or currents are present ($\varrho_{\text{ext}} = \varrho = 0$ and $\mathbf{j}_{\text{ext}} = \mathbf{j} = 0$), the equations may be combined in order to obtain the wave equation

$$\nabla^2 \mathbf{e} + \frac{\omega^2}{c^2} \mathbf{e} = 0, \tag{2.2}$$

where $c = 1/\sqrt{\epsilon_0\mu_0}$ is the speed of light in vacuum. The solutions to the wave equation are plane-waves of the form

$$\mathbf{e} = \mathbf{e}_0 \exp(i\mathbf{k}\cdot\mathbf{r}), \tag{2.3}$$

where $\omega = ck$. In a material, where charges and currents *are* present, the solutions to Maxwell's equations are not generally as simple as this. To help visualize this, one may imagine the presence of the charges and currents in the medium disrupting the vacuum field, leading to complicated variations of field over microscopic length scales. As an example, consider the field in the layered dielectric structure shown in Fig. 2.3a: The white layers correspond with vacuum, while the shaded layers correspond with a dielectric material. Within the shaded regions rapid variations of the field occur. At the same time, one observes a slowly varying envelope function, corresponding to a wavelength much longer than the structural variations of the structure. Often one is primarily interested in macroscopic effects of the system. Little error is therefore incurred if one simply treats the structure as effectively continuous with a smoothly varying macroscopic field as illustrated in Fig. 2.3b. An analogy from everyday life may be helpful here: When watching a movie on an LED screen, the microscopic reality of the bewildering number of discrete pixels is uninteresting. Since the microscopic variations across the screen are minuscule in comparison to typical image features, very little error is incurred if one assumes that the screen is continuous. In order to arrive at the macroscopic picture of Fig. 2.3b one needs to *average* the microscopic fields $\mathbf{e}(\mathbf{r})$ and $\mathbf{b}(\mathbf{r})$, and thereby obtain *macroscopic fields* $\mathbf{E}(\mathbf{r})$ and $\mathbf{B}(\mathbf{r})$. The Russakoff-Jackson formulation of effective, macroscopic fields relies on an average procedure of the form

$$\langle \mathbf{F}(\mathbf{r}) \rangle = \int f(\mathbf{r}')F(\mathbf{r}-\mathbf{r}')\mathrm{d}^3r', \tag{2.4}$$

where $f(\mathbf{r})$ is an arbitrary test function that varies slowly over the size of a unit cell (and may extend over several such cells)[37, 38]. Nothing so far has been assumed regarding length scales. Homogenization theories have traditionally concerned themselves with molecular media in which molecules or atoms are averaged over (Fig. 2.2b). With the interest in composite media during the last century, it became evident that structures which are large on the atomic length scale, but small compared with the wavelength of the field, can be treated as *artifical atoms* to which homogenization theories can be applied (Fig. 2.2c). This is the crucial idea behind metamaterials, where the structural freedom leads to electromagnetic properties not found in nature.

It shall now be assumed that a metamaterial with a *periodic* structure is under consideration. Futhermore, only a single spatial Fourier component of the source

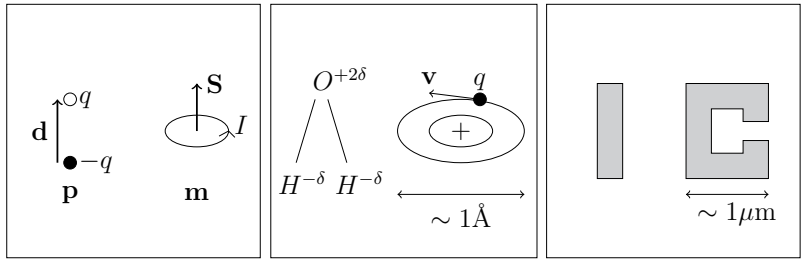

Figure 2.2: Qualitative explanation of dipole analogy for material constituents. (a) Elementary dipoles. (b) Possible molecular analogies: An H_2O molecule is polarized due to the greater electron affinity of the Oxygen atom and resembles the electrical dipole $\mathbf{p}$, while the simple atomic model of an electron circulating an ion resembles the magnetic dipole $\mathbf{m}$ (of course the more appropriate quantum mechanical picture is more complicated than this). (c) Possible metamaterial analogies: A wire can be polarized and thereby resemble the electrical dipole $\mathbf{p}$, and induced currents in the C-ring structure may resemble the magnetic dipole $\mathbf{m}$.

shall be considered:

$$\mathbf{J}_{\text{ext}} = \overline{\mathbf{J}}_{\text{ext}} \mathrm{e}^{i\mathbf{k}\cdot\mathbf{r}}, \tag{2.5a}$$

$$\rho_{\text{ext}} = \overline{\rho_{\text{ext}}} \mathrm{e}^{i\mathbf{k}\cdot\mathbf{r}}. \tag{2.5b}$$

In other words, the wavenumber is $\mathbf{k}$ is controlled by the choice of the source. It is also assumed that the test function in (2.4) is band-limited, or rather, that its fourier transform $f(\mathbf{k})$ vanishes outside the first Brillouin zone. This is approximately the case for any sufficiently smooth function $f(\mathbf{r})$ which extends over several unit cells. The averaging procedure (2.4) may then be expressed (see for example [39])

$$\langle \mathbf{F}(\mathbf{r}) \rangle = \overline{\mathbf{F}} \mathrm{e}^{i\mathbf{k}\cdot\mathbf{r}}, \tag{2.6a}$$

where

$$\overline{\mathbf{F}} = \frac{f(\mathbf{k})}{V} \int_v \mathbf{F}(\mathbf{r}) \mathrm{e}^{-i\mathbf{k}\cdot\mathbf{r}} \mathrm{d}^3 r, \tag{2.6b}$$

and the integral is taken over the volume of a unit cell of the periodic medium. Here the fact that the microscopic fields are Bloch waves of the form

$$\mathbf{e}(\mathbf{r}) = \mathbf{U}_E(\mathbf{r}) \mathrm{e}^{i\mathbf{k}\cdot\mathbf{r}}, \tag{2.7a}$$

$$\mathbf{h}(\mathbf{r}) = \mathbf{U}_H(\mathbf{r}) \mathrm{e}^{i\mathbf{k}\cdot\mathbf{r}}, \tag{2.7b}$$

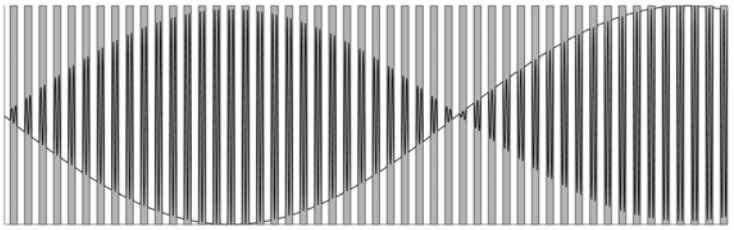

(a)

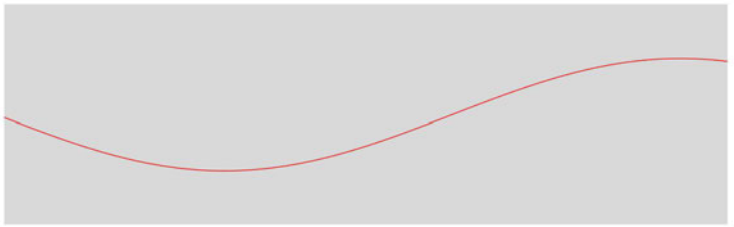

(b)

Figure 2.3: Microscopic and macroscopic points of view when considering the electric field in a periodically layered dielectric structure. (a) Microscopic field $\mathbf{e}$ is seen to vary rapidly, although a clear slowly varying modulation is observed. (b) The effective macroscopic picture: A smooth macroscopic field $\mathbf{E}$ in an effetively continuous background medium.

has been used, where $\mathbf{U}_{E,H}(\mathbf{r})$ has the same periodicity as the metamaterial. This results from the periodicity of the metamaterial and that the source too may be considered to be a Bloch wave. The operation (2.6b), when applied to these, therefore essentially represents the spatial average of their periodic modulations $\mathbf{U}_E(\mathbf{r})$ and $\mathbf{U}_H(\mathbf{r})$. If the test function is chosen so that $f(\mathbf{k}) \approx 1$ well inside the first Brillouin zone, negligible error is incurred for small $\mathbf{k}$ by setting $f(\mathbf{k}) = 1$ in (2.6b), making it then correspond to the averaging procedure utilized in [40, 41]. Therefore, in the following the test function shall be set $f(\mathbf{k}) = 1$.

Application of (2.6) to (2.1a)-(2.1b) gives

$$i\mathbf{k} \times \mathbf{E} = i\omega\mathbf{B}, \tag{2.8a}$$

$$i\mathbf{k} \times \frac{\mathbf{B}}{\mu_\mathbf{0}} = -i\omega\epsilon_0\mathbf{E} - i\omega\langle\mathbf{p}\rangle + \overline{\mathbf{J}}_{\text{ext}} e^{i\mathbf{k}\cdot\mathbf{r}}. \tag{2.8b}$$

In arriving at this result the Bloch property of the fields (2.7) and the divergence

theorem have been used to show

$$\int_V \nabla \times [\mathbf{e}\exp(-i\mathbf{k}\cdot\mathbf{r})]\mathrm{d}^3r = \int_s \mathrm{d}\mathbf{S} \times \mathbf{U}_E(\mathbf{r}) = 0. \tag{2.9}$$

where V and S indicate integration over the volume and surface of the unit cell. In (2.1) the induced current density has been expressed $\mathbf{j} = -i\omega\mathbf{p}$. The reason for this may be seen from the Maxwell-Ampere equation (2.1b): The induced current can be described through the microscopic electric displacement field $\mathbf{d}$ according to

$$\begin{aligned}\nabla \times \frac{\mathbf{b}}{\mu_0} &= -i\omega\epsilon_0\mathbf{e} + \mathbf{j} + \mathbf{j}_{\text{ext}} \\ &= -i\omega\mathbf{d} + \mathbf{j}_{\text{ext}}.\end{aligned} \tag{2.10}$$

Hence, using the relation $\mathbf{d} = \epsilon_0\mathbf{e} + \mathbf{p}$, the polarization may be expressed

$$\mathbf{p} = \mathbf{d} - \epsilon_0\mathbf{e} \tag{2.11a}$$

$$= -\frac{\mathbf{j}}{i\omega}. \tag{2.11b}$$

As a side remark, for linear media in which $\mathbf{d}$ and $\mathbf{e}$ are related through the microscopic permittivity ε according to $\mathbf{d} = \epsilon_0\varepsilon\mathbf{e}$, one may derive the expression $\mathbf{p} = \epsilon_0(\varepsilon - 1)\mathbf{e}$ from (2.11a), which will be used frequently later on in Sec. 5.2.

The next step in the homogenization process is to multipole expand $\langle\mathbf{p}\rangle$. From (2.6) with the expansion $\exp(-i\mathbf{k}\cdot\mathbf{r}) \approx 1 - i\mathbf{k}\cdot\mathbf{r} - (\mathbf{kr})^2/2$ one obtains [41,42] (to the second order in k)

$$\langle\mathbf{p}\rangle = \frac{\mathrm{e}^{i\mathbf{k}\cdot\mathbf{r}}}{V}\int_V \mathbf{p}\mathrm{e}^{-i\mathbf{k}\cdot\mathbf{r}}\mathrm{d}^3r \tag{2.12a}$$

$$= \frac{\mathrm{e}^{i\mathbf{k}\cdot\mathbf{r}}}{V}\cdot\left(\int_V \mathbf{p}\mathrm{d}^3r - i\mathbf{k}\cdot\int_V \mathbf{r}\mathbf{p}\mathrm{d}^3r - \frac{1}{2}\int_V (\mathbf{k}\cdot\mathbf{r})^2\mathbf{p}\mathrm{d}^3r\right)$$

$$\equiv \mathbf{P} - \frac{\mathbf{k}\times\mathbf{M}}{\omega} - i\mathbf{k}\cdot\mathbf{Q} + \mathbf{R}, \tag{2.12b}$$

where

$$\mathbf{P} = \frac{\mathrm{e}^{i\mathbf{k}\cdot\mathbf{r}}}{V}\int_V \mathbf{p}\mathrm{d}^3r, \tag{2.13a}$$

$$\mathbf{M} = -\frac{i\omega}{2}\frac{\mathrm{e}^{i\mathbf{k}\cdot\mathbf{r}}}{V}\int_V \mathbf{r}\times\mathbf{p}\mathrm{d}^3r, \tag{2.13b}$$

$$\mathbf{Q} = \frac{1}{2}\frac{\mathrm{e}^{i\mathbf{k}\cdot\mathbf{r}}}{V}\int_V (\mathbf{rp} + \mathbf{pr})\mathrm{d}^3r, \tag{2.13c}$$

$$\mathbf{R} = -\frac{1}{2}\frac{\mathrm{e}^{i\mathbf{k}\cdot\mathbf{r}}}{V}\int_V (\mathbf{k}\cdot\mathbf{r})^2\mathbf{p}\mathrm{d}^3r. \tag{2.13d}$$

and where the tensor **rp** has been decomposed into its antisymmetric and symmetric parts,

$$\begin{aligned}\mathbf{k}\cdot\mathbf{rp} &= \mathbf{k}\cdot(\mathbf{rp}-\mathbf{pr})/2 + \mathbf{k}\cdot(\mathbf{rp}+\mathbf{pr})/2 \\ &= -\mathbf{k}\times(\mathbf{r}\times\mathbf{p})/2 + \mathbf{k}\cdot(\mathbf{rp}+\mathbf{pr})/2. \end{aligned} \tag{2.14}$$

It is common to neglect the higher order term **R** in (2.12b), although Paper 5 of this thesis will later show that this is not generally warranted for metamaterials – the electrical electrical quadrupole **Q** *and* the higher order term **R** are generally as important as **M** when second order effects are concerned (e.g. magnetism).

Insertion of (2.12) into (2.8b) gives

$$i\mathbf{k}\times\left[\frac{\mathbf{B}}{\mu_0}-\mathbf{M}\right] = -i\omega\left[\epsilon_0\mathbf{E}+\mathbf{P}\right] - \omega\mathbf{k}\cdot\mathbf{Q} - i\omega\mathbf{R} + \overline{\mathbf{J}}_{\text{ext}}\,e^{\mathbf{k}\cdot\mathbf{r}} \tag{2.15}$$

The aim of a homogenization procedure is often to arrive at effective parameters ϵ and μ that describe the effective electromagnetic response of the metamaterial. In the so-called Casimir formulation, the parameters are defined according to

$$\epsilon'(\omega,\mathbf{k})\mathbf{E} = \mathbf{E} + \frac{\mathbf{P}}{\epsilon_0}, \tag{2.16a}$$

$$[1-\mu'^{-1}(\omega,\mathbf{k})]\mathbf{B} = \mu_0\mathbf{M}, \tag{2.16b}$$

usually assuming that the terms **Q** and **R** are negligible. Then introducing these parameters allows (2.15) to be expressed in similar form as (2.1b) where instead of using vacuum parameters ϵ_0 and μ_0 the fields are described using parameters $\epsilon_0\epsilon'$ and $\mu_0\mu'$. In other words, the effective parameters describe an effective continuous *medium* which takes into account the effective properties of the electric and magnetic *dipoles* through (2.13a) and (2.13b). Note that these parameters generally depend on **k**, meaning that they are spatially *non-local* and the system is *spatially dispersive*, i.e. the response of the system at a given point depends on the fields at other positions. This is analogous to frequency dispersion where ω-dependent parameters imply a non-local response in time. For a discussion of the importance of spatial dispersion in metamaterials, consider Chapter 5.

Instead of allocating terms from the multipole expansion (2.12b) to parameters $\epsilon'(\omega,\mathbf{k})$ and $\mu'(\omega,\mathbf{k})$, characteristic of Russakoff-Jackson homogenization, one may alternatively choose to include *all* terms of the expansion of the macroscopic polarization $\langle\mathbf{p}\rangle$ in (2.8b) into a single parameter according to

$$\epsilon(\omega,\mathbf{k})\mathbf{E} = \mathbf{E} + \frac{\langle\mathbf{p}\rangle}{\epsilon_0} \tag{2.17}$$

which is characteristic of the Landau-Lifshitz formulation presented in [40]. This is evidently a good option when **Q** and **R** are significant. That this parameter

generally depends on the wavenumber $\mathbf{k}$ is clear from the expansion (2.12b). It is sometimes useful to operate with both a permittivity *and* a permeability, so the parameter $\epsilon(\omega, \mathbf{k})$ shall now be converted into two parameters [40, 43]. Observe that the macroscopic quantities $\mathbf{B}$ and $\mathbf{E}$ are left invariant upon the transformation

$$-i\omega\langle\mathbf{p}\rangle \rightarrow -i\omega\tilde{\mathbf{P}} + i\mathbf{k}\times\tilde{\mathbf{M}}, \tag{2.18}$$

when inserting into (2.8). We can express the left hand side in terms of the non-local parameter $\epsilon(\omega, \mathbf{k})$ by (2.17), and the right hand side terms of two new parameters ϵ and μ^{-1} utilizing analogous relations to (2.16), in order to obtain

$$\epsilon(\omega, \mathbf{k}) = \epsilon - \frac{c^2}{\omega^2}\mathbf{k} \times [\mathbb{1} - \mu^{-1}] \times \mathbf{k}, \tag{2.19}$$

where we have used (2.8a), and the last term is expressed as a dyadic vector product. Non-gyrotropic media carry the symmetry [44],

$$\epsilon(\omega, -\mathbf{k}) = \epsilon(\omega, \mathbf{k}), \tag{2.20}$$

meaning that the first order $\mathbf{k}$-term in the expansion of $\epsilon(\omega, \mathbf{k})$ must vanish. Hence any first order $\mathbf{k}$-dependence in the new parameters ϵ and μ must cancel in (2.19), and it is therefore possible to define these parameters so that they have no such first order $\mathbf{k}$-dependence. Furthermore, *if* all the second order $\mathbf{k}$-dependence of the new parameter ϵ can be placed into the term containing μ, then it is possible to construct a set of *local parameters* (i.e. $\mathbf{k}$-independent) for the system to the second order in $\mathbf{k}$. Due to the cross-products applied to the tensor μ, however, this is not always possible: Any longitudinal component, parallel with $\mathbf{k}$, vanishes from the cross product. Explicit expressions for ϵ and μ are given in Paper 5 of this thesis [45]. Note that in the special case where the non-local parameter $\epsilon(\omega, \mathbf{k})$ can be decomposed into two local parameters ϵ and μ, the system is still spatially dispersive in the sense that magnetism can be viewed as a second order spatially dispersive effect, although it is common to think of a medium with local ϵ and μ as non-spatially dispersive. For clarity, this thesis considers a medium to be spatially dispersive if the Landau-Lifshitz parameter (2.17) is $\mathbf{k}$-dependent.

As the above discussions show, a given metamaterial system can be described in terms of a variety of effective parameters. One may for instance choose to use the Casimir formulation (2.16) or the Landau-Lifshitz formulation (2.17), or any arbitrary division of the latter into parameters ϵ and μ according to (2.19). The following Sec. 2.2.1 will for instance describe a metamaterial consisting of a periodic array of cylinders in terms of the Casimir formulation, where the currents flowing around cylinders lead to a permeability $\mu' \neq 1$ for the system. However, one may equally well have used the non-local Landau-Lifshitz parameter $\epsilon(\omega, \mathbf{k})$,

for which one has no permeability function (i.e. $\mu = 1$). The fact that different descriptions are possible for the same physics may seem odd, but is a consequence of the division of the macroscopic polarization (2.18) being non-unique. Note that in the subsequent discussions, primed parameters ϵ' and μ' specifically imply the definition (2.16), and the permittivity function $\epsilon(\omega, \mathbf{k})$ with explicit dependence on $\mathbf{k}$ implies the Landau-Lifshitz parameter (2.17), whereas unprimed parameters generally do not pertain to any specific definition unless otherwise stated.

2.2 Make your own metamaterial

A good definition of a metamaterial is offered by *Wiktionary*[1].

> *Any material that obtains its electromagnetic properties from its structure rather than from its chemical composition; especially a material engineered to have features of a size less than that of the wavelength of a class of electromagnetic radiation.*

The key ingredients here are **"electromagnetic properties"**, **"size less than the wavelength"** and **"structure"**. In order to get a feel for how these ingredients combine into a metamaterial, this section considers the design of a negative refraction medium relying on household items such as aluminium cans and wires. In other words, this section presents a *do-it-yourself* metamaterial – an approach that has proven to be pedagogical in both lectures and conference presentations, although the resulting homemade metamaterial of course is not likely to have any state-of-the-art properties.

The interesting phenomenon of negative refraction occurs when one simultaneously achieves $\epsilon < 0$ and $\mu < 0$. While there does exist natural media where both $\epsilon < 0$ and $\mu < 0$ can be achieved *separately*, it was first by virtue of metamaterial structures that one was able to achieve both *simultaneously* in the same medium. The following sections shall design a metamaterial consisting of wire and resonator structures such as those proposed by Pendry and Smith. et. al [11, 16], beginning a structure which achieves $\mu < 0$.

2.2.1 Negative permeability through resonance

A popular science experiment is to drop a magnet through a conducting cylinder (such as a copper pipe) and observe the magnet *fall slowly* (Fig. 2.4a). Due to the change in magnetic flux through the cylinder, current is induced around the cylinder according to Faraday's law. The potential energy of the magnet is

[1] `https://en.wiktionary.org/wiki/metamaterial` on the 16th of January 2017.

converted into kinetic energy *and* heat dissipation of the currents. The magnet is slowed down the most when the cylinder is made of a good conductor, thus yielding large currents and a large opposing field according to Lenz' law.

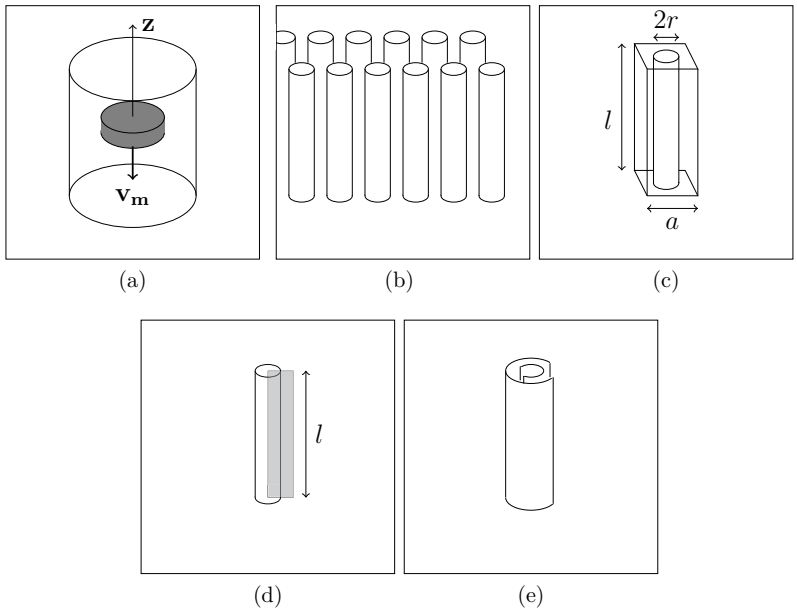

Figure 2.4: (a) Falling magnet in a conducting cylinder. (b) Metamaterial consisting of a periodic arrangement of conducting cylinders. (c) Unit cell of the metamaterial. (d) Contour-curve for the evaluation of $\mathbf{b}_I$ in (2.26). (e) Split ring cylinder: One cylinder that has been cut vertically is placed inside of another cylinder that also has been cut vertically.

The above experiment demonstrates the usefulness of conducting, non-magnetic cylinders to generate a magnetic response. When desiring to design a metamaterial with a magnetic response (i.e. $\mu \neq 1$), a structure of cylinders such as shown in Fig. 2.4b may therefore be a good place to begin. Such a structure may for instance be made using an array of empty aluminium cans. According to (2.16b) one needs to determine the dipole density vector $\mathbf{M}$ and the macroscopic field $\mathbf{B}$ in order to find the effective permeability μ' for the system. According to the averaging procedure (2.6) the macroscopic field is given by

$$\mathbf{B} = \frac{\mathrm{e}^{i\mathbf{k}\cdot\mathbf{r'}}}{a^2 l} \int \mathbf{b}\mathrm{e}^{-i\mathbf{k}\cdot\mathbf{r'}}\mathrm{d}^3 r', \tag{2.21}$$

where l represents the length of the cylinders, a^2 is the area of the unit cell cross section, and $\mathbf{b}$ is the microscopic magnetic flux density. The coordinates are represented by the primed vector $\mathbf{r}'$ (to distinguish it from the cylinder radius r). From (2.13b) and (2.11b)

$$\mathbf{M} = -\frac{i\omega \mathrm{e}^{i\mathbf{k}\cdot\mathbf{r}'}}{2a^2 l}\int_V \mathbf{r}' \times \frac{\mathbf{j}}{-i\omega}\mathrm{d}^3 r' \tag{2.22}$$

$$= \frac{\mathrm{e}^{i\mathbf{k}\cdot\mathbf{r}'}}{2a^2 l}\int_{-l/2}^{l/2}\int_0^{2\pi}\int_{a^2} \mathbf{r}' \times \mathbf{j}\rho \mathrm{d}\rho \mathrm{d}\phi \mathrm{d}z, \tag{2.23}$$

where $\mathbf{r}' = \langle \rho\cos(\phi), \rho\sin(\phi), z\rangle$, and where the origin has been placed in the center of the unit cell. Assuming a symmetric distribution of current density in the $\hat{\mathbf{z}}$-direction $\mathbf{j}(z) = \mathbf{j}(-z)$, which is zero everywhere except on the thin cylinder walls where $j = I/l\mathrm{d}r$, this expression simplifies to

$$\mathbf{M} = \frac{\pi r^2}{a^2} j \mathrm{e}^{i\mathbf{k}\cdot\mathbf{r}'}\hat{\mathbf{z}}, \tag{2.24}$$

where j hereafter represents the current per cylinder length $j = I/l$, and where r again is the cylinder radius. Both j and $\mathbf{b}$ need to be determined in order to find μ', and the latter shall be considered first. The field inside of a cylinder in Fig. 2.4b may be expressed as a superposition of fields

$$\mathbf{b} = \mathbf{b}_{\text{ext}} + \mathbf{b}_{\text{I}} - \mathbf{b}_r, \quad \{\text{within a cylinder}\} \tag{2.25}$$

where $\mathbf{b}_{\text{ext}} = b_{\text{ext}}\hat{\mathbf{z}}$ represents the external field (i.e. the field one would have if the cylinders were replaced by empty space) which is assumed to be uniform over the unit cell along the cylinder axis, $\mathbf{b}_{\text{I}}$ represents the induced field due to the current flow around the cylinder, and $\mathbf{b}_r$ represents the coupling field with the neighboring cylinders. The induced field $\mathbf{b}_{\text{I}}$ may be determined from the integral form of (2.1b) assuming quasi-statics

$$\oint_c \mathbf{b}_{\text{I}} \cdot \mathrm{d}\mathbf{l} = \mu_0 I, \tag{2.26}$$

over the closed contour-curve displayed in Fig. 2.4d. When $l \gg r$ we may assume that $\mathbf{b}_I = b_I\hat{\mathbf{z}}$ inside the cylinder, while $\mathbf{b}_I = 0$ outside, thus giving

$$\mathbf{b}_I = \frac{\mu_0 I}{l}\hat{\mathbf{z}} = \mu_0 j\hat{\mathbf{z}}. \tag{2.27}$$

In order to determine the coupling field $\mathbf{b}_r$, one may note that 2.1d implies that the magnetic flux through a cylinder $\Phi = b_I \pi r^2$ must return back again all over

the metamaterial (i.e. every field line must bite its tail). Furthermore, when $l \gg r$ one may show that the net return flux from *all N cylinders* is spread out evenly over all the cylinders. Together these effects allow for the coupling field $\mathbf{b}_r$ between cylinders to be expressed

$$\mathbf{b}_r = \frac{N\Phi}{Na^2}\hat{\mathbf{z}} = \frac{b_I \pi r^2}{a^2}\hat{\mathbf{z}} = \frac{\mu_0 \pi r^2}{a^2} j\hat{\mathbf{z}}. \tag{2.28}$$

The microscopic field may therefore be expressed

$$\mathbf{b} = \begin{cases} b_{\text{ext}}\hat{\mathbf{z}} + \mu_0 j(1 - \frac{\pi r^2}{a^2})\hat{\mathbf{z}} & \text{inside cylinder,} \\ b_{\text{ext}}\hat{\mathbf{z}} - \mu_0 j \frac{\pi r^2}{a^2}\hat{\mathbf{z}} & \text{outside cylinder.} \end{cases} \tag{2.29}$$

Insertion into (2.21) now yields

$$\begin{aligned} \mathbf{B} &= \frac{\hat{\mathbf{z}}}{a^2}\left[b_{\text{ext}} + \mu_0 j(1 - \frac{\pi r^2}{a^2})\right]\pi r^2 + \frac{\hat{\mathbf{z}}}{a^2}\left[b_{\text{ext}}\hat{\mathbf{z}} - \mu_0 j\frac{\pi r^2}{a^2}\right](a^2 - \pi r^2), \\ &= b_{\text{ext}}\hat{\mathbf{z}}. \end{aligned} \tag{2.30}$$

Note that the wavenumber has been set to $\mathbf{k} = 0$ in (2.21), in line with the assumption that the external field $\mathbf{b}_{\text{ext}}$ is uniform. The same applies to the magnetization (2.24) in the following.

We now proceed to solve j by using Faraday's law (2.1a)

$$IR_\Omega = i\omega\pi r^2\left[b_{\text{ext}} + \mu_0 j\left(1 - \frac{\pi r^2}{a^2}\right)\right], \tag{2.31}$$

where R_Ω represents the electrical resistance of the cylinder wall, and a $\exp(-i\omega t)$ time dependence has been assumed. Re-writing the left hand side in terms of resistance per circumference-length ratio ρ

$$IR_\Omega = 2\pi r\rho j, \tag{2.32}$$

and solving for j in (2.31) gives

$$j = \frac{b_{\text{ext}}}{\frac{2\rho}{i\omega r} - \mu_0(1 - \frac{\pi r^2}{a^2})}. \tag{2.33}$$

Now that expressions for $\mathbf{B}$ and j have been obtained, the effective parameter μ' is found by inserting (2.24) and (2.30) into (2.16b). One then obtains

$$\mu' = 1 - \frac{\omega\frac{\pi r^2}{a^2}}{\omega + \frac{i2\rho}{\mu_0 r}}. \tag{2.34}$$

A plot of μ' against scaled frequency is presented in Fig. 2.5a. It is clear that the arrangement of cylinders has succeeded in creating a magnetic response out of non-magnetic cylinders ($\mu' \neq 1$). However, the arrangement does not give $\mu' < 0$. In order to achieve negative values, the geometry of the cylinders must be modified: Consider the split ring cylinder in Fig. 2.4e. One can think of it as one cylinder placed inside of another, with a small strip of each cylinder cut away on opposite sides. It will now be shown that a periodic array of such split-ring cylinders enables the achievement of negative permeability.

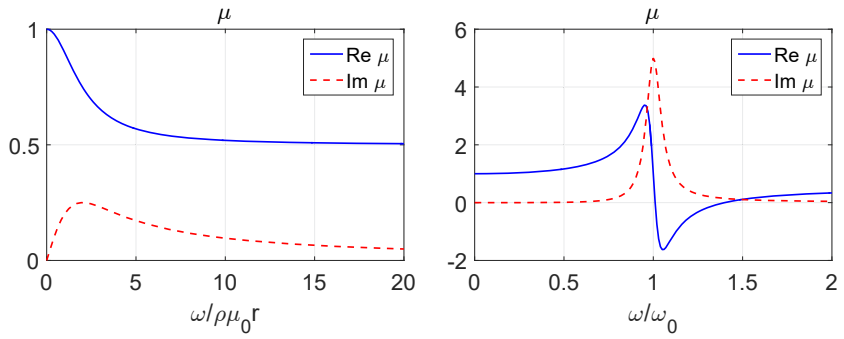

(a) (b)

Figure 2.5: Effective permeability of metamaterials consisting of (a) A periodic arrangement of cylinders with filling fraction $\pi r^2/a^2 = 0.5$. (b) A periodic arrangement of split ring cylinders with filling fraction $\pi r^2/a^2 = 0.5$ and $\frac{2\rho}{\omega_0 \mu_0 r} = 0.1$.

The split-ring cylinder is different from the normal cylinder in that there has been introduced a capacitance between the cylinder walls. Figure 2.6 shows how one may treat the split-ring cylinder as capacitors in series. If it is assumed that the spacing between the two cylinder walls is small compared with the radius r, the only significant difference between the derivation of μ for the hollow cylinder and for the split-ring cylinder is the different expression of the *emf* used in (2.31)

$$\text{emf} = I(R_\Omega + Z_c), \tag{2.35}$$

where $Z_c = -1/i\omega C_{\text{net}}$ is the impedance of the effective series capacitor in Fig. 2.6b. Using

$$\frac{1}{C_{\text{net}}} = \frac{1}{C} + \frac{1}{C} = \frac{2d}{\epsilon_0 A} \tag{2.36}$$

and using that the area $A = \pi r l$ corresponds to half of the cylinder surface area (since the surface area of the split ring cylinder walls in Fig. 2.6a corresponds to two capacitors as shown in Fig. 2.6b) gives

$$C_{\text{net}} = \frac{\epsilon_0(A/2)}{d} = \frac{\epsilon_0(\pi r l/2)}{d}. \tag{2.37}$$

I.e. the net capacitance corresponds to an effective area of $\pi r l/2$. Introducing a quantity $C = C_{\text{net}}/(\pi r l/2)$ which represents the capacitance per effective area, allows the following expression for the permeability to be found

$$\mu'(\omega) = 1 + \frac{\omega^2 \frac{\pi r^2}{a^2}}{\omega_0^2 - \omega^2 - i\omega\frac{2\rho}{\mu_0 r}}, \tag{2.38}$$

by following the same steps as earlier. Here $\omega_0 = \sqrt{2/\pi^2\mu_0 C r^3}$ represents the resonance frequency. This response is plotted in Fig. 2.5b against scaled frequency ω/ω_0. One observes that a negative permeability $\mu' < 0$ is achieved in a frequency bandwidth above resonance.

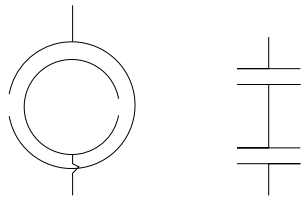

Figure 2.6: (a) Cross-section of a split ring cylinder. (b) Capacitors in series.

2.2.2 Negative permittivity through plasma response

As shall be shown here, negative permittivities $\epsilon < 0$ can be obtained by using conducting wires. Consider first a *slab* of a good conductor (Fig. 2.7a): The microscopic field is that of a continuous medium $\mathbf{e} = e\exp(i\mathbf{k}\cdot\mathbf{r'})\hat{\mathbf{z}}$ polarized along the axis of the slab, and the macroscopic field is then obtained from (2.6)

$$\mathbf{E} = \frac{\mathrm{e}^{i\mathbf{k}\cdot\mathbf{r'}}}{a^2 l}\int \mathbf{e}\mathrm{e}^{-i\mathbf{k}\cdot\mathbf{r'}}\mathrm{d}^3 r' = e\mathrm{e}^{i\mathbf{k}\cdot\mathbf{r'}}\hat{\mathbf{z}}, \tag{2.39}$$

i.e. equal to the microscopic field. It is common to model the motion of the charges as a damped spring system. Each charge is then assumed to be bound by a spring

with spring constant κ according to Hooke's law, and the motion is damped by an amount proportional with the velocity of the charge. This proportionality constant is τ^{-1}, where τ represents a characteristic distance of collision-free travel. From Newton's second law one may thus express

$$\ddot{z} + \frac{1}{\tau}\dot{z} + \frac{\kappa}{m}z = \frac{q}{m}e_0 \exp(-i\omega t). \tag{2.40}$$

The solution to this equation for finite values of τ and k yields the Lorentzian response which is discussed further in Sec. 4.2.2. Given that the slab is made of a good conductor, it is in order to simplify and assume no collisions, $\tau \to \infty$, and free charges, $k = 0$. In other words, the charges are assumed to behave like a gas. The velocity of the charges are then given by integrating the right hand side of (2.40), which yields

$$\dot{z} = \frac{iq}{m\omega}e, \tag{2.41}$$

having assigned the initial velocity equal to zero. This expression may be used in (2.13a), to calculate the polarization density

$$\mathbf{P} = \frac{\mathrm{e}^{i\mathbf{k}\cdot\mathbf{r}'}}{a^2 l}\int \frac{\mathbf{j}}{-i\omega}\mathrm{d}^3 r', \tag{2.42}$$

$$= \frac{\hat{\mathbf{z}}\mathrm{e}^{i\mathbf{k}\cdot\mathbf{r}'}}{a^2 l}\int \frac{Nq\dot{z}}{-i\omega}\mathrm{d}^3 r', \tag{2.43}$$

$$= -\frac{Nq^2}{m\omega^2}e\mathrm{e}^{i\mathbf{k}\cdot\mathbf{r}'}\hat{\mathbf{z}}. \tag{2.44}$$

Here N represents the number density of charges. From (2.16a) the permittivity may then be found

$$\epsilon' - 1 = \frac{P}{\epsilon_0 E} = -\frac{Nq^2}{\epsilon_0 m\omega^2} = -\frac{\omega_p^2}{\omega^2}, \tag{2.45}$$

where $\omega_p^2 = Nq^2/\epsilon_0 m$. This is known as the *plasma response*. Clearly it yields negative values when $\omega < \omega_p$.

Now, instead of a slab, consider a periodic arrangement of solid conducting rods (or wires) (Fig. 2.7b). Gaps between the rods give room for placing the split-ring cylinder structures discussed in the previous section, as pictured in Fig. 2.7c. This is desirable given the goal of achieving $\epsilon < 0$ and $\mu < 0$ simultaneously. Compared with the bulk conductor, the air gaps between the rods will lead to scattering of the field, which has not been accounted for in the derivation above. The exact

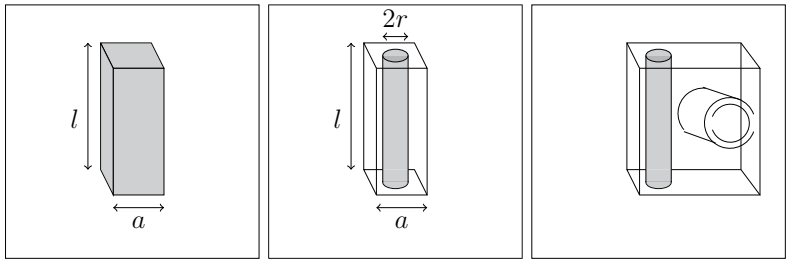

Figure 2.7: (a) Conducting slab, (b) Unit cell of a metamaterial consisting of conducting rods, (c) Possible unit cell of a metamaterial which can realize simultaneous $\epsilon < 0$ and $\mu < 0$.

solution for the periodic rod array may be found in [46]. When simplified in the limit $\omega a/c \to 0$ and assuming uniform fields $\mathbf{k} = 0$, the solution becomes

$$\epsilon' - 1 = -\frac{\omega_p^2}{\omega^2}\frac{\pi r^2}{a^2}, \tag{2.46}$$

I.e. in the exact treatment the plasma response is weighted by the volume fraction of the cylinder to the unit cell.

The needed structures to obtain negative refraction have thus been found: The wire and split-ring metamaterial of which Fig. 2.7c shows a unit cell. A similar design was used by Smith et al. in 2000 to demonstrate negative refraction experimentally [16]. Although the design discussed here *can* be made of household aluminium cans and copper wire, one must remember that any application as a metamaterial necessitates fields with wavelengths much longer than the structure sizes. Thus the effective properties of a homemade structure may easily lie in the radio-frequency regime. Note also that determining ϵ and μ separately for the wire and split-ring structures, respectively, does not necessarily imply that a combined structure (Fig. 2.7c) will exhibit the same parameters. However, due to the complexity involved in treating a combined system, it is not straightforward to obtain analytical expressions.

2.3 Transmission line metamaterials

Networks of lumped elements can emulate electromagnetic media. This section will demonstrate this by determining the effective permittivity ϵ and effective permeability μ for a lumped circuit consisting of repetitions of the unit cell shown below.

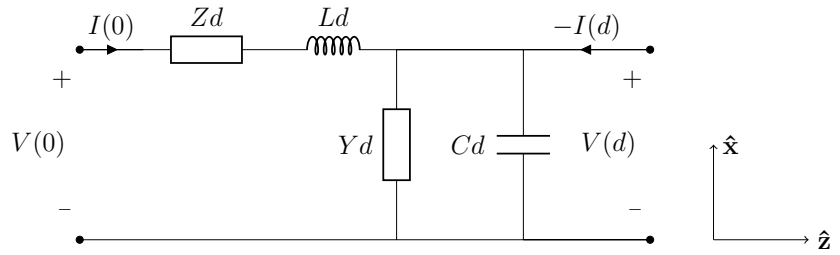

The quantities Z, L, Y and C are per unit length; i.e. Zd and Yd represent the distributed impedance and admittance of generic lumped elements (to be specified later) over the distance d, and likewise Ld and Cd represent the distributed intrinsic inductance and capacitance of the transmission line. The circuit is a unit cell of a 2d network: I.e. it is repeated to the left and right, as well as above and below the page. From Kirchoff's voltage law one can derive

$$\underbrace{\frac{V(d)-V(0)}{d}}_{=\mathrm{d}V/\mathrm{d}z} = -ZI(0) - L\frac{\mathrm{d}I(0)}{\mathrm{d}t}, \tag{2.47a}$$

where Faraday's law has been used to express the voltage drop over the inductor as the negative of the electromotive force $L\partial I/\partial t$. Similarily, from Kirchoff's current law

$$\underbrace{\frac{I(0)-I(d)}{d}}_{=-\mathrm{d}I/\mathrm{d}z} = YV(d) + C\frac{\mathrm{d}V(d)}{\mathrm{d}t}, \tag{2.47b}$$

where the definition of capacitance has been used to express the current over the capacitor $I_C = \partial Q/\partial t = C\partial V/\partial t$. These equations are known as the *telegrapher equations* of the transmission line. Assuming a time dependence of $\exp(-i\omega t)$ then gives

$$\frac{\mathrm{d}V}{\mathrm{d}z} = -(Z - i\omega L)I(0), \tag{2.48a}$$

$$\frac{\mathrm{d}I}{\mathrm{d}z} = -(Y - i\omega C)V(d). \tag{2.48b}$$

The telegrapher equations can be mapped to the Maxwell's equations. In order to do this the potential and current in the circuit shall be related to the fields. One may express $V = -Ed$. Using Ampere's law over a contour of dimensions $\Delta y = d$ and Δx with surface normal along the upper circuit line gives $H(z) = I(z)/2d$. It has been assumed that the magnetic field points uniformly along the $\hat{\mathbf{y}}$ direction,

typical of the field above a sheet distribution of current. This is approximately the case if there are many parallel lines of current on either side of the circuit drawn above. Inserting for the fields gives

$$\frac{\mathrm{d}E}{\mathrm{d}z} = 2(Z - i\omega L)H, \tag{2.49a}$$

$$\frac{\mathrm{d}H}{\mathrm{d}z} = \frac{(Y - i\omega C)}{2}E. \tag{2.49b}$$

Introducing the parameter definitions

$$\mu \equiv -\frac{2Z}{i\omega\mu_0} + \frac{2L}{\mu_0}, \tag{2.50a}$$

$$\epsilon \equiv -\frac{Y}{2i\omega\epsilon_0} + \frac{C}{2\epsilon_0}, \tag{2.50b}$$

allows for the mapping of the telegrapher equations (2.48) to the Maxwell equations for the system

$$\frac{\mathrm{d}E}{\mathrm{d}z} = -i\omega\mu_0\mu H, \tag{2.51a}$$

$$\frac{\mathrm{d}H}{\mathrm{d}z} = -i\omega\epsilon_0\epsilon E. \tag{2.51b}$$

Thus the circuit clearly models an electromagnetic medium with parameters ϵ and μ. Furthermore, following the recent discussions of *effective media*, it is natural to interpret such circuits as a form of metamaterials in which effective permittivity and permeability functions arise from structures with characteristic lengths that are small compared to the wavelength $d \ll \lambda$. As is discussed in [47], one may for instance design a negative permittivity metamaterial by replacing the generic admittance Y with that of an inductor $Y = 1/Z_L = -1/i\omega L$ for which

$$\epsilon = \frac{C}{2\epsilon_0} - \frac{\omega_L^2}{\omega^2}, \tag{2.52a}$$

having defined $\omega_L^2 \equiv 1/2\epsilon_0 L$. Hence the functional resemblance with the plasma-response discussed in Sec. 2.2.2 is apparent. Similarily, if the generic impedance element is replaced with that of a capacitor $Z = -1/i\omega C$, one may obtain a negative permeability metamaterial

$$\mu = \frac{2L}{\mu_0} - \frac{\omega_C^2}{\omega^2}, \tag{2.52b}$$

having defined $\omega_C^2 \equiv 2/\mu_0 C$. I.e. one ends up with a plasma-response equivalent for the permeability. At low frequency, the frequency dependent terms in (2.52a) and (2.52b) dominate (i.e. intrinsic capacitance and inductance effects are negligible), thus yielding $\epsilon < 0$ and $\mu < 0$. Thus it is possible to realize a negative index medium with a transmission line metamaterial consisting of periodically placed inductors and capacitors [47], when placed as in the unit cell circuit below.

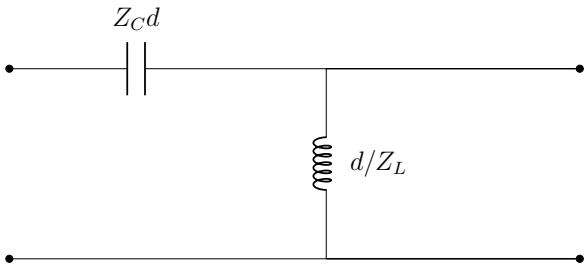

Transmisions lines thus present a simple, yet powerful, method of testing and designing metamaterial phenomena. Furthermore, rational functions can often be realized in terms of lumped elements, for instance by use of algorithms such as Brune synthesis [48]. This opens up for the possibility of starting with a desired function of ϵ or μ, and find the needed circuit which realizes them, i.e. the inverse to the process of homogenization discussed in Sec. 2.1, where one starts with a given structure and determines the parameters ϵ and μ. For instance, imagine that one is interested in finding circuits which realize a Lorentzian resonance in $\mu(\omega)$ according to

$$\mu(\omega) = 1 + \frac{\alpha}{\omega_0^2 - \omega^2 - i\omega\Gamma}, \tag{2.53}$$

where ω_0 is the resonance frequency, while Γ and α characterize the resonance width and amplitude, respectively. The following section shows how a circuit can be built up to obtain this.

2.3.1 Brune synthesis of RLC impedances

Here the procedure of Brune synthesis [48] will be illustrated. The goal is to determine the necessary circuit elements which together give the needed impedance Z such that $\mu(\omega)$ by (2.50) gives the Lorentzian response (2.53). Introducing $s = -i\omega$ and neglecting the influence of intrinsic inductance means that the target function becomes

$$Z(s) = \frac{\mu_0}{2} s + \frac{\mu_0}{2} \frac{s\alpha}{\omega_0^2 + s^2 + s\Gamma} \tag{2.54}$$

1. **If $Z(s)$ has a pole at infinity, remove a series inductance and obtain a positive real remainder $Z_1(s)$.**
   Following this a series inductance with $Z_L = -i\omega\frac{\mu_0}{2} = s\frac{\mu_0}{2}$ is removed, thereby letting us define

$$\begin{aligned} Z_1(s) &= Z(s) - \frac{\mu_0}{2}s, \\ &= \frac{\mu_0}{2}\frac{s\alpha}{\omega_0^2 + s^2 + s\Gamma}. \end{aligned} \tag{2.55}$$

   The first element of the circuit for $Z(s)$ has thus been found:

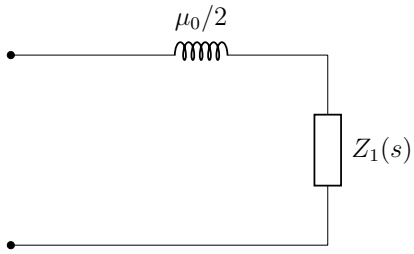

   The next step is to perform the Brune synthesis on $Z_1(s)$. $Z_1(s)$ does not have a pole at infinity, so we move on to the next step:

2. **If $Z_1(s)$ has a pole at zero, remove a series capacitor and obtain a positive real remainder.**
   This is not the case for $Z_1(s)$, so we move on to the next step.

3. **If $Z_1(s)$ has a zero at infinity, remove a shunt capacitor from $Y_1(s) = 1/Z_1(s)$ and obtain a positive remainder $Y_2(s)$.**
   Following this step a shunt capacitor with admittance $Y_C = 1/Z_C = -i\omega C = sC$ is removed, leaving

$$Y_2(s) = \frac{2}{\mu_0}\frac{\omega_0^2 + s^2 + s\Gamma}{\alpha s} - s\frac{2}{\alpha\mu_0}, \tag{2.56}$$

$$= \frac{2}{\mu_0}\frac{\omega_0^2 + s\Gamma}{\alpha s}. \tag{2.57}$$

   Hence another component of the circuit of $Z(s)$ has been found

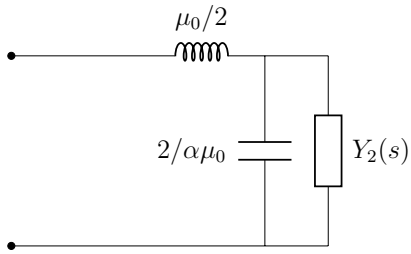

Next, brune synthesis shall be applied to $Z_2(s) = 1/Y_2(s)$. Steps 1-3 do not apply, so the next step is applied.

4. **If $Z_2(s)$ has a zero at zero, remove a shunt inductor from $Y_2(s) = 1/Z_2(s)$ and obtain a positive real remainder $Y_3(s)$.**
Following this step a shunt inductor with $Y_L = 1/Z_L = -1/i\omega L = 1/sL$ is removed, leaving

$$\begin{aligned} Y_3(s) &= \frac{2}{\mu_0}\frac{\omega_0^2 + s\Gamma}{\alpha s} - \frac{1}{s\frac{\mu_0\alpha}{2\omega_0^2}}, \\ &= \frac{2\Gamma}{\alpha\mu_0}. \end{aligned} \tag{2.58}$$

The remainder $Y_3(s)$ is constant and thus corresponds with a resistor. Hence the circuit for $Z(s)$ has thus been found

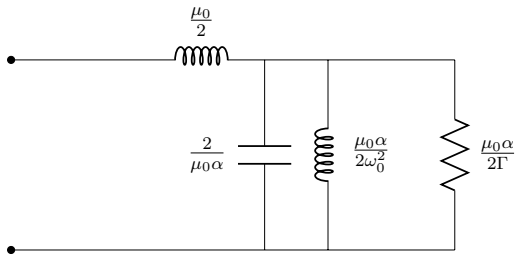

Naming $L_1 = \mu_0/2$, $C = 2/\mu_0\alpha$, $L_2 = \mu_0\alpha/2\omega_0^2$ and $R = \mu_0\alpha/2\Gamma$ and calculating the total impedance of the above circuit gives

$$Z(\omega) = -i\omega L_1 - \frac{1}{i\omega C + \frac{1}{i\omega L_2} - \frac{1}{R}}. \tag{2.59}$$

Using (2.50) allows for the determination of $\mu(\omega)$

$$\begin{aligned}\mu(\omega) &= -\frac{2}{\mu_0}\frac{Z}{i\omega}, \\ &= \frac{2}{\mu_0}L_1 + \frac{\frac{2}{\mu_0}}{-\omega^2 C + \frac{1}{L_2} - \frac{i\omega}{R}}\end{aligned} \tag{2.60}$$

Introducing the values of the circuit for L_1, C, L_2, and R yields the Lorentzian response (2.53).

Brune synthesis may also be applied to obtain a Lorentzian response for $\epsilon(\omega)$, as shown in Paper 3 of this thesis [49]. Also, Sec. 4.2.2 discusses how Lorentzian resonances can be superposed to obtain any desired causal response function. This therefore implies that any desired causal metamaterial response can be modelled by transmission line circuits as those above. Furthermore, circuit model metamaterials can sometimes be realized as circuit equivalent systems: Consider e.g. the acoustic cloak designed by a circuit equivalent [50]. To some extent, therefore, using Brune synthesis for the design of transmission line metamaterials can serve as a complete inverse-homogenization procedure, by which metamaterial realizations of desired parameters $\epsilon(\omega)$ and $\mu(\omega)$ can be realized in physical systems beyond circuits.

2.4 Model breakdown

Over the previous sections several metamaterial systems have been considered for which functions for the effective parameters $\epsilon(\omega)$ and $\mu(\omega)$ have been derived. Recall, for instance, the LC-loaded transmission line proposed in [47] of which the effective parameters are stated to be of the form

$$\epsilon = -\frac{\omega_L^2}{\omega^2}, \tag{2.61a}$$

$$\mu = -\frac{\omega_C^2}{\omega^2}, \tag{2.61b}$$

which can yield negative refraction. It is sometimes interesting to know the values of $\epsilon(\omega)$ or $\mu(\omega)$ as $\omega \to \infty$: As discussed in Sec. 4.2.1, the real and imaginary components of an effective parameter can be related through the use of Kramers-Kronig relations in which the parameters are integrated over all frequencies. Evaluating (2.61) as $\omega \to \infty$ reveals that $\epsilon = \mu = 0$. However, if one takes $\epsilon(\omega)$ and $\mu(\omega)$ to represent the electric and magnetic response of the medium, this result is clearly odd: In the vacuum limit $\omega \to \infty$ one usually expects $\epsilon \to 1$ and $\mu \to 1$, implying that the system no longer is responsive. Contrary to this, a permittivity and

permeability near zero usually indicate a strong response. A similar observation can be made in the effective permeability of the split ring cylinder metamaterials considered in Eq. (2.38) of Sec. 2.2.1: In the vacuum limit one finds that $\mu \to 1 - \pi r^2/a^2 \neq 1$.

The above issues reveal that it is important to remember that metamaterials are only *effectively* continuous media. That is, they may be treated as continuous media insofar as the characteristic sizes of their discrete structures may be neglected. However, at high frequencies $\omega \to \infty$ the corresponding wavelength becomes vanishingly small, $\lambda \to 0$, for which it is no longer possible to assume that the metamaterial behaves as an effectively continuous medium. It therefore follows that the effective parameters ϵ and μ no longer represent any effective electric or magnetic response – i.e. they no longer describe the effective permittivity or permeability. Consider again (2.61): Behind these equations rest two assumptions: i. that the medium can be described as a circuit, and ii. that the intrinsic capacitance and inductance can be neglected (compare with eqs. (2.50)). As ω increases both of these assumptions break down, first the latter when by (2.50) $\epsilon(\infty)$ and $\mu(\infty)$ clearly are no longer zero, and then the former (when the description in terms of a circuit becomes meaningless due to the wavelength being small compared circuit dimensions).

Note that the breakdown of the effective parameters discussed so far assumes eigenmodal propagation where ω and k are related by a dispersion relation. In the presence of sources, however, ω and k can in principle be chosen independently of each other: Think for instance of the field in a capacitor where it is possible to oscillate at a desired frequency ω while having $k \to 0$. It then turns out to be possible to have analytic permeability functions $\mu \neq 1$ as $\omega \to \infty$, while keeping $kd \ll 1$, thereby not necessarily leading to model-breakdown (as discussed in Paper 6 of this thesis). However, it can be shown that the magnetization tends to zero in this limit, meaning that $\mu(\infty)$ nevertheless loses its physical significance: Since the magnetization tends to zero, this means that there is no material response despite the fact that $\mu(\infty) \neq 1$.

Although it is true that effective parameters $\epsilon(\omega)$ and $\mu(\omega)$ may lose either their physical meaning as effective permittivity and permeability (eigenmodal propagation) or physical significance (source-driven systems) *locally* at high frequency, this does not mean that their functional form there is without *global* physical importance. Owing to the analytic properties of the parameters, as discussed in Sec. 4.2, the values of $\epsilon(\omega)$ or $\mu(\omega)$ for large ω determine their functional values for small ω where the parameters describe the effective properties of the system. The fact that $\epsilon(\omega)$ and $\mu(\omega)$ can approach values other than unity as $\omega \to \infty$ thus turns out to imply that metamaterials can have a greater dispersional *freedom* at low ω than conventional media. This is the topic of Paper 4 of this thesis [51].

Chapter 3

Making Maxwell's equations do something new

Maxwell's equations in linear media are

$$\nabla \times \mathbf{E} = i\omega\mu_0\mu\mathbf{H}, \tag{3.1a}$$
$$\nabla \times \mathbf{H} = -i\omega\epsilon_0\epsilon\mathbf{E} + \mathbf{J}, \tag{3.1b}$$
$$\nabla \cdot \mathbf{D} = \rho, \tag{3.1c}$$
$$\nabla \cdot \mathbf{B} = 0. \tag{3.1d}$$

Here it is evident that the material parameters ϵ and μ directly influence the field solutions $\mathbf{E}$ and $\mathbf{B}$. As mentioned in the introduction, the breakthrough which lead to the field of metamaterials was the discovery that simultaneous $\epsilon < 0$ and $\mu < 0$ could be realized [16]. Such media soon became known as *left-handed* media, as opposed to all known natural media which are termed *right-handed* (i.e. having $\epsilon > 0$ and $\mu > 0$). In this way, metamaterials opened up an unprobed area of Maxwell's equations – the result of which has lead to the discovery of novel phenomena of both theoretical and practical interest. This chapter considers some of the consequences of making the Maxwell's equations *do something new*, that is, by solving them for a new range of ϵ and μ values.

3.1 Left-handed media

Consider a transverse electromagnetic (TEM) wave with

$$\mathbf{E} = E_0 \exp(i\mathbf{k} \cdot \mathbf{r})\hat{\mathbf{x}}, \tag{3.2a}$$
$$\mathbf{H} = H_0 \exp(i\mathbf{k} \cdot \mathbf{r})\hat{\mathbf{y}}, \tag{3.2b}$$

in a continuous, source free, linear medium. Insertion of the fields in (3.1a) and (3.1b) gives

$$\mathbf{k} \times \mathbf{E} = \omega \mu_0 \mu \mathbf{H}, \tag{3.3a}$$
$$\mathbf{k} \times \mathbf{H} = -\omega \epsilon_0 \epsilon \mathbf{E}. \tag{3.3b}$$

In conventional media, where $\epsilon > 0$ and $\mu > 0$, the above equations place the vectors $\mathbf{k}, \mathbf{E}$ and $\mathbf{H}$ according to Fig. 3.1a. Since $\mathbf{k}$ is in the direction of $\mathbf{E} \times \mathbf{H}$, in accordance with the right-hand rule, such media are often referred to as *right-handed*. On the other *hand*, in the event that $\epsilon < 0$ and $\mu < 0$, (3.3) give vectors $\mathbf{k}, \mathbf{E}$ and $\mathbf{H}$ placed as shown in Fig. 3.1b (changing the signs of ϵ and μ is equivalent to changing the sign of $\mathbf{H}$). Here $\mathbf{k}$ points in the opposite direction of $\mathbf{E} \times \mathbf{H}$, in accordance with the *left-hand rule*. This is why such media are often referred to as *left-handed* media. The direction of energy flow is given by the *Poynting vector* $\mathbf{S} = \mathbf{E} \times \mathbf{H}$. Hence, in left-handed media one is left with the surprising result that the energy flow $\mathbf{S}$ and wave propagation $\mathbf{k}$ point in *opposite* directions! Figure 3.2 displays a simulation of a plane wave incident on a negative index medium.

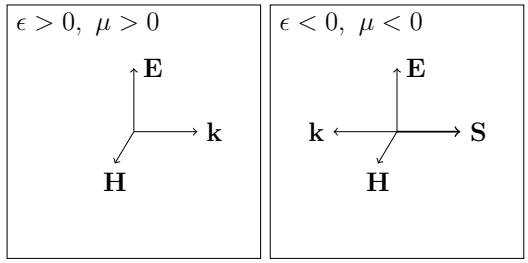

Figure 3.1: (a) Right handed medium (b) Left-handed medium.

It is at the interface between a right-handed and left-handed medium that the interesting phenomenon of *negative refraction* occurs. Consider Fig. 3.3 which displays the wavefronts on two sides of an interface. The boundary conditions across the interface are

$$\mathbf{E}_{1t} = \mathbf{E}_{2t}, \tag{3.4a}$$
$$\mathbf{H}_{1t} = \mathbf{H}_{2t}, \tag{3.4b}$$

where the subscripts $1t$ and $2t$ refer to the tangential components of the field on the left and right side of the interface, respectively. These require that the wavefronts are connected over the boundary. Furthermore, energy conservation requires that

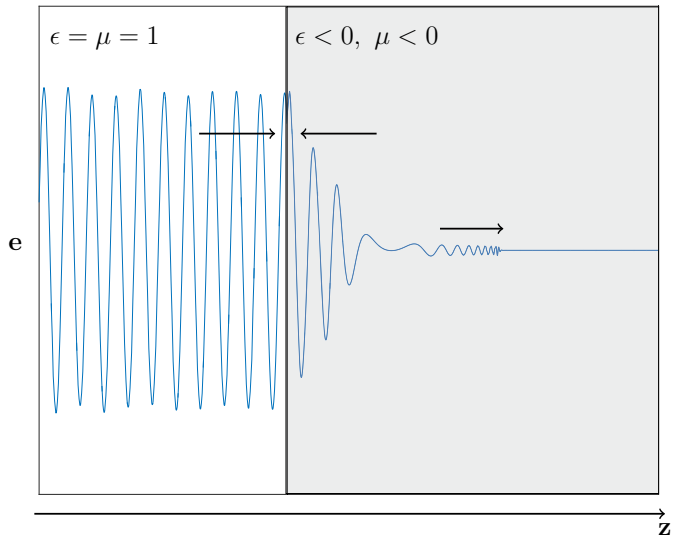

Figure 3.2: The wave propagation of a plane wave incident to a negative index medium. The arrow towards the right displays the forerunner of the wave, while the wave vector points towards the left. The negative index medium is modeled $\epsilon = \mu = 1 + F\omega_0^2/(\omega_0^2 - \omega^2 - i\Gamma\omega)$, where $F = 20$, $\omega_0 = 1$, $\Gamma = 0.1$, and the chosen frequency $\omega_{\text{obs}} = \sqrt{11}$. The simulation has been kindly provided by Hans Olaf Hågenvik at NTNU.

the normal component of the Poynting vector is continuous over the boundary: $(\mathbf{E} \times \mathbf{H})_{1n} = (\mathbf{E} \times \mathbf{H})_{2n}$, where the subscript n refers to the normal component. In the case that the interface rests between a right-handed and left-handed medium, such as shown in Fig. 3.3b, the result is that the normal component of $\mathbf{k}$ changes direction over the interface: The direction of $\mathbf{k}$ in the left-handed medium is given by the left-hand rule, and must point in the opposite direction of the Poynting vector. Comparing Fig. 3.3a with Fig. 3.3b we observe that the wavefronts in the latter refract with the negative of the angle in the former – in other words *negative refraction* has occurred. In terms of Snell's law

$$n_1 \sin\theta_1 = n_2 \sin\theta_2, \tag{3.5}$$

where $n_{1,2}$ and $\theta_{1,2}$ represent the refractive index and angle of incidence in the left and right medium, respectively, it makes sense to describe the negative refraction

by setting $n_2 < 0$. We have, however, not yet linked the index of refraction n to the material parameters ϵ and μ. To do so, one may combine (3.3a) and (3.3b) in order to obtain the dispersion equation

$$k^2 = \frac{\omega^2}{c^2}\epsilon\mu, \tag{3.6}$$

where it has been used that $c^2 = 1/\sqrt{\epsilon_0\mu_0}$. Inserting the definitions $v_p = \omega/k$ and $n = v_p/c$ allows us to find

$$n^2 = \epsilon\mu. \tag{3.7}$$

Expressing ϵ and μ in polar form then gives

$$n = \sqrt{|\epsilon\mu|}\exp i\left(\frac{\theta_\epsilon + \theta_\mu}{2}\right), \tag{3.8}$$

where θ_ϵ and θ_μ are the complex phases of ϵ and μ respectively. For $\epsilon = \mu = \exp(i\pi) = -1$, one finds $n = \exp(\pi) = -1$.

Evidently, a negative refractive index is achieved when $\epsilon < 0$ and $\mu < 0$, but this does not exhaust all possibilities: Clearly another possibility is to have $\epsilon = \exp(i2\pi) = 1$ and $\mu = 1$. In this case $n = -1$ while $\epsilon > 0$ and $\mu > 0$, i.e. in a right-handed medium. One is therefore left with two cases of right-handed media with $\epsilon = \mu = 1$ which yield different signs of n: The recent case where $\epsilon = \exp(i2\pi) = 1$ and $\mu = 1$, and the other being vacuum. The difference between them is of course the *amount of phase* $\arg(\epsilon)$. The polar plots in Fig. 3.4 reveal the importance this phase difference plays: The plot starts with $\theta_\epsilon = 0$ at infinite frequency $\omega \to \infty$, and traverses a circular path towards the phase $\theta_\epsilon = \theta_{\epsilon,\text{obs}}$ at a certain observation frequency $\omega = \omega_{\text{obs}}$. Correspondingly the phase of the refractive index changes as shown in Fig. 3.4b. With an accumulated phase of $\theta_\epsilon \approx 2\pi$ one achieves $n \approx -1$. Figure 3.4a reveals that in accumulating a phase $\theta_\epsilon \approx 2\pi$ at $\omega = \omega_{\text{obs}}$, there must be frequencies at which $\text{Im}\,\epsilon > 0$ and frequencies at which $\text{Im}\,\epsilon < 0$. The latter implies that the system is active, i.e. that it is a gain medium. Hence the right-handed, negative index medium with $\epsilon = \exp(i2\pi) = 1$ and $\mu = 1$, achieves its negative index through gain, and is therefore a very different medium than vacuum.

The above example shows that is not generally possible in *active media* to consider ϵ and μ at a single frequency and simply determine the sign of n. Adding a phase $\theta = j2\pi$, where j is an integer, to θ_ϵ or θ_μ does not alter the numerical values of ϵ or μ, respectively, but does change the sign of n according to (3.8). Negative refraction is a *global phenomenon* and the values of ϵ and μ must be traced from infinite frequency in order to identify the local sign of n. The correct sign is found by demanding that $n(\omega) \to +1$ in the vacuum limit $\omega \to \infty$. However,

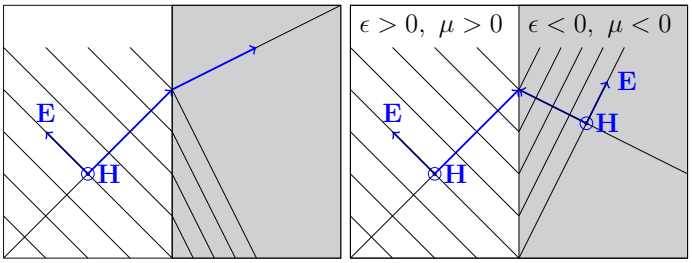

Figure 3.3: (a) Positive refraction, (b) Negative refraction at an interface between a right-handed and left-handed medium.

in the special case of a passive medium, it is sufficient to choose that sign which gives Im $n > 0$.

Since there are many challenges involved in designing prospective gain metamaterials, the possibility of negative refraction in right handed media is perhaps primarily of theoretical nature. Commonly in literature, therefore, a negative index medium implies a left-handed medium. Note that these discussions have assumed that active media do not contain any zeros in the product $\epsilon\mu$ for frequencies in the upper complex half-plane $\operatorname{Im}\omega < 0$. When this is not the case, however, the refractive index as defined by (3.8) may be non-analytic and the medium electromagnetically unstable, i.e. the fields diverge [52,53]. For the appropriate definition of the refractive index under such circumstances the reader is referred to [52].

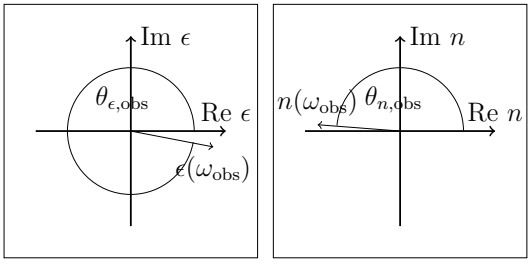

Figure 3.4: Polar representations of (a) The permittivity ϵ and (b) The refractive index n, in non-magnetic medium.

3.2 Flying fish and perfect lenses

In everyday life the phenomenon of *positive* refraction can be encountered when looking into a pond or lake. Figure 3.5a illustrates how positive refraction makes the virtual image of a fish appear to be closer to the surface than the actual fish. If the water had been replaced with a negative index medium, however, (and if the fish was able to swim in it!) a rather different virtual image results – the fish would appear to be *swimming above the surface* as shown in Fig. 3.5b! This is understood by ray-tracing from the fish, as shown. Clearly negative index media have interesting properties. In the following we shall consider how a negative index medium can be put to more practical use – to create a perfect lens.

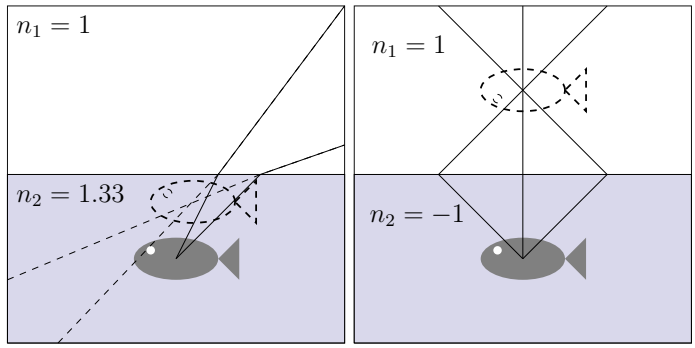

Figure 3.5: Illustrations of (a) Fish and virtual image of fish as seen from observer above the water-air interface. (b) Fish and image of fish as seen from observer above interface between negative index medium and air.

Consider the slab of a left-handed medium with $\epsilon = \mu = -1$ in vacuum, as shown in Fig. 3.6. Ray tracing from the object plane at $z = 0$ reveals that an image is formed to the right of the slab. Hence this arrangement functions as an unconventional lens. It was proposed by Veselago in 1967 [22], however, further theoretical work was done on it by Pendry in 2000 [25] where the arrangement was shown to be more than merely an uncoventional lens. It was shown to have infinite resolution! A hand-waving argument can be made to demonstrate this [25]. Expanding the field at the object plane in terms of its spatial Fourier-components in the $\hat{\mathbf{y}}$-direction gives

$$\mathbf{E}(y,0) = \int_{-\infty}^{\infty} \mathbf{A}(k_y) \exp(ik_y y) \mathrm{d}k_y. \tag{3.9}$$

Assuming source free, isotropic, continuous media, it follows that propagation of each component along $\hat{\mathbf{z}}$ is given by $\exp(ik_z z)$. Note that the system is impedance matched despite the sign changes in ϵ and μ, since the impedance $\eta = \sqrt{\mu_0\mu/\epsilon_0\epsilon}$ does not change. Thus there is no scattering at the interface, and the field along $\hat{\mathbf{z}}$ is given by

$$\mathbf{E}(y,z) = \int_{-\infty}^{\infty} \mathbf{A}(k_y)\exp(ik_y y + ik_z z)\mathrm{d}k_y. \tag{3.10}$$

Using (3.6) the $\hat{\mathbf{z}}$ and $\hat{\mathbf{y}}$ components of $\mathbf{k}$ can be related through the Pythagorean theorem

$$k_z = \sqrt{\frac{\omega^2}{c^2} - k_y^2}, \tag{3.11}$$

which allows for classification of two types of wave modes: *Normal modes* where $k_y \leq \omega/c$ and *evanescent modes* where $k_y > \omega/c$. The evanescent modes thus have imaginary values of k_z meaning that they decay exponentially with z when traveling from the object towards the slab: With $k_z = i|k_z|$ the evanescent field decays according to $\exp(-k_z z)$. However, as discussed in relation with Fig. 3.3b earlier, the sign of k_z changes over the boundary between the right- and left-handed media. Thus, within the negative index slab the evanescent field is amplified rather than attenuated, according to $\exp(+|k_z|z)$! Although this may seem surprising given that the medium is assumed passive, it is possible due to the fact that the evanescent field does not transport energy. Figure 3.6 shows that the fields propagate equal distances within and outside the slab in arriving at the image plane. The evanescent field is therefore attenuated and amplified over equal distances, so that the evanescent field amplitude at the object plane is restored at the image plane.

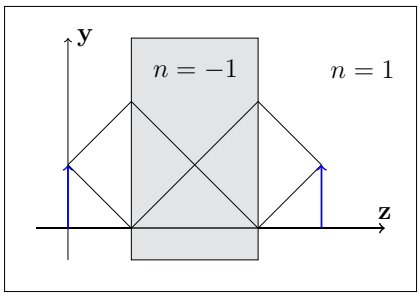

Figure 3.6

In order to perfectly restore the field of the object at the image plane, it is necessary that all Fourier coefficients in (3.10) arrive through the lens arrangement.

Herein lies the problem of limited resolution in conventional lens systems: Only the normal modes with $k_y \leq \omega/c$ make it through to the image plane, since the evanescent field is attenuated. The *upper* bound on k_y translates to a *lower* bound on the wavelengths that can be resolved $\lambda_{\text{res}} \geq 2\pi/\omega c$. In conventional lens systems, therefore, the resolution λ_{res} can only be improved by increasing the frequency ω of the field; or equivalently reducing the wavelength $\lambda \propto 1/\omega$. This is why electron microscopes are typically used to resolve molecular distances, due to the electron having a smaller wavelength than visible light. In the arrangement discussed here, however, no attenuation of the evanescent field occurs and thus perfect resolution is obtained.

The above analysis has not included the effect of material losses. In practice all materials are lossy, a fact that poses significant challenges towards realizing a perfect lens. One solution may be to compensate by gain, but this too involves certain challenges [54].

3.3 Step-by-step guide to invisibility

When driving on the highway on a warm and sunny summer day one may perhaps see what appears to be small puddles on the road ahead which mystically *vanish* as they are approached. What one is actually looking at is the sky! According to Fermat's principle, light follows that trajectory which minimizes its optical path

$$s = \int n \mathrm{d}l, \tag{3.12}$$

where n is the refractive index and $\mathrm{d}l$ is a length element. On sunny days the air may be warmer nearer to the ground, and gradually cooler towards the sky. Thus near to the ground, the air density gradually increases upwards towards the sky, and therefore also the refractive index. Rather than following a straight path from the sky and to the observer, a light ray will bend as shown in Fig. 3.7, since n is smaller nearer to the ground. This phenomenon, referred to as a *mirage*, is an example of how varying the refractive index may be used to control the trajectory of light. The refractive index is of course given by the permittivity and permeability ϵ and μ according to (3.7). With the control metamaterials offer over ϵ and μ, this section investigates the possibility creating metamaterial cloaks that bend light *around* objects –thus rendering them *invisible*! The section is based on derivations found in [32].

It is not difficult to become *almost* invisible. If you paint yourself green and lie down in the grass, you may very well become *almost* invisible. It is the method of becoming *perfectly* invisible which shall be presented here. Essentially this method consists of three steps – two of which are relatively easy, one of which is severely difficult (perhaps bordering on impossible).

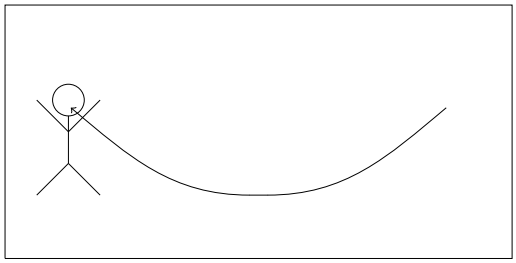

Figure 3.7: Illustration of the optical illusion of a mirage. Due to a smaller refractive index in the warmer air near to the ground, the optical path (3.12) is minimized by following a bent trajectory. The observer believes she is looking at the ground, when she in reality is looking at the sky!

3.3.1 Step 1: Find a transform

If you should happen to find yourself in a strong gravitational field (e.g. in vicinity of a black hole) the very fabric of physical reality, *space and time*, is deformed according to Einstein's theory of general relativity. Unlike equations (3.1), Maxwell's equations must then be expressed in *curvilinear coordinates*. However, it turns out that this also may be the case in metamaterials – far away from any black holes. In terms of the notation of differential geometry presented in [32], the Maxwell's equations may be expressed

$$[ijk]E_{k,j} = -\frac{\partial}{\partial t}\left(\sqrt{g}g^{ij}B_j\right), \tag{3.13a}$$

$$[ijk]B_{k,j} = \frac{1}{c^2}\frac{\partial}{\partial t}\left(\sqrt{g}g^{ij}E_j\right) + \mu_0\sqrt{g}j^i, \tag{3.13b}$$

$$(\sqrt{g}g^{ij}E_j)_{,i} = \frac{\sqrt{g}\rho}{\epsilon_0}, \tag{3.13c}$$

$$(\sqrt{g}g^{ij}B_j)_{,i} = 0. \tag{3.13d}$$

In this notation repeated indices are summed over, e.g. $g^{ij}B_j = g^{i1}B_1 + g^{i2}B_2 + B^{i3}B_3$. The tensor g_{ij} is called the metric tensor, from which the inverse metric tensor g^{ij} is defined: $g^{ij}g_{jk} = \delta^i{}_k$. The parameter $\delta^i{}_k = 1$ if $i = k$ and otherwise equals zero. The quantity g is the determinant of the metric tensor g_{ij}. The bracket $[ijk]$ follows the rule

$$[ijk] = \begin{cases} +1 & \text{if } ijk \text{ is an even permutation of 123 (e.g. 312 and 231),} \\ -1 & \text{if } ijk \text{ is an odd permutation of 123 (e.g. 132 and 213),} \\ 0 & \text{otherwise (e.g. 113 and 223).} \end{cases} \tag{3.14}$$

The subscript $_{,i}$ refers to the differential operation

$$V^j_{\ ,i} = \frac{\partial V^j}{\partial x^i}. \tag{3.15}$$

Mathematically (3.13) define the Maxwell's equations in curved *space*, where the metric tensor g_{ij} characterizes the space-geometry. I.e. in non-deformed, Cartesian space (Fig. 3.8a)

$$g^{ij} = g_{ij} = \begin{bmatrix} 1 & 0 & 0 \\ 0 & 1 & 0 \\ 0 & 0 & 1 \end{bmatrix}, \tag{3.16}$$

and hence $g = 1$. One may verify that (3.13) then simplifies to the usual form (2.1). However, in a space described in cylindrical coordinates (which is a form of curved space, relative to a Cartesian grid, as seen in Fig. 3.8b)

$$g^{ij} = \begin{bmatrix} 1 & 0 & 0 \\ 0 & \frac{1}{r^2} & 0 \\ 0 & 0 & 1 \end{bmatrix}. \tag{3.17}$$

In this manner, the Maxwell's equations in any geometry of space is found through the tensor g_{ij}.

Try to now imagine a *deformation* of space that works to our advantage – i.e. one that can make objects invisible. For instance, consider deforming the cylindrical coordinate system by expanding the point-coordinate $r = 0$ into an extended circle, as shown in Fig. 3.8c. This is achieved through the transform

$$r \to r' = R_1 + \frac{R_2 - R_1}{R_2} r \qquad \text{for } r < R_2, \tag{3.18a}$$

$$r \to r \qquad \text{for } r \geq R_2, \tag{3.18b}$$

by which the r-coordinates are compressed inside an annulus of inner and outer radii R_1 and R_2, respectively [27]. In other words, that space (i.e. the coordinates) which earlier occupied $r < R_2$ in Fig. 3.8b has now been compressed into the region $R_1 < r < R_2$, constituting a deformation of space. Hence the area within the extended circle in Fig. 3.8c corresponds to an empty *void* – an area without any coordinates. Any fields present in the coordinate system of Fig. 3.8b are thus confined outside of the extended circle in Fig. 3.8c, meaning that the area of the extended circle is unprobed by the fields. The basic idea is that since the fields cannot probe the inside of the extended circle, then this area is invisible (no coordinates means that it is literally off the grid). Of course, one may object that the area is merely invisible because it does not exist (no coordinates corresponds to non-existent space). The next section, however, will show that the void can correspond to the interior of a metamaterial (illustrated in Fig. 3.8d).

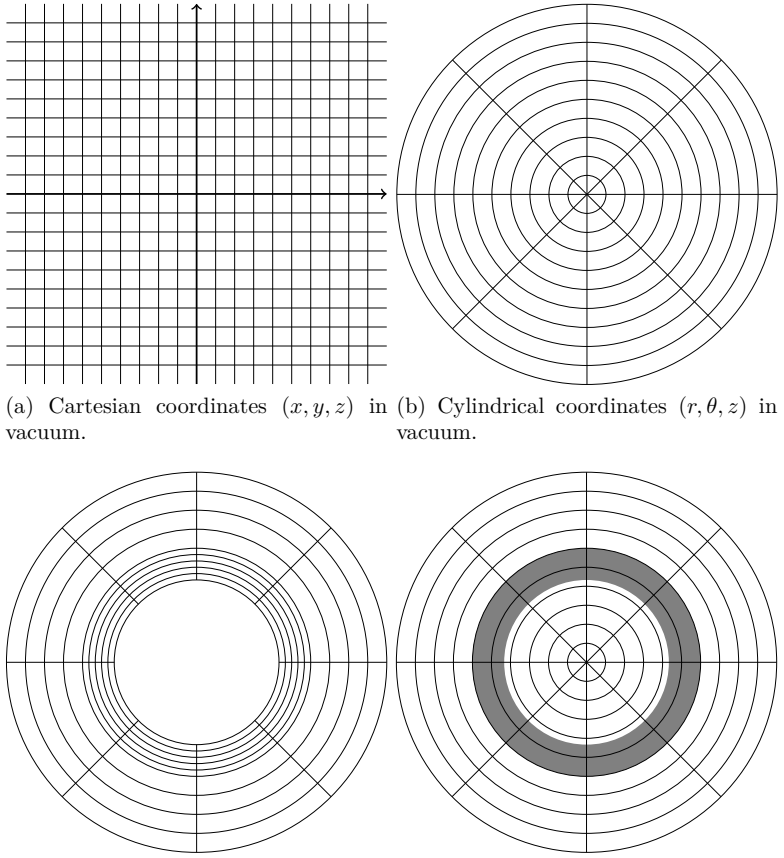

(a) Cartesian coordinates (x, y, z) in vacuum.

(b) Cylindrical coordinates (r, θ, z) in vacuum.

(c) Transformed cylindrical coordinates (r', θ, z) in vacuum.

(d) Cylindrical coordinates (r, θ, z), with an anisotropic medium.

Figure 3.8: Different coordinate systems. Inspired by figures in [32].

3.3.2 Step 2: Determine the needed effective parameters

This section will show how the field equations for *curved space* (3.13), reduce to the familiar field equations in a *medium* (3.1) through the introduction of a metamaterial with anisotropic parameters ϵ and μ. This implies that the deformed coordinate system pictured in Fig. 3.8c corresponds to a metamaterial with exotic parameters in non-deformed space, as illustrated in Fig. 3.8d.

The deformed coordinate system displayed in Fig. 3.8c, corresponding to the transform (3.18) of a cylindrical coordinate system, is characterized by *some* metric

tensor g_{ij}. Its explicit expression is not important for the present discussion. With this g_{ij}, the fields can be solved from (3.13) in terms of the deformed coordinates. Since (3.13) apply for vacuum, one may replace B_i with $\mu_0 H_i$. Considering (3.13a),

$$\underbrace{[ijk]E_{k,j}}_{=(\nabla\times\mathbf{E})_i} = -\frac{\partial}{\partial t}\Bigg(\underbrace{\sqrt{g}g^{ij}\mu_0 H_j}_{\equiv\mu_0\mu^{ij}H_j}\Bigg),$$
$$\rightarrow \nabla\times\mathbf{E} = -\mu_0\frac{\partial\mu\mathbf{H}}{\partial t}. \tag{3.19}$$

I.e. the metric tensor quantities have been hidden in a parameter $\mu^{ij} \equiv \sqrt{g}g^{ij}$, allowing (3.13a) to be expressed in the familiar form of Maxwell's equations in linear media for non-deformed, Cartesian coordinates (2.1a). Similarly, considering (3.13b),

$$\underbrace{\mu_0[ijk]H_{k,j}}_{=\mu_0(\nabla\times\mathbf{H})_i} = \frac{1}{c^2}\frac{\partial}{\partial t}\Bigg(\underbrace{\sqrt{g}g^{ij}E_j}_{\equiv\epsilon^{ij}E_j}\Bigg) + \mu_0\underbrace{\sqrt{g}j^i}_{\equiv j'^i},$$
$$\rightarrow \nabla\times\mathbf{H} = \frac{\partial\epsilon\mathbf{E}}{\partial t} + \mathbf{j}', \tag{3.20}$$

the metric tensor quantities have now been hidden in a parameter $\epsilon^{ij} \equiv \sqrt{g}g^{ij}$, and the current density has been scaled according to $j'^i \equiv \sqrt{g}j^i$, in order that (3.13b) may be expressed in the familiar form of Maxwell's equations in linear media for non-deformed, Cartesian coordinates (3.1b). The same procedure when applied to (3.13c) and (3.13d) gives

$$\nabla\cdot\epsilon\mathbf{E} = \frac{\rho'}{\epsilon_0}, \tag{3.21}$$
$$\nabla\cdot\mu\mathbf{H} = 0, \tag{3.22}$$

where the scaled charge density $\rho' \equiv \sqrt{g}\rho$ has been introduced. These correspond with the familiar Maxwell's equations in linear media for non-deformed, Cartesian coordinates (3.1c) and (3.1d).

Let us pause a moment to summarize the above findings. The unfamiliar field equations (3.13) for the deformed coordinate system displayed in Fig. 3.8c, have been shown to attain the same form as the familiar Maxwell's equations in linear media for flat, Cartesian coordinates (3.1) through the introduction of tensors

$$\epsilon^{ij} = \mu^{ij} = \sqrt{g}g^{ij}. \tag{3.23}$$

The order of this argument may be reversed: Given that we have a metamaterial in flat, Cartesian space with effective parameters ϵ and μ given by (3.23), the

fields will behave *as if* the coordinate system is deformed according to Fig. 3.8c. Knowing that this particular coordinate transform renders the area $r < R_1$ invisible, it follows that a metamaterial which attains parameters (3.23) may work as a cloaking device!

3.3.3 Step 3: Realize effective parameters in a metamaterial

As mentioned, the last step towards perfect invisibility is not trivial. It involves making metamaterials with effective parameters that fulfill conditions analogous to (3.23) [32]. The famous experimentally realized metamaterial cloak for microwave frequencies [29] in fact only manages to realize the needed parameters partially. Indeed, even if the needed parameters could be attained perfectly, they will likely only yield invisibility within a narrow frequency bandwidth. In order to understand this, consider the fact that an invisibility cloak will work perfectly only if the fields that interact with it behave as if there was no cloak there. This means that if a cloak in air bends light around and object, then the light must exit the cloak as if it had been travelling in pure air all along, in a straight line. The only way in which the field phase-front along a bent trajectory exits the cloak as if it had travelled in a straight line, is if the phase velocity is greater within the cloak than in the outside medium. Simply put, the fields inside the cloak must travel faster than the velocity of light in the external medium. In air, where the speed of light is close to that of vacuum, this implies that the phase velocity of the field within the cloak must be faster than $c \approx 3 \cdot 10^8$m/s. Although it is possible to have phase velocities greater than c without violating relativistic causality, this can only be achieved in a narrow band of frequencies. To say that that broadband invisibility remains challenging is therefore likely an understatement.

Of course, one way to increase the bandwidth of operation is to slow down the speed of light in the external medium. For instance, as an analogy to the electromagnetic invisibility cloak, an acoustic cloak for applications in water has been demonstrated [50]. Another interesting analogy is the heat cloak [55].

If one abandons the idea of full invisibility, a number of ideas exist. For instance, carpet cloaks can be used to make an object resting on a conducting surface appear as the background conductor [56]. Again, also acoustic analogies have been made [57]. A broadband cloak, covering the visible spectrum, is possible for diffusive light (e.g. light in smoke) [58], however this does not rely on the concept of transformations. This is rather to be understood along the lines of scattering reduction, for which a number of other ideas exist [59].

Chapter 4

The far-reaching consequences of causality

The principle of *cause* and *effect*, or *causality*, is one of the first tools a child acquires to make sense of the world. The ceaseless pleasures of repeatedly dropping a spoon from a high chair may very well be a statistical experiment in which the toddler is testing causal relationships [60], and perhaps also a social experiment on the dismayed parents. However, the topic of causality does not only generate enthusiasm among the smallest minds. It has been a controversial topic among many great names in philosophy –from Aristotle to David Hume and Immanuel Kant, and beyond. The topics of this chapter, however, are related to the far-reaching consequences the principle of causality carries with it for the theory of electromagnetism.

4.1 Analyticity of the response function ϵ

The functions ϵ and μ of a medium are often interpreted as response functions due to an applied influence. When this is the case, the parameters ϵ and μ are *analytic functions* in the upper complex frequency half-plane. That is, the complex functions ϵ and μ are then defined and infinitely differentiable for all ω with Im $\omega > 0$, [61, 62]. This section considers the argument for the analyticity of ϵ.

One may express the relationship between the polarization density and electric field as

$$\mathbf{P}(\omega) = \epsilon_0(\underbrace{\epsilon - 1}_{\equiv\chi(\omega)})\mathbf{E}(\omega), \tag{4.1}$$

where $\chi(\omega)$ is the electric susceptibility. Transforming to the time domain yields

the convolution

$$\boldsymbol{\mathcal{P}}(t) = \epsilon_0 \int_{-\infty}^{\infty} x(\tau)\boldsymbol{\mathcal{E}}(t-\tau)\mathrm{d}\tau, \tag{4.2}$$

where $\boldsymbol{\mathcal{P}}(t), x(t)$ and $\boldsymbol{\mathcal{E}}(t)$ are the inverse transforms of $\mathbf{P}(\omega), \chi(\omega)$, and $\mathbf{E}(\omega)$, respectively. Among textbook treatments it is common to argue that the time-domain susceptibility

$$x(t) = 0 \text{ for } t < 0, \tag{4.3}$$

where $t = 0$ corresponds to the time at which the field $\boldsymbol{\mathcal{E}}(t)$ is switched on. This is because the field $\boldsymbol{\mathcal{E}}(t)$ is assumed to be the *influence* and the induced polarization density $\boldsymbol{\mathcal{P}}(t)$ the resulting *change*. Causality dictates that any cause precedes the effect, and therefore there cannot be any response until after the influence is applied. The property (4.3) implies that $\chi(\omega) = \epsilon - 1$ is analytic according to the Titchmarsh theorem[1].

The above argument is intuitive, but unfortunately not entirely rigorous. This is because the polarization density $\boldsymbol{\mathcal{P}}(t)$ and field $\boldsymbol{\mathcal{E}}(t)$ should *both* be viewed as output of the source current density $\mathbf{J}_{\text{ext}}$ [63]: Given the complex dynamics by which the total field $\boldsymbol{\mathcal{E}}(t)$ arises under the influence of a source $\mathbf{J}_{\text{ext}}$, it is not obvious that it should always precede the polarization density $\boldsymbol{\mathcal{P}}(t)$. The proper relationship between the influence and change shall therefore be determined now. Considering Maxwell's equations in a linear, isotropic and time-shift invariant medium

$$i\mathbf{k} \times \mathbf{E} = i\omega\mu_0\mu\mathbf{H}, \tag{4.4a}$$
$$i\mathbf{k} \times \mathbf{H} = -i\omega\epsilon_0\epsilon(\omega, \mathbf{k})\mathbf{E} + \mathbf{J}_{\text{ext}}, \tag{4.4b}$$

where the Landau-Lifshitz parameter $\epsilon(\omega, \mathbf{k})$ by (2.17) includes the induced current, one finds

$$k^2\mathbf{E}_\perp = \frac{\omega^2}{c^2}\mu(\epsilon_\perp\mathbf{E}_\perp + \epsilon_\parallel\mathbf{E}_\parallel) + i\omega\mu_0\mu(\mathbf{J}_{\text{ext},\perp} + \mathbf{J}_{\text{ext},\parallel}), \tag{4.5}$$

[1]Titchmarsh Theorem: if $\chi(\omega)$ is square integrable over the real ω-axis, then any one of the following implies the other two:

1. Causality: The fourier transform $x(t) = F_\omega[\chi(\omega)]$ is zero for $t < 0$
2. Analyticity: The function $\chi(\omega)$ is analytic for $\mathrm{Im}(\omega) > 0$. Furthermore, $\chi(\omega)$ is uniformly square integrable along a line parallel to the real axis in the upper half-plane: $\int_{-\infty+i\gamma}^{\infty+i\gamma} |\chi(\omega)|^2 d\omega < k$ for some number k and all γ.
3. Kramers-Kronig: The real and imaginary parts of $\chi(\omega)$ (where $\omega \in \mathbb{R}$) are Hilbert transforms of each other.

when dividing into orthogonal and longitudinal components relative to the $\mathbf{k}$ vector. Here $\epsilon_\perp$ and $\epsilon_\parallel$ are elements of the diagonal tensor $\epsilon(\omega, \mathbf{k})$ in the basis of vectors orthogonal and parallel with $\mathbf{k}$. From this relation one may express

$$\mathbf{E}_\perp = \frac{i\omega\mu_0\mu}{k^2 - \frac{\omega^2}{c^2}\mu\epsilon_\perp}\mathbf{J}_{\text{ext},\perp}, \tag{4.6a}$$

$$\mathbf{E}_\parallel = \frac{1}{i\omega\epsilon_0\epsilon_\parallel}\mathbf{J}_{\text{ext},\parallel}. \tag{4.6b}$$

These equations provide a proper relationship between an influence $\mathbf{J}_{\text{ext}}$ and its effected change $\mathbf{E}$, and hence the quantities multiplied with $\mathbf{J}_{\text{ext},\perp}$ and $\mathbf{J}_{\text{ext},\parallel}$ are response functions that are analytic. It is however not possible from this to argue that ϵ and μ are separately generally analytic. In (4.6a) it is for instance possible that $\epsilon_\perp$ and μ are of themselves not analytic, while contributing to an overall analytic response function. In (4.6b) the analyticity of $\epsilon_\parallel^{-1}$ for Im $\omega > 0$ does not preclude $\epsilon_\parallel$ from having poles at those frequencies, which would make $\epsilon_\parallel$ non-analytic. A conditional case for the analyticity of ϵ can nevertheless be made by use of a somewhat technical argument involving Poisson's integral formula for the upper half-plane

$$\text{Im}\left\{\frac{1}{\epsilon_\parallel(\omega' + i\omega'')}\right\} = \frac{1}{\pi}\int_{-\infty}^{\infty}\frac{\omega''}{(\omega' - \tau)^2 + \omega''^2}\text{Im}\left\{\frac{1}{\epsilon_\parallel(\tau)}\right\}\text{d}\tau. \tag{4.7}$$

This expresses the harmonic extension of Im $\epsilon_\parallel^{-1}$ to the upper complex half-plane from its values along the real frequency axis. Here ω' and ω'' represent the real and imaginary parts of the frequency $\omega = \omega' + i\omega''$. Due to the reality of the field and the reality of the polarization density in (4.2), it follows that $x(t) \in \mathbb{Re}$, and from the inverse fourier transform of $\chi = \epsilon - 1$ one observes

$$\epsilon(-\omega) = \epsilon^*(\omega^*). \tag{4.8}$$

The same symmetry applies for the elements $\epsilon_\perp$ and $\epsilon_\parallel$ of the tensor, and hence one observes the same symmetry for $\epsilon_\parallel^{-1}(\omega) = \epsilon_\parallel^*(\omega)/|\epsilon_\parallel(\omega)|^2$. It follows that Im $\epsilon_\parallel^{-1}(-\tau) = -$Im $\epsilon_\parallel^{-1}(\tau)$, which may be used to re-write (4.7)

$$\text{Im}\left\{\frac{1}{\epsilon_\parallel(\omega' + i\omega'')}\right\} = \frac{1}{\pi}\int_0^{\infty}\frac{4\omega'\omega''\tau}{[(\omega - \tau)^2 + \omega''^2][(\omega + \tau)^2 + \omega''^2]}\text{Im}\left\{\frac{1}{\epsilon_\parallel(\tau)}\right\}\text{d}\tau. \tag{4.9}$$

Assuming a passive medium without spatial dispersion implies Im $\epsilon_\parallel > 0$ for positive real frequencies (Sec. 5.3 and [64]), which in turn implies Im $\epsilon_\parallel^{-1} < 0$

when assuming that there are no poles in $\epsilon_\parallel$ along the real frequency axis. From (4.9) it is thus clear that Im $\epsilon_\parallel^{-1} \neq 0$ in the upper complex half-plane, showing that there are no poles in $\epsilon_\parallel$. Furthermore, if there is no spatial dispersion in the system (i.e. no dependence on $\mathbf{k}$), then there cannot be any difference between $\epsilon_\parallel$ and $\epsilon_\perp$, i.e. ϵ becomes a scalar with $\epsilon_\parallel = \epsilon_\perp = \epsilon$. To summarize, therefore, in a continuous, isotropic, passive medium without spatial dispersion for which ϵ has no poles on the real frequency axis, ϵ is an analytic function in the upper complex half-plane.

When the system is spatially dispersive, it can be shown that the Landau-Lifshitz parameter $\epsilon(\omega, \mathbf{k})$ is analytic and obeys the Kramers-Kronig relations for fixed $\mathbf{k}$ as long as the microscopic permittivity is analytic [65].

4.2 Consequences of analyticity

4.2.1 Kramers-Kronig relations

A consequence of ϵ being analytic is that it is infinitely differentiable. One immediate implication of this is seen from the Taylor expansion evaluated around $\omega = a$

$$\epsilon(\omega) = \sum_{n=0}^{\infty} \frac{(\omega - a)^n}{n!} \frac{\mathrm{d}^n \epsilon}{\mathrm{d}\omega^n}\bigg|_{\omega=a}. \tag{4.10}$$

Knowing $\epsilon(\omega)$ in vicinity of $\omega = a$, and thereby being able to calculate an infinite number of derivatives due to analyticity, it is thus possible to find the function $\epsilon(\omega)$ for all frequencies ω. This implies that the extrapolation of $\epsilon(\omega)$ outside of a known frequency bandwidth is *unique*. This has certain implications. For instance, if the real component, Re $\epsilon(\omega)$, is known for all ω it is possible to determine Im $\epsilon(\omega)$, and vice versa. This is done by use of *Kramers-Kronig relations*, which shall be derived below. Given that the real component ϵ may be interpreted to describe field scattering while the imaginary component Im ϵ describes losses or damping, it is interesting that these physical processes turn out to be intricately related.

Let the analytic permittivity function be expressed as

$$\epsilon = a + \chi, \tag{4.11a}$$

where

$$a = \lim_{\omega \to \infty} \epsilon, \tag{4.11b}$$

$$\chi \in L^2. \tag{4.11c}$$

It is usual to let $a = 1$, considering that the permittivity in most conventional media asymptotically approach unity at high frequencies (such as the plasma response (2.45) considered earlier). However, on the background of the discussions in Sect. 2.4 and in Paper 4 of this thesis, it may in some cases be appropriate to set $a \neq 1$ in metamaterial systems. The condition that $\chi \in L^2$ means that it is square integrable

$$\int_{-\infty}^{\infty} |\chi(\omega)|^2 \mathrm{d}\omega < \infty. \tag{4.12}$$

Consider the function

$$\frac{\epsilon(\nu) - a}{\nu - \omega}, \tag{4.13}$$

in the complex plane for the frequency ν in Fig. 4.1. Due to the analyticity of ϵ in the upper complex half-plane, this function is analytic within the bounded region shown (the area between the two semicircles, where the radius of the larger semicircle tends to infinity, and the radius of the smaller tends to zero). By Cauchy's integral theorem one therefore has

$$\oint \frac{\epsilon(\nu) - a}{\nu - \omega} \mathrm{d}\nu = 0, \tag{4.14}$$

where the integral is taken over the contour bounding the region of analyticity in Fig. 4.1. The contour of integration may be divided into three sections: c_∞ corresponding to the larger semicircle, c_ω corresponding to the small semicircle surrounding ω, and the real axis excluding the vicinity of $\nu = \omega$, such that (4.14) can be re-written

$$\mathcal{P} \int_{-\infty}^{\infty} \frac{\epsilon(\nu) - a}{\nu - \omega} \mathrm{d}\nu + \int_{c_\infty} \frac{\epsilon(\nu) - a}{\nu - \omega} \mathrm{d}\nu + \int_{c_\omega} \frac{\epsilon(\nu) - a}{\nu - \omega} \mathrm{d}\nu = 0. \tag{4.15}$$

Here $\mathcal{P}$ represents Cauchy's principle value. The integral over c_∞ is bounded by

$$\left| \int_{c_\infty} \frac{\epsilon(\nu) - a}{\nu - \omega} \mathrm{d}\nu \right| \leq \int_{c_\infty} \left| \frac{\epsilon(\nu) - a}{\nu - \omega} \right| |\mathrm{d}\nu| \leq \max \left\{ \left| \frac{\epsilon(\nu) - a}{\nu - \omega} \right| \right\} \pi |\nu|. \tag{4.16}$$

It shall be assumed that $\epsilon(\nu) - a \to 0$ as $\nu \to \infty$, making the integral negligible. The integral over c_ω can be simplified by substituting $\nu - \omega = r \exp(i\theta)$, where r gives the radius of the small semicircle surrounding $\nu = \omega$, and θ the angle at that point with respect to the real frequency axis. One obtains

$$\begin{aligned} \int_{c_\omega} \frac{\epsilon(\nu) - a}{\nu - \omega} \mathrm{d}\nu &= \lim_{r \to 0} \int_{\pi}^{0} i(\epsilon(\nu) - a) \mathrm{d}\theta \\ &= \int_{\pi}^{0} i(\epsilon(\omega) - a) \mathrm{d}\theta \\ &= -i\pi(\epsilon(\omega) - a). \end{aligned} \tag{4.17}$$

In the second line, the limit was moved inside the integral. This is permitted due to uniform convergence by analyticity of ϵ, and can e.g. be shown explicitly by the Lebesgue dominated convergence theorem. As a result one may therefore express from (4.15)

$$\epsilon(\omega) = a - \frac{i\mathcal{P}}{\pi}\int_{-\infty}^{\infty}\frac{\epsilon(\nu)-a}{\nu-\omega}\mathrm{d}\nu. \tag{4.18}$$

Separating into real and imaginary components and using the symmetry property (4.8) permits this to be re-written

$$\mathrm{Re}\,\epsilon(\omega) = a + \frac{2\mathcal{P}}{\pi}\int_{0}^{\infty}\frac{\nu\mathrm{Im}\,\epsilon(\nu)}{\nu^2-\omega^2}\mathrm{d}\nu, \tag{4.19a}$$

$$\mathrm{Im}\,\epsilon(\omega) = -\frac{2\omega\mathcal{P}}{\pi}\int_{0}^{\infty}\frac{\mathrm{Re}\,\epsilon(\nu)-a}{\nu^2-\omega^2}\mathrm{d}\nu. \tag{4.19b}$$

These are relations relate the real and imaginary parts of $\epsilon(\omega)$ and are known as Kramers-Kronig relations.

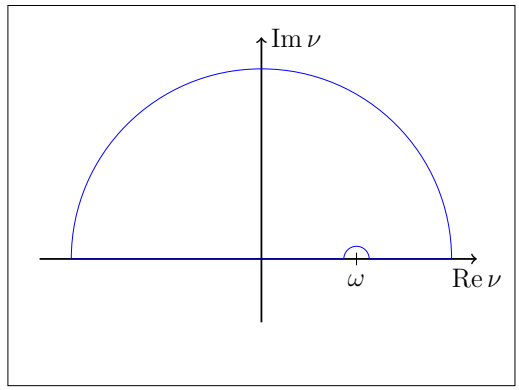

Figure 4.1

4.2.2 Decomposition into Lorentzian functions

Another interesting consequence of $\epsilon(\omega) = a + \chi(\omega)$ being analytic is that it can be decomposed into a superposition of Lorentzian response functions according to

$$\chi(\omega) = \frac{2}{\pi}\lim_{\Gamma\to 0}\int_{0}^{\infty}\mathrm{Im}\,\chi(\omega_0)\frac{\omega_0}{\omega_0^2-\omega^2-i\omega\Gamma}\mathrm{d}\omega_0, \tag{4.20}$$

as derived in papers 2 and 3 of this thesis [49,66]. The Lorentzian response

$$L(\omega) = \frac{\omega_0}{\omega_0^2 - \omega^2 - i\omega\Gamma}, \tag{4.21}$$

has its resonance at frequency ω_0 and its width is given by Γ (see Fig. 4.2). The decomposition (4.20) may be understood intuitively by observing that the imaginary part of the Lorentzian response function approaches a δ-function as a distribution under the limit $\Gamma \to 0$ [66]. Hence the imaginary part of the left and right sides of the equality in (4.20) are clearly identical. Since the real part is uniquely given by (4.19) from the imaginary part, it follows that also the real part is equal on both sides of the equality. On a more fundamental level, the decomposition (4.20) is a consequence of $\chi(\omega)$ being analytic in the upper complex half-plane, and may be deduced from Cauchy's integral theorem in a manner similar to the Kramers-Kronig relations, as shown in Paper 3 of this thesis [49].

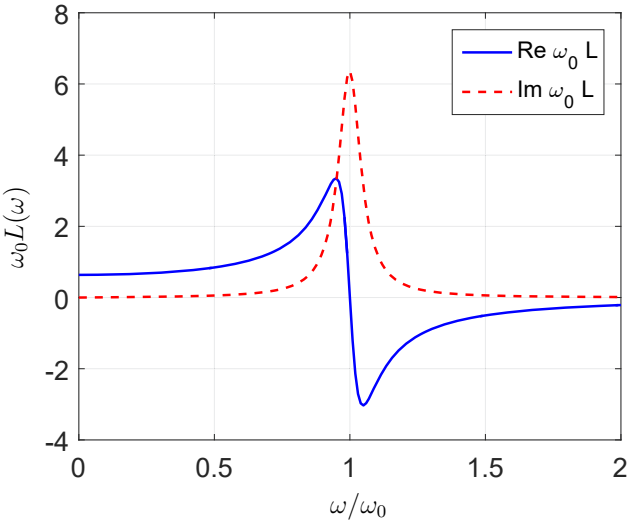

Figure 4.2: Lorentzian response function where $\Gamma/\omega_0 = 0.1$.

The decomposition (4.20) is interesting given the wide variety of systems which display resonant behavior with response functions resembling (4.21). The Lorentzian response function arises from the Lorentz model by Eq. (2.40) in Sec. 2.2.2, which describes resonant behavior in terms of a spring-constant k and a damping coefficient τ^{-1}. When defining $k = m\omega_0^2$ and $\tau^{-1} = \Gamma$, the particular case of charge

displacement z in Sec. 2.2.2 yields

$$z = \frac{1}{\omega_0^2 - \omega^2 + i\omega\Gamma} q e_0 \exp(-i\omega t), \tag{4.22}$$

for the charge q due to an external field $e_0 \exp(i\omega t)$. The Lorentzian resonance response is observed. The damped spring model is applicable to a wide variety of resonant behavior like RLC circuits, photon absorption (interband transitions), the metamaterial response μ considered in Eq. (2.38) of Sec. 2.2.1 and the metamaterial response ϵ in SiC particles [67], to mention a few.

The significance of the decomposition (4.20) is both of theoretical and practical interest. For instance, superpositions of Lorentzian responses are popular in textbook treatments on dispersion, but are commonly regarded as subsets of the class of causal functions. To mention an example from an authoritative textbook in electromagnetics, Jackson's *Classical electrodynamics*, the section on frequency dispersion characteristics [38, p. 309] begins with the words

> *Almost* all of the physics of dispersion is illustrated by ... [the Lorentz model],

(emphasis added). In reality, (4.20) and its Riemann sum equivalent discussed in Paper 2 of this thesis [66], reveal that superpositions of Lorentzians encompass the entire space of causal functions. The practical consequence of this is observed when one reverses order: Any causal response can be engineered by superpositions of common Lorentzian response functions. Considering the abundance of Lorentzian-like responses in metamaterial systems, this may be considered a feasible means by which desired dispersions may be engineered. For instance, modifying the split-ring cylinder metamaterial discussed in Sec. 2.2.1 to allow for several cylinders of different radii, capacitances and resistivities within the unit cell (Fig. 4.3), the effective permeability of the system becomes a simple sum of the single cylinder response functions (2.38)

$$\mu - 1 = \sum_k \frac{\omega^2 F_k}{\omega_{0,k}^2 - \omega^2 - i\omega\Gamma_k}, \tag{4.23a}$$

where

$$F_k = \frac{\pi r_k^2}{a^2} \tag{4.23b}$$

$$\omega_{0,k} = \frac{2}{\pi^2 \mu_0 C_k r_k^3}, \tag{4.23c}$$

$$\Gamma_k = \frac{2\rho_k}{r_k \mu_0}, \tag{4.23d}$$

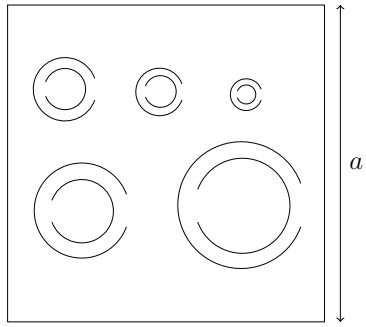

Figure 4.3: Cross section of unit cell for a metamaterial consisting of split-ring cylinders of varying structural and material parameters.

as shown in Paper 2 of this thesis [66]. This simple relation is a result of the cylinder coupling affecting each cylinder equally when the cylinder lengths are long compared with the radii. In general, when considering other systems, the coupling between Lorentz resonators is more complex. The single cylinder response function (2.38) is similar to the Lorentzian (4.21) near resonance. Thus by tayloring the amplitude F_k, the resonance frequency $\omega_{0,k}$ and width Γ_k of each cylinder k by modifying the filling factor $\pi r_k^2/a^2$, the capacitance per area C_k, and the resistance per circumference-length ratio ρ_k, respectively, one can in principle realize a desired response μ.

Chapter 5

Spatial dispersion in metamaterials

The similarity between conventional and metamaterial *homogenization* was highlighted in Sec. 2.1. Metamaterial structures were then thought of as *artificial atoms* or *molecules* which are averaged over in the same manner as in the effective medium theories for molecular media. However, given the fact that metamaterials after all can have very different structures from molecular media, there are nevertheless some important differences [39–41, 68–73]; in particular, the importance of *spatial dispersion*. The fact that metamaterial homogenization generally leads to non-local effective parameters was noted in the presentation of homogenization theory in Sec. 2.1. That is, the field response at a particular point $\mathbf{r}$ of the metamaterial depends also on the fields around that point, analogously to how the response at a given time t depends on the earlier fields in temporally dispersive media. This leads to $\mathbf{k}$-dependent effective parameters, in much the same way that temporal dispersion gives frequency dependent parameters. The following sections presents some considerations on the presence of spatial dispersion in metamaterials.

5.1 Obtaining local parameters

Section 2.1 discusses how the non-local Landau-Lifshitz permittivity (2.17) ($\mathbf{k}$-dependent) in some cases could be transformed into two local parameters ($\mathbf{k}$-independent) by (2.19). This is an example of how one in special cases may be able to obtain local parameters in spatially dispersive media. It turns out that the Casimir parameters (2.16) can also be made *more local* in some circumstances. This is the topic of this section.

Consider the fact that the terms in the multipole expansion of the averaged

polarization $\langle \mathbf{p} \rangle$ expressed in (2.13) depends on the choice of coordinate origin: If the coordinate origin is shifted by a vector $\mathbf{r}_0 = \langle \Delta x, \Delta y, \Delta z \rangle$ according to the coordinate transformation $\tilde{\mathbf{r}} = \mathbf{r} - \mathbf{r}_0$, the multipoles $\mathbf{P}$ and $\mathbf{M}$ are transformed according to

$$\tilde{\mathbf{P}} = [1 - i\mathbf{k} \cdot \mathbf{r}_0 - \frac{1}{2}(\mathbf{k} \cdot \mathbf{r}_0)^2]\mathbf{P}, \tag{5.1a}$$

$$\tilde{\mathbf{M}} = [1 - i\mathbf{k} \cdot \mathbf{r}_0][\mathbf{M} + i\omega \frac{\mathbf{r}_0 \times \mathbf{P}}{2}], \tag{5.1b}$$

where orders of $\mathbf{k}$ are included such that $\langle \mathbf{p} \rangle$ is second order in $\mathbf{k}$ upon their insertion into (2.12b). By combining (2.16a) and (5.1a), and noting that $\mathbf{E}$ is invariant under the coordinate transformation, the Casimir permittivity (2.16a) after the coordinate transformation can be expressed:

$$\tilde{\epsilon}' - 1 = [1 - i\mathbf{k} \cdot \mathbf{r}_0 - \frac{1}{2}(\mathbf{k} \cdot \mathbf{r}_0)^2](\epsilon' - 1). \tag{5.2}$$

The Casimir permittivity can be made *more local* if $\mathbf{r}_0$ can be chosen in such a way that the first order $\mathbf{k}$-term in $\tilde{\epsilon}'$ can be cancelled. The condition for this can be found by demanding that the gradient with respect to the $\mathbf{k}$-component k_k vanishes as $\mathbf{k} \to 0$, which gives the result

$$r_{0k} = -\sum_l \sum_m \frac{i}{\epsilon'_{lm}(\omega, 0) - \delta_{lm}} \frac{\partial \epsilon'_{lm}}{\partial k_k}\bigg|_{\mathbf{k}=0}, \tag{5.3}$$

where ϵ'_{lm} represents the lm-th element of the $\epsilon'(\omega, \mathbf{k})$ tensor, and $\delta_{lm} = 1$ when $l = m$ and $\delta_{ml} = 0$ otherwise. This therefore represents the components of the origin shift $\mathbf{r_0}$ necessary to avoid any first order $\mathbf{k}$-dependence. Of course, should (5.3) give complex values, or values that lie outside the unit cell, then the required coordinate shift is non-realizable. Section 5.2 below presents a case where the condition (5.3) yields more local Casimir parameters. This highlights an important point: That local parameters do not necessarily imply that the system is spatially non-dispersive. As is shown in Sec. 5.2, the coordinate shift given by (5.3) gives more local parameters, but does not modify the system. Similar comments apply in the case of the generally non-local Landau-Lifshitz parameter $\epsilon(\omega, \mathbf{k})$: One may note that (2.19) implies that it is possible in some cases to express this parameter in terms of two local parameters ϵ and μ. Generally, a system with local parameters ϵ, μ or ϵ', μ' should be viewed as spatially dispersive to the second order of $\mathbf{k}$. This is shown explicitly in Paper 5 of this thesis [45].

The appendix of Paper 5 demonstrates a particular case where modifiying the definition of the Casimir parameters (2.16) to include the terms $\mathbf{Q}$ and $\mathbf{R}$ from the expansion (2.12b), leads to a further localization of the parameters.

5.2 Homogenization of a 1d metamaterial

The metamaterial homogenization of Secs. 2.2.1 and (2.2.2) applied to systems for which the source was assumed to be constant over all space (i.e. $\mathbf{k} = 0$ in (2.5)), leading to uniform *external* or *applied* fields. This section considers homogenization of a simple 1d metamaterial for which the source has a finite wavenumber $\mathbf{k}$, in which non-local effective parameters arise. A comparison with homogenization methods utilizing eigenvalue problems is also made. The 1d metamaterial consists of a dielectric structure of alternating layers with refractive indices n_1 and n_2 as shown in Fig. 5.1. It will be demonstrated that shifting the coordinate origin allows for the Casimir parameters to become more local.

5.2.1 Model

In line with assumptions of the homogenization theory presented in Sec. 2.1, the following source is assumed

$$\mathbf{j}_{\text{ext}} = \bar{J}_{\text{ext}} \exp(ikx)\hat{\mathbf{y}}, \tag{5.4}$$

I.e. $\mathbf{k} = k\hat{\mathbf{x}}$. The wave equation thus becomes

$$\frac{\partial^2 e(x)}{\partial x^2} + \frac{\omega^2}{c^2}\varepsilon(x)e(x) = -i\omega\mu_0 j_{\text{ext}} \tag{5.5}$$

for which it can be shown that the solutions are Bloch-waves, owing to the periodicity of microscopic permittivity $\varepsilon(x)$ and the periodic (constant) source amplitude $\bar{J}_{\text{ext}}$. The wave equation may alternatively be solved within each layer where $\varepsilon(x)$ may be considered a constant equal to $\varepsilon_1 = n_1^2$ in layer 1, and $\varepsilon_2 = n_2^2$ in layer 2, and the field solutions can be expressed as a sum of right- and leftwards moving homogeneous solutions (subscript $+$ and $-$, respectively), and particular solutions (subscript p)

$$e_1(x) = e_{1+}\exp(ik_1x) + e_{1-}\exp(-ik_1x) + e_{p1}\exp(ikx), \tag{5.6a}$$

$$e_2(x) = e_{2+}\exp[ik_2(x-d_1)] + e_{2-}\exp[-ik_2(x-d_1)] + e_{p2}\exp[ik(x-d_1)], \tag{5.6b}$$

in layers 1 and 2, respectively, where

$$e_{p1} = \frac{i\omega\mu_0\bar{J}_{\text{ext}}}{k^2 - \frac{\omega^2}{c^2}\varepsilon_1}, \qquad e_{p2} = \frac{i\omega\mu_0\bar{J}_{\text{ext}}}{k^2 - \frac{\omega^2}{c^2}\varepsilon_2}\mathrm{e}^{ikd_1}. \tag{5.7}$$

For the homogeneous solutions one has $k_1 = n_1\omega/c$ and $k_2 = n_2\omega/c$ where ω is the frequency, whereas in the particular solutions k is the wavenumber of the source

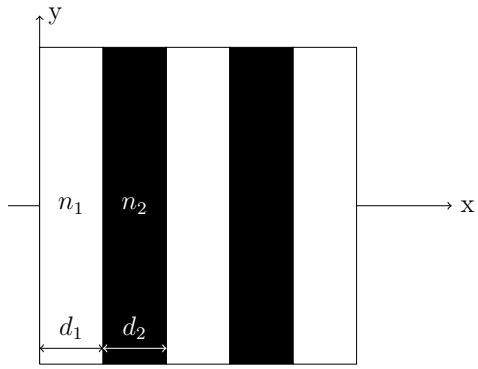

Figure 5.1: A section of a layered medium (1D metamaterial) which extends infinitely to the left and right

(5.4). According to the boundary conditions, $e(x)$ and $e'(x) \equiv \partial e(x)/\partial x = i\omega b(x)$ are continuous over the boundaries. This allows for the field solution to (5.5) to be expressed in terms of the matrix notation

$$\begin{bmatrix} e(x) \\ \frac{de(x)}{dx} \end{bmatrix} = \begin{cases} \mathbf{M_1}(x)\mathbf{E_0} + e_{p1}\mathbf{x_1}(x) \text{ for } 0 \le x \le d_1 \\ \\ \mathbf{M_2}(x-d_1)\mathbf{M_1}(d_1)\mathbf{E_0} + \mathbf{M_2}(x-d_1)e_{p1}\mathbf{x_1}(d_1) \\ \qquad\qquad + e_{p2}\mathbf{x_2}(x-d_1) \text{ for } d_1 \le x \le d_1+d_2, \end{cases} \tag{5.8}$$

where the matrices $\mathbf{M}_1, \mathbf{M}_2$ are expressed

$$\mathbf{M_{1,2}(x)} = \begin{bmatrix} \cos(k_{1,2}x) & \frac{1}{k_{1,2}}\sin(k_{1,2}x) \\ -k_{1,2}\sin(k_{1,2}x) & \cos(k_{1,2}x) \end{bmatrix}, \tag{5.9}$$

and the vectors $\mathbf{x}_1, \mathbf{x}_2$ are

$$\mathbf{x_{1,2}} = \begin{bmatrix} -\cos(k_{1,2}x) - i\frac{k}{k_{1,2}}\sin(k_{1,2}x) + \exp(ikx) \\ k_{1,2}\sin(k_{1,2}x) - ik\cos(k_{1,2}x) + ik\exp(ikx) \end{bmatrix}. \tag{5.10}$$

Here the vector $\mathbf{E}_0 = [e(0), de(0)/dx]^{\mathrm{T}}$ represents the field quantities at $x = 0$, and is solved from

$$\begin{bmatrix} e(d_1+d_2) \\ \frac{de(d_1+d_2)}{dx} \end{bmatrix} = \exp(ik[d_1+d_2])\mathbf{E}_0, \tag{5.11}$$

which follows from the Bloch property of the fields.

5.2.2 Eigenvalue problems

In the absence of a source, (5.5) constitutes an *eigenvalue problem* where $e(x)$ and ω represent the *eigenfunction* and *eigenvalue*, respectively. In literature, it is common to use eigenvalue problems as a means to obtain effective parameters for the system. A brief example will be considered here for comparison with *current-driven homogenization*, which shall be considered next.

When $\mathbf{j}_{\text{ext}} = 0$, the dispersion relation for the crystal is obtained from (5.11): Since then $e_{p1} = e_{p2} = 0$, a non-zero solution of $\mathbf{E}_0$ implies that

$$\det\Big[\mathbf{M}_2(d_2)\mathbf{M}_1(d_1) - \exp(ik[d_1 + d_2])\mathbf{I}\Big] = 0. \tag{5.12}$$

From this, one may find an explicit expression of the dispersion relation

$$\cos(kd) = \cos\left([n_1 d_1 + n_2 d_2]\frac{\omega}{c}\right) - \frac{(n_1 - n_2)^2}{2n_1 n_2}\sin\left(n_1 d_1 \frac{\omega}{c}\right)\sin\left(n_2 d_2 \frac{\omega}{c}\right). \tag{5.13}$$

I.e. a non-linear relationship between frequency ω and the Bloch wavenumber k. This relationship is obeyed under so-called *eigenmodal propagation*. One notices that with sufficient index contrast $n_2 - n_1$ the right hand side of (5.13) may for certain frequency bands become greater than unity, in which no real solutions of k exist. These are known as *photonic band gaps*. They occur for Bloch wavenumbers around $k(d_1 + d_2) = l\pi$, where l is a non-zero integer. At such wavelengths the structure in Fig. 5.1 should be considered a *photonic crystal*. In the context of homogenization, however, one is generally concerned with the metamaterial limit $k(d_1 + d_2) \ll 1$. In this limit an effective medium approach is appropriate, and one may then Taylor-expand the cosine and sine functions of (5.13) to obtain an expression for the effective refractive index $n \equiv ck/\omega$

$$n^2 = \frac{\varepsilon_1 d_1 + \varepsilon_2 d_2}{d_1 + d_2}. \tag{5.14}$$

5.2.3 Current-driven homogenization

Introducing the source (5.4) means that the dispersion relation (5.13) no longer holds. This implies that the parameters ω and k may be chosen independently of each other through the choice of the source (5.4), and propagation is *non-eigenmodal*. Homogenization of such *current driven* systems allows for a more general determination of the effective parameters of the system, in the sense that $\epsilon(\omega, \mathbf{k})$ and $\mu(\omega, \mathbf{k})$ can be determined for any pair of $(\omega, \mathbf{k})$ and not only those that fulfill (5.13).

In order to gain some intuition, the limit $\omega \to 0$ with fixed k shall be considered for which simple analytical expressions can be obtained. Then it can be shown

that the somewhat complicated solution of the field $\mathbf{e}(x)$ in (5.8) reduces to a plane wave of the form

$$\mathbf{e}(x) = \frac{i\omega\mu_0\bar{J}_{\text{ext}}}{k^2}\exp(ikx)\hat{\mathbf{y}}. \tag{5.15}$$

This solution can be understood from the wave equation (5.5): When $\omega \ll ck$ the term containing $\varepsilon(x)$ becomes negligible, meaning that the influence of the structure vanishes. The Landau-Lifshitz and Casimir effective permittivity functions $\epsilon(\omega, k)$ and $\epsilon'(\omega, k)$ according to (2.17) and (2.16a), respectively, shall now be derived for the field (5.15).

The macroscopic field $\mathbf{E}(x) \equiv \bar{E}\exp(ikx)\hat{\mathbf{y}}$ is by insertion of (5.15) into (2.6) simply equal to the microscopic field

$$E(x) = \frac{\exp(ikx)}{d_1+d_2}\int_0^{d_1+d_2} e(x)\exp(-ikx)\mathrm{d}x = \frac{i\omega\mu_0\bar{J}_{\text{ext}}}{k^2}\exp(ikx). \tag{5.16}$$

The microscopic field (5.15) may therefore equivalently be expressed

$$\mathbf{e}(x) = \bar{E}\exp(ikx)\hat{\mathbf{y}}, \tag{5.17}$$

which shall hereafter be done for brevity. One may express the microscopic polarization $\mathbf{p}(x) = \epsilon_0(\varepsilon(x)-1)\mathbf{e}(x)$. The averaged polarization $\langle\mathbf{p}\rangle$ is then

$$\begin{aligned}\langle p\rangle &= \frac{\exp(ikx)}{d_1+d_2}\int_0^{d_1+d_2}\epsilon_0(\varepsilon(x)-1)\bar{E}\mathrm{d}x \\ &= \frac{\epsilon_0\exp(ikx)\bar{E}}{d_1+d_2}\Big[d_1(\varepsilon_1-1)+d_2(\varepsilon_2-1)\Big].\end{aligned} \tag{5.18}$$

From (2.17) one thus has

$$\begin{aligned}\epsilon(0,k) &= 1+\frac{\langle p\rangle}{\epsilon_0 E}, \\ &= 1+\frac{1}{d_1+d_2}\Big[d_1(\varepsilon_1-1)+d_2(\varepsilon_2-1)\Big], \\ &= \frac{\varepsilon_1 d_1+\varepsilon_2 d_2}{d_1+d_2}.\end{aligned} \tag{5.19}$$

Thus the Landau-Lifshitz parameter for $\omega \to 0$ and fixed k becomes identical with the eigenmodal result (5.14).

In order to solve for the Casimir permittivity (2.16a), one must determine the polarization density according to (2.13a). Inserting for (5.15) gives

$$\begin{aligned} P &= \frac{\exp(ikx)\epsilon_0\bar{E}}{d_1+d_2}\left[(\varepsilon_1-1)\int_0^{d_1}\exp(ikx)\mathrm{d}x + (\varepsilon_2-1)\int_{d_1}^{d_1+d_2}\exp(ikx)\mathrm{d}x\right] \\ &= \frac{\exp(ikx)\epsilon_0\bar{E}}{ik(d_1+d_2)}\left[(\varepsilon_1-1)\Big(\exp(ikd_1)-1\Big) + (\varepsilon_2-1)\exp(ikd_1)\Big(\exp(ikd_2)-1\Big)\right] \\ &\overset{k(d_1+d_2)\ll 1}{=} \frac{\exp(ikx)\epsilon_0\bar{E}}{ik(d_1+d_2)}\left[(\varepsilon_1-1)ikd_1 + (\varepsilon_2-1)(1+ikd_1)ikd_2\right] \end{aligned} \tag{5.20}$$

From (2.16a) one therefore has

$$\begin{aligned} \epsilon'(0,k) &= 1+\frac{P}{\epsilon_0 E} \\ &\overset{k(d_1+d_2)\ll 1}{=} \frac{\varepsilon_1 d_1+\varepsilon_2 d_2}{d_1+d_2} + O(k). \end{aligned} \tag{5.21}$$

This becomes identical with the eigenmodal result (5.14) in the limit $k \to 0$.

The Casimir permeability (2.16b) can be expressed through

$$1-\frac{1}{\mu'} = \frac{\mu_0\omega M}{kE}, \tag{5.22}$$

where (2.8a) has been used to replace B. Unless the term $M/E \to 0$ as $O(k)$, or faster, one obtains $\mu' \to 0$ in (5.22) as $k \to 0$. Due to the dependence of the magnetization density M on the choice of coordinate origin by (2.13b), it turns out that it is possible to achieve $M/E \to 0$ as $O(k)$ for the 1D system of Fig. 5.1 by shifting the origin of the coordinate system. Considering (2.13b) where the coordinate origin is shifted by Δx

$$\frac{M}{E} = -\frac{i\omega\epsilon_0}{2(d_1+d_2)}\int_{-\Delta x}^{d_1+d_2-\Delta x} x[\varepsilon(x)-1]\exp(ikx)\mathrm{d}x, \tag{5.23}$$

one observes that if the exponential in the integrand is expanded, the integral may be expressed as two terms

$$\int_{-\Delta x}^{d_1+d_2-\Delta x} x[\varepsilon(x)-1]\mathrm{d}x + ik\int_{-\Delta x}^{d_1+d_2-\Delta x} x^2[\varepsilon(x)-1]\mathrm{d}x. \tag{5.24}$$

If the shift Δx is chosen in such a way that the first term is zero, then $M/E \to 0$ as $O(k)$ and a finite value of μ' results. Solving the first integral in (5.24) reveals that this is achieved if

$$\Delta x = \frac{(\varepsilon_1 - 1)d_1^2 + d_2(\varepsilon_2 - 1)(2d_1 + d_2)}{2(\varepsilon_1 - 1)d_1 + 2(\varepsilon_2 - 1)d_2}. \tag{5.25}$$

This reduces to points of inversion symmetry for the following particular choices of material parameters ε_1 and ε_2

$$\Delta x = \begin{cases} d_1/2 & \text{if } \varepsilon_2 = 1, \\ d_1 + d_2/2 & \text{if } \varepsilon_1 = 1. \end{cases} \tag{5.26}$$

Note that introducing the shift Δx in the coordinate origin also influences the value of the Casimir permittivity $\epsilon'(\omega, k)$ in accordance with (5.2). It turns out that the shift (5.25) is the same shift obtained from (5.3), i.e. the shift necessary to remove any first order k dependence of $\epsilon'(\omega, k)$, thus making the parameter more local. Given the dependence of the Casimir parameters on the coordinate origin, it seems reasonable that the coordinate origin should be chosen so as to ensure localized parameters, if possible, when operating with the Casimir formulation. Eq. (5.25) however seems to suggest that it is not generally possible to identify such suitable coordinate points on the basis of symmetry arguments, since Δx is not restricted to points of symmetry for general choices of ε_1 and ε_2.

The shift Δx may be interpreted as redistributing averaged current between P and M, and therefore between $\epsilon'(\omega, k)$ and $\mu'(\omega, k)$: From (2.12a) it is seen that $\langle \mathbf{j} \rangle = -i\omega \langle \mathbf{p} \rangle$ is invariant to any coordinate shift, making it clear from (2.12b) that any change in $\mathbf{M}$ must be balanced by a change in $\mathbf{P}$, $\mathbf{Q}$ and $\mathbf{R}$. The Landau-Lifshitz permittivity $\epsilon(\omega, \mathbf{k})$, however, is independent of the choice of coordinate origin, due to the invariance of $\langle \mathbf{p} \rangle$ and $\mathbf{E}$ by (2.6) to any coordinate shift.

5.3 Passivity in a spatially dispersive metamaterial

Negative imaginary parts of the permittivity and permeability are often interpreted as the presence of gain in a medium [43]. In the presence of spatial dispersion, however, it is not always this simple. This shall now be shown in terms of the treatments given in [43, Chapter 80] and [38, chapter 6.7], which here are generalized to spatially dispersive systems including a plane wave source. The macroscopic Maxwell's equations (2.8) may be expressed in terms of the decomposition of the Landau-Lifshitz parameter $\epsilon(\omega, \mathbf{k})$ into two parameters ϵ and μ by (2.19) as follows

$$i\mathbf{k} \times \mathbf{E} = i\omega \mathbf{B}, \tag{5.27a}$$

$$i\mathbf{k} \times \mathbf{H} = -i\omega \mathbf{D} + \bar{\mathbf{J}}_{\text{ext}} \mathrm{e}^{i\mathbf{k} \cdot \mathbf{r}}, \tag{5.27b}$$

where $\mu_0\mu\mathbf{H} = \mathbf{B}$ and $\epsilon_0\epsilon\mathbf{E} = \mathbf{D}$. Note that it is assumed that *all* electromagnetic effects are included in ϵ and μ (i.e. multipole terms $\mathbf{Q}$ and $\mathbf{R}$ from the expansion (2.12b) either are included or are negligible). Equations (5.27) may be considered to be the Fourier transforms of corresponding space and time domain counterparts given by

$$\nabla \times \boldsymbol{\mathcal{E}} = -\frac{\partial \boldsymbol{\mathcal{B}}}{\partial t}, \tag{5.28a}$$

$$\nabla \times \boldsymbol{\mathcal{H}} = \frac{\partial \boldsymbol{\mathcal{D}}}{\partial t} + \boldsymbol{\mathcal{J}}_{\text{ext}}. \tag{5.28b}$$

The relationship between $\boldsymbol{\mathcal{D}}$ and $\boldsymbol{\mathcal{E}}$, and $\boldsymbol{\mathcal{B}}$ and $\boldsymbol{\mathcal{H}}$ is generally non-local in both space and time. The following equation is found

$$-\nabla \cdot (\boldsymbol{\mathcal{E}} \times \boldsymbol{\mathcal{H}}) = \boldsymbol{\mathcal{E}} \cdot \boldsymbol{\mathcal{J}}_{\text{ext}} + \boldsymbol{\mathcal{E}} \cdot \frac{\partial \boldsymbol{\mathcal{D}}}{\partial t} + \boldsymbol{\mathcal{H}} \cdot \frac{\partial \boldsymbol{\mathcal{B}}}{\partial t}. \tag{5.29}$$

The left hand side of this equation is usually expressed in terms of the Poynting vector $\boldsymbol{\mathcal{S}} = \boldsymbol{\mathcal{E}} \times \boldsymbol{\mathcal{H}}$, however, as shall be now shown the interpretation of the Poynting vector is not straightforward in this case. Equations (5.28) correspond with a description in which all induced current is considered to be *bound*, whereas it is often usual to distinguish between *bound* and *free* currents, $\boldsymbol{\mathcal{J}}_{\text{b}}$ and $\boldsymbol{\mathcal{J}}_{\text{f}}$ respectively. The Maxwell-Ampère equation may then be expressed

$$\nabla \times \boldsymbol{\mathcal{H}}' = \boldsymbol{\mathcal{J}}_{\text{ext}} + \boldsymbol{\mathcal{J}}_{\text{f}} + \frac{\partial \boldsymbol{\mathcal{D}}'}{\partial t}, \tag{5.30}$$

in which the fields $\boldsymbol{\mathcal{H}}' = \boldsymbol{\mathcal{B}}/\mu_0 - \boldsymbol{\mathcal{M}}'$ and $\boldsymbol{\mathcal{D}}' = \epsilon_0\boldsymbol{\mathcal{E}} + \boldsymbol{\mathcal{P}}'$ are different from $\boldsymbol{\mathcal{H}} = \boldsymbol{\mathcal{B}}/\mu_0 - \boldsymbol{\mathcal{M}}$ and $\boldsymbol{\mathcal{D}} = \epsilon_0\boldsymbol{\mathcal{E}} + \boldsymbol{\mathcal{P}}$, respectively, but the fields $\boldsymbol{\mathcal{B}}$ and $\boldsymbol{\mathcal{E}}$ are left unchanged. The following relation is found

$$-\nabla \cdot (\boldsymbol{\mathcal{E}} \times \boldsymbol{\mathcal{H}}') = \boldsymbol{\mathcal{E}} \cdot (\boldsymbol{\mathcal{J}}_{\text{ext}} + \boldsymbol{\mathcal{J}}_{\text{f}}) + \boldsymbol{\mathcal{E}} \cdot \frac{\partial \boldsymbol{\mathcal{D}}'}{\partial t} + \boldsymbol{\mathcal{H}}' \cdot \frac{\partial \boldsymbol{\mathcal{B}}}{\partial t}. \tag{5.31}$$

It is clear that the corresponding Poynting vector $\boldsymbol{\mathcal{S}}' = \boldsymbol{\mathcal{E}} \times \boldsymbol{\mathcal{H}}'$ is generally different from $\boldsymbol{\mathcal{S}} = \boldsymbol{\mathcal{E}} \times \boldsymbol{\mathcal{H}}$. It is therefore not evident how the usual interpretation of the Poynting vector as energy flux density of the fields relate to these quantities, since they seem to change depending on the arbitrary division into bound and free currents. This complication can be bypassed by noting that the term $\boldsymbol{\mathcal{E}} \cdot \boldsymbol{\mathcal{J}}_{\text{f}}$ in (5.31) can be expressed

$$\boldsymbol{\mathcal{E}} \cdot \boldsymbol{\mathcal{J}}_{\text{f}} = -\nabla \cdot (\boldsymbol{\mathcal{E}} \times \Delta\boldsymbol{\mathcal{M}}) + \boldsymbol{\mathcal{E}} \cdot \frac{\partial \Delta\boldsymbol{\mathcal{P}}}{\partial t} - \Delta\boldsymbol{\mathcal{M}} \frac{\partial \boldsymbol{\mathcal{B}}}{\partial t}, \tag{5.32}$$

where $\Delta\boldsymbol{\mathcal{P}} = \boldsymbol{\mathcal{P}} - \boldsymbol{\mathcal{P}}'$ and $\Delta\boldsymbol{\mathcal{M}} = \boldsymbol{\mathcal{M}} - \boldsymbol{\mathcal{M}}'$. Insertion of this into (5.31) reveals that the difference between $\boldsymbol{\mathcal{S}}$ and $\boldsymbol{\mathcal{S}}'$ amounts to the term $-\nabla \cdot (\boldsymbol{\mathcal{E}} \times \Delta\boldsymbol{\mathcal{M}})$. This

is a flux-term which vanishes by the divergence theorem when Eqs. (5.29) and (5.31) is integrated over all time and space. Doing so, the following term

$$\int \mathcal{E} \cdot \mathcal{J}_{\text{ext}} \mathrm{d}t\mathrm{d}^3r, \tag{5.33}$$

represents the total work by the source. Since all media to some extent are dissipative [43], $\int -\nabla \cdot \mathcal{S} \mathrm{d}t\mathrm{d}^3r = 0$ by the divergence theorem because the propagating energy away from the localized source must tend to zero in an infinitely extended medium. Hence (5.33) must balance with

$$\int \left(\boldsymbol{\mathcal{E}} \cdot \frac{\partial \mathcal{D}}{\partial t} + \boldsymbol{\mathcal{H}} \cdot \frac{\partial \mathcal{B}}{\partial t} \right) \mathrm{d}t\mathrm{d}^3r, \tag{5.34}$$

which then represents the total work of moving charges and altering the fields. By convention that work performed by the system is positive, it follows that (5.34) must be positive for a passive system. By expressing the fields in (5.34) through Fourier-transforms of the $(\omega, \mathbf{k})$-space fields $\mathbf{E}(\omega, \mathbf{k})$, $\mathbf{D}(\omega, \mathbf{k})$, $\mathbf{H}(\omega, \mathbf{k})$, and $\mathbf{B}(\omega, \mathbf{k})$ one may express

$$\int \int \mathcal{E}_i \frac{\partial \mathcal{D}_i}{\partial t} \mathrm{d}t\mathrm{d}^3r = \int \omega \epsilon''_{ij} (E'_i E'_j + E''_i E''_j) \mathrm{d}\omega\mathrm{d}^3k, \tag{5.35}$$

where $\epsilon''_{ij} = \operatorname{Im} \epsilon_0 \epsilon_{ij}$, $E'_i = \operatorname{Re} E_i$ and $E''_i = \operatorname{Im} E_i$, as well as an analogous expression for the second term in the integrand of (5.34). The passivity condition thus becomes

$$\operatorname{Im} \epsilon_0 (\epsilon)_{ij} (E'_i E'_j + E''_i E''_j) + \operatorname{Im} \mu_0 (\mu)_{ij} (H'_i H'_j + H''_i H''_j) > 0. \tag{5.36}$$

For the 1D layered metamaterial considered in Sec. 5.2, this condition becomes the familiar

$$\operatorname{Im} \epsilon_0 \epsilon |E|^2 + \operatorname{Im} \mu_0 \mu |H|^2 > 0. \tag{5.37}$$

At first glance (5.37) may seem to suggest that both $\operatorname{Im} \epsilon > 0$ and $\operatorname{Im} \mu > 0$ in a passive medium; as in the case of non-spatially dispersive media, where $|E|$ and $|H|$ independently can be made arbitrarily small [43]. However, since in the spatially dispersive periodic metamaterial we have $B = kE/\omega$ by (2.8a) we may re-write (5.37) as

$$\left[\operatorname{Im} \epsilon_0 \epsilon + \frac{k^2 \mu_0}{\omega^2} \frac{\operatorname{Im} \mu}{\mu_0^2 |\mu|} \right] |E|^2 > 0, \tag{5.38a}$$

$$\Rightarrow \operatorname{Im} \left[\epsilon + \frac{k^2 c^2}{\omega^2} \left(1 - \frac{1}{\mu} \right) \right] > 0, \tag{5.38b}$$

$$\Rightarrow \operatorname{Im} \epsilon(\omega, \mathbf{k}) > 0, \tag{5.38c}$$

where we have used (2.19) in arriving to the last line. From (5.38b) it is clear that it for instance is possible to have $\operatorname{Im}\mu < 0$ in a passive medium, given that $\operatorname{Im}\epsilon$ is sufficiently positive [74].

This derivation has assumed that the parameters ϵ and μ represent the decomposition of the Landau-Lifshitz parameter $\epsilon(\omega, \mathbf{k})$ by (2.19). However, note that if $\mathbf{Q}$ and $\mathbf{R}$ can be considered negligible in the multipole expansion (2.12b) then the Casimir parameters ϵ' and μ' by (2.16) can be viewed as a special case of this decomposition, and the above discussion applies also to them.

Chapter 6

Summary and future work

The many novel dispersion characteristics offered by metamaterial structures, implies significant freedom in attainable dispersions compared with conventional media. It therefore becomes interesting to characterize the possibilities and limitations of the effective parameters in metamaterials. The papers of this thesis contribute in various ways to do so along the lines of causality and homogenization theory.

Paper 1 concerns itself with the amount of loss or gain in negative index media. While it is shown that negative indices $n < 0$ are compatible with arbitrarily low loss in passive media, the necessity of attaining sufficient complex phase $\arg(n)$ means that significant loss or gain will generally be present in the dispersion of metamaterials. Papers 2 and 3 demonstrate how any causal dispersion function can be approximated as a superposition of Lorentzian resonances, to any precision. Paper 2 does so by outlining the conditions under which a Lorentzian superposition χ_Γ converges to a target susceptibility χ under the L^2-norm, while Paper 3, a conference paper, extends this analysis by showing more fundamentally how the result is obtained directly from Cauchy's integral theorem for analytic functions. This result carries both theoretical and practical implications. Theoretically, the typical textbook treatment on dispersion, relying on Lorentz-resonators, can be interpreted to cover all causal response functions. With regards to practical implications, expressing a desired dispersion as a Lorentzian superposition offers a possible route towards finding a possible structure of realization (i.e. an inverse-homogenization procedure) in terms of metamaterial structures which yield Lorentzian resonances. This latter aspect has been emphasized in Paper 3. Paper 4 addresses the fact that certain effective parameter functions found in literature do not obey standard Kramers-Kronig relations. Indeed, this may be interpreted as a relaxation of the dispersion constraints which apply to conventional media. For instance it is argued that the permeability function for Pendry's famous array of split-ring cylinders has the dispersion of an active medium, despite being

passive. The additional dispersion freedom of a metamaterial is characterized by formulating generalized Kramers-Kronig relations, which take this freedom into account. Papers 5 and 6 are concerned with the consequences of spatial dispersion on the effective parameters. Paper 5 demonstrates that certain higher order multipole terms, above the electrical quadrupole, are generally as important as the magnetic dipole and electrical quadrupole terms when second order spatially dispersive effects are considered (e.g. magnetism). This despite the fact that the magnetic dipole and electrical quadrupole terms are of a lower order, and are therefore generally larger in value. Paper 6 shows how spatial dispersion may explain the occurrence of diamagnetism in causal, passive media. It is argued that spatially dispersive media may have analytic permeability functions which do not tend to unity for high frequencies and fixed wave number k, which explains that it is possible to have a positive imaginary part Im $\mu(\omega) > 0$ for all frequencies, and simultaneously $\mu(0) < 1$. This is a general result, not limited to metamaterials, although metamaterial examples of permeability functions which do not tend to unity at high frequency for fixed wave numbers are given.

Based on the variation of the topics covered above, there exist several lines of inquiry for further work. Regarding the most recent work on spatial dispersion (Papers 5 & 6), the next step should be to attempt to translate the effect of the higher order terms into transmission- and reflection coefficients. This will help to get a more direct appreciation of the importance that the higher order terms play in homogenization. However, obtaining these coefficients involves finding Fresnel-equations for non-local parameters, which is a subject matter of its own. Another interesting question is related to the arbitrariness by which the electromagnetic properties are divided into parameters ϵ and μ. In particular, one may imagine a number of physically reasonable definitions of the permeability μ. An investigation of the different properties of different permeability-definitions is therefore of interest. This thesis has also shown in Sec. 5.2.3 that the Casimir parameters depend on the choice of coordinates, and that the optimum coordinates towards obtaining local parameters do not seem to generally relate to symmetry properties of the system. As it is generally desirable to obtain local parameters, a fruitful topic is to investigate further the conditions under which the Casimir parameter become local, and if there are any guiding principles that can be used to ensure this.

With regards to the work on relaxed dispersion constraints for metamaterials (Paper 4), it will be interesting to examine further examples of practical use. A potentially interesting case could be the reduction of *overall* scattering in invisibility cloaks. In the recent review article by Alù et al. [59], a section titled *Do cloaked objects scatter less?* assesses that although an invisibility cloak suppresses scattering within a narrow bandwidth, the cloak simultaneously increases scattering

outside of this bandwidth. Over all frequencies the net contribution of the cloak is therefore to increase scattering. This assessment is based on the assumption that the static electric susceptibility is always positive for passive media, due to the conventional Kramers-Kronig relation

$$\chi(0) = \mathrm{Re}[\epsilon(0) - 1] = \frac{2}{\pi} \int_0^\infty \frac{\mathrm{Im}\epsilon(x)}{x} \mathrm{d}x. \tag{6.1}$$

However, as has been discussed in Sec. 2.4, there exist metamaterials in literature which display plasma-response susceptibilities $\chi(0) < 0$ [46, 47]. The Kramers-Kronig relations which describe these systems must take into account poles at $\omega = 0$, as can be found by deriving Kramers-Kronig relations for the quantity $\omega\chi$ following the derivation in [75]. It could be interesting to see if the relaxed dispersion constraints represented by such Kramers-Kronig relations can have any relevance towards reducing the global scattering in invisibility cloaks. A final suggestion for further work, is to investigate the possibility of developing a systematic inverse-homogenization procedure based on the findings of Papers 2 & 3. That is, rather than find the effective parameters of a given structure, find the needed structure for a desired dispersion. For instance, given the possibility of approximating any causal function as a superposition of Lorentzian resonance functions, it is in principle possible to express this superposition in terms of a circuit equivalent. Circuit equivalents in turn can offer a pragmatic means towards finding a corresponding structure (e.g. [50] which realizes an acoustic cloak by a circuit equivalent). It would be interesting to investigate whether a systematic algorithm for such inverse-homogenization could be developed.

Chapter 7

Contribution in papers

This section lists the papers of this thesis, and describes my contribution to each of them. Their numbering follows chronological order and corresponds to the numbering used elsewhere in this thesis. The publications are categorized according to *Journal publications* and *Conference publications* below.

Journal Publications

Paper 1

Christopher A. Dirdal and Johannes Skaar, *Negative refraction in causal media by evaluating polar paths for rational functions*, J. Opt. Soc. Am. B Vol. 30 No. 2 February 2013.

The analysis of section 4 and of the response displayed in Fig. 9 are primarily my own work, utilizing the method of polar paths and rational functions outlined in the previous sections to which I contributed significantly. I wrote the manuscript except the introduction and appendix, made the plots, figures and calculations therein, and participated in the review process.

Paper 2

Christopher A. Dirdal and Johannes Skaar, *Superpositions of Lorentzians as the class of causal functions*, Phys. Rev. A 88, 033834 (2013).

The initial idea of using superpositions of Lorentzian response functions to approximate *arbitrary* functions was an innovation of mine, inspired by the earlier work of Johannes in which such a superposition had been used to obtain a response function that achieves negative refraction with arbitrary small amounts of loss. Under the supervision and suggestions of Johannes, I produced the proofs of delta-convergence (appendix A) and the L^2-convergence (appendix B), although the

latter relies on the Riemann sum error derived by Johannes (Sec. IV B.1). The L^2 proof also relies on a δ-approximation of Sec. IV B.2, of which was proposed by me, and made rigorous with the help of Johannes.

I wrote the manuscript and produced the examples in which known dispersions from Johannes' earlier work were approximated by sums of Lorentzian response functions. I was the corresponding author under the review process.

Paper 4

Christopher A. Dirdal, Tarjei Bondevik, and Johannes Skaar, *Relaxed dispersion constraints and metamaterial effective parameters with physical meaning for all frequencies*, Phys. Rev. B 91, 134102 (2015).

I have been significantly involved in the development of the ideas and the derivation of the theory. I have performed the simulations, written the manuscript and been the corresponding author through the review process.

Paper 5

Christopher A. Dirdal, Hans Olaf Hågenvik, Haakon Aamot Haave, and Johannes Skaar, *Higher order terms in metamaterial homogenization*, submitted for journal publication.

I have been significantly involved in the development of the ideas and the derivation of the theory, together with Hågenvik and Skaar. I discovered the significance of the higher order term R. I performed the 1D simulations, while assisting Haakon in the 2D simulations. I wrote the manuscript and I am currently the corresponding author in the review process.

Paper 6

Christopher A. Dirdal and Johannes Skaar, *Diamagnetism and the dispersion of the magnetic permeability*, submitted for journal publication.

I contributed to the original idea of the article, supplied the calculation of the permeability function for the split ring cylinder metamaterial at high frequencies, performed the 1D simulations and contributed significantly in the analyticity proof of μ^{-1} in the appendix. The main ideas were developed by Johannes, who also wrote the manuscript and is the corresponding author in the review process.

Conference publications

Paper 3

Christopher A. Dirdal and Johannes Skaar, *Superposing Lorentzian resonance functions towards engineering target responses*, Proceedings of META'14 Singapore, The 5th International Conference on Metamaterials, Photonic Crystals and Plasmonics, ISBN 978-2-9545460-4-9.

In relation to journal paper 2 on the same topic, the novelty value of this article lies (i) in the derivation of the fundamental superposition equation directly from Cauchy's Integral Formula, instead of relying on the proof of delta-convergence of the imaginary part of a Lorentzian function, and (ii) in a greater emphasis on the possibility of superposing Lorentzian response functions for dispersion engineering. Building on an idea of Johannes which had not been pursued further during our work on the journal paper, I proposed the basic outline for the derivation of (i). Subsequently Johannes contributed to simplify the derivation to the form presented in the conference paper. The dispersion engineering perspective (ii) is primarily my work.

Bibliography

[1] John Brown, "Artificial dielectrics having refractive indices less than unity," Proceedings of the IEE-Part IV: Institution Monographs **100**, 51–62 (1953)

[2] RN Bracewell *et al.*, "Analogues of an ionized medium," Wireless Engineer **31**, 320–326 (1954)

[3] Walter Rotman, "Plasma simulation by artificial dielectrics and parallel-plate media," IRE Transactions on Antennas and Propagation **10**, 82–95 (1962)

[4] J Van Kranendonk and JE Sipe, "V foundations of the macroscopic electromagnetic theory of dielectric media," Progress in Optics **15**, 245–350 (1977)

[5] Vladimir M. Shalaev, "Electromagnetic properties of small-particle composites," Physics Reports **272**, 61 – 137 (1996), ISSN 0370-1573, `http://www.sciencedirect.com/science/article/pii/0370157395000763`

[6] Ari H Sihvola, *Electromagnetic mixing formulas and applications*, 47 (Iet, 1999)

[7] Graeme W Milton, "The theory of composites (cambridge monographs on applied and computational mathematics)," (2002)

[8] Sergei Tretyakov, *Analytical modeling in applied electromagnetics* (Artech House, 2003)

[9] Jagadis Chunder Bose, "On the rotation of plane of polarisation of electric waves by a twisted structure," Proceedings of the Royal Society of London **63**, 146–152 (1898)

[10] JC Maxwell Garnett, "Colours in metal glasses and in metallic films.[abstract]," Proceedings of the Royal Society of London, 443–445(1904)

[11] J.B. Pendry, A.J. Holden, D.J. Robbins, and W.J. Stewart, "Magnetism from conductors and enhanced nonlinear phenomena," Microwave Theory and Techniques, IEEE Transactions on **47**, 2075–2084 (Nov 1999), ISSN 0018-9480

[12] S.A. Schelkunoff and H.T. Friis, *Antennas: theory and practice*, Applied mathematics series (Wiley, 1952) https://books.google.no/books?id=SvOvDAEACAAJ

[13] AN Lagarkov, VN Semenenko, VA Chistyaev, DE Ryabov, SA Tretyakov, and CR Simovski, "Resonance properties of bi-helix media at microwaves," Electromagnetics **17**, 213–237 (1997)

[14] AP Vinogradov, AN Lagarkov, and VE Romanenko, "Some peculiarities in the resonant behavior of the bi-helix microstructure," Electromagnetics **17**, 239–249 (1997)

[15] G. W. Milton, "Analytic materials," Proceedings of the Royal Society of London Series A **472**, 20160613 (Nov. 2016), arXiv:1610.06059 [physics.class-ph]

[16] D. R. Smith, Willie J. Padilla, D. C. Vier, S. C. Nemat-Nasser, and S. Schultz, "Composite medium with simultaneously negative permeability and permittivity," Phys. Rev. Lett. **84**, 4184–4187 (May 2000), http://link.aps.org/doi/10.1103/PhysRevLett.84.4184

[17] Richard A Shelby, David R Smith, and Seldon Schultz, "Experimental verification of a negative index of refraction," science **292**, 77–79 (2001)

[18] J. B. Pendry, A. J. Holden, W. J. Stewart, and I. Youngs, "Extremely low frequency plasmons in metallic mesostructures," Phys. Rev. Lett. **76**, 4773–4776 (Jun 1996), http://link.aps.org/doi/10.1103/PhysRevLett.76.4773

[19] J B Pendry, A J Holden, D J Robbins, and W J Stewart, "Low frequency plasmons in thin-wire structures," Journal of Physics: Condensed Matter **10**, 4785 (1998), http://stacks.iop.org/0953-8984/10/i=22/a=007

[20] L. I. Mandelstam, "Lectures on optics, relativity theory and quantum mechanics," in *Nauka Eds., Moscow, 1972. 440 pp. Under the revision by corresponding member of the Academy of Sciences of U.S.S.R. S.M. Rytov. (Russian Title: Lektsii po optike, teorii otnositel'nosti i kvantovoi mehanike)* (1971)

[21] Vladimir M Agranovich and Yu N Gartstein, "Spatial dispersion and negative refraction of light," Physics-Uspekhi **49**, 1029 (2006)

[22] Viktor G Veselago, "The electrodynamics of substances with simultaneously negative values of ϵ and μ," Soviet physics uspekhi **10**, 509 (1968)

[23] Horace Lamb, "On group-velocity," Proceedings of the London Mathematical Society **2**, 473–479 (1904)

[24] Arthur Schuster, *An introduction to the theory of optics* (E. Arnold, 1904)

[25] J. B. Pendry, "Negative refraction makes a perfect lens," Phys. Rev. Lett. **85**, 3966–3969 (Oct 2000), http://link.aps.org/doi/10.1103/PhysRevLett.85.3966

[26] Ulf Leonhardt, "Optical conformal mapping," Science **312**, 1777–1780 (2006)

[27] J. B. Pendry, D. Schurig, and D. R. Smith, "Controlling electromagnetic fields," Science **312**, 1780–1782 (2006), ISSN 0036-8075, http://science.sciencemag.org/content/312/5781/1780.full.pdf, http://science.sciencemag.org/content/312/5781/1780

[28] D. Schurig, J. B. Pendry, and D. R. Smith, "Calculation of material properties and ray tracing in transformation media," Opt. Express **14**, 9794–9804 (Oct 2006), http://www.opticsexpress.org/abstract.cfm?URI=oe-14-21-9794

[29] D. Schurig, J. J. Mock, B. J. Justice, S. A. Cummer, J. B. Pendry, A. F. Starr, and D. R. Smith, "Metamaterial electromagnetic cloak at microwave frequencies," Science **314**, 977–980 (2006), ISSN 0036-8075, http://science.sciencemag.org/content/314/5801/977.full.pdf, http://science.sciencemag.org/content/314/5801/977

[30] Nanfang Yu, Patrice Genevet, Mikhail A. Kats, Francesco Aieta, Jean-Philippe Tetienne, Federico Capasso, and Zeno Gaburro, "Light propagation with phase discontinuities: Generalized laws of reflection and refraction," Science **334**, 333–337 (2011), ISSN 0036-8075, http://science.sciencemag.org/content/334/6054/333.full.pdf, http://science.sciencemag.org/content/334/6054/333

[31] Xingjie Ni, Alexander V Kildishev, and Vladimir M Shalaev, "Metasurface holograms for visible light," Nature communications **4** (2013)

[32] Ulf Leonhardt and Thomas G. Philbin, "Transformation optics and the geometry of light," Prog. Opt. **53**, 69–152 (2009)

[33] B. Reznik, "Origin of the thermal radiation in a solid-state analogue of a black hole," Phys. Rev. D **62**, 044044 (Jul 2000), http://link.aps.org/doi/10.1103/PhysRevD.62.044044

[34] U. Leonhardt and P. Piwnicki, "Optics of nonuniformly moving media," Phys. Rev. A **60**, 4301–4312 (Dec 1999), http://link.aps.org/doi/10.1103/PhysRevA.60.4301

[35] Ulf Leonhardt and Thomas G Philbin, "General relativity in electrical engineering," New Journal of Physics **8**, 247 (2006)

[36] Igor I Smolyaninov and Evgenii E Narimanov, "Metric signature transitions in optical metamaterials," Physical Review Letters **105**, 067402 (2010)

[37] G. Russakoff, "A derivation of the macroscopic maxwell equations," Am. J. Phys. **38**, 1188 (1970)

[38] John David Jackson, *Classical electrodynamics*, 3rd ed. (Wiley, New York, 1999) ISBN 9780471309321, http://cdsweb.cern.ch/record/490457

[39] M. G. Silveirinha, "Nonlocal homogenization theory of structured materials," in *Metamaterials Handbook: Theory and phenomena of metamaterials*, edited by Filippo Capolino (CRC Press, London, 2009) Chap. 10

[40] Mário G. Silveirinha, "Metamaterial homogenization approach with application to the characterization of microstructured composites with negative parameters," Phys. Rev. B **75**, 115104 (Mar 2007), http://link.aps.org/doi/10.1103/PhysRevB.75.115104

[41] Andrea Alù, "First-principles homogenization theory for periodic metamaterials," Phys. Rev. B **84**, 075153 (Aug 2011), http://link.aps.org/doi/10.1103/PhysRevB.84.075153

[42] J. van Bladel, *Electromagnetic fields* (IEEE Press, Hoobken, NJ, 2007)

[43] L. D. Landau, L. P. Pitaevskii, and E. M. Lifshitz, *Electrodynamics of Continuous Media, Second Edition: Volume 8 (Course of Theoretical Physics)*, 2nd ed. (Butterworth-Heinemann, 1984)

[44] V.M. Agranovich and V.L. Ginzburg, *Crystal optics with spatial dispersion, and excitons:*, Springer series in solid-state sciences (Springer-Verlag, 1984) ISBN 9783540115205, https://books.google.no/books?id=ckksAAAAYAAJ

[45] C. A. Dirdal, H. Olaf Hågenvik, H. Aamot Haave, and J. Skaar, "Higher order terms and locality in metamaterial homogenization," ArXiv e-prints(Jan. 2017), arXiv:1701.01708 [physics.optics]

[46] Mário G. Silveirinha, "Nonlocal homogenization model for a periodic array of ϵ-negative rods," Phys. Rev. E **73**, 046612 (Apr 2006), http://link.aps.org/doi/10.1103/PhysRevE.73.046612

[47] G.V. Eleftheriades, A.K. Iyer, and P.C. Kremer, "Planar negative refractive index media using periodically l-c loaded transmission lines," Microwave Theory and Techniques, IEEE Transactions on **50**, 2702–2712 (Dec 2002), ISSN 0018-9480

[48] Omar Wing, *Classical Circuit Theory* (Springer US, 2009)

[49] *Superposing Lorentzian resonance functions towards engineering target responses* (Meta'14 Singapore Proceedings, 2015)

[50] Shu Zhang, Chunguang Xia, and Nicholas Fang, "Broadband acoustic cloak for ultrasound waves," Phys. Rev. Lett. **106**, 024301 (Jan 2011), `http://link.aps.org/doi/10.1103/PhysRevLett.106.024301`

[51] Christopher A Dirdal, Tarjei Bondevik, and Johannes Skaar, "Relaxed dispersion constraints and metamaterial effective parameters with physical meaning for all frequencies," Physical Review B **91**, 134102 (2015)

[52] Johannes Skaar, "Fresnel equations and the refractive index of active media," Phys. Rev. E **73**, 026605 (Feb 2006), `http://link.aps.org/doi/10.1103/PhysRevE.73.026605`

[53] Hans Olaf Hågenvik, Markus E Malema, and Johannes Skaar, "Fourier theory of linear gain media," Physical Review A **91**, 043826 (2015)

[54] Marte P. Hatlo Andresen, Aleksander V. Skaldebø, Magnus W. Haakestad, Harald E. Krogstad, and Johannes Skaar, "Effect of gain saturation in a gain compensated perfect lens," J. Opt. Soc. Am. B **27**, 1610–1616 (Aug 2010), `http://josab.osa.org/abstract.cfm?URI=josab-27-8-1610`

[55] Robert Schittny, Muamer Kadic, Sebastien Guenneau, and Martin Wegener, "Experiments on transformation thermodynamics: Molding the flow of heat," Phys. Rev. Lett. **110**, 195901 (May 2013), `http://link.aps.org/doi/10.1103/PhysRevLett.110.195901`

[56] Jensen Li and JB Pendry, "Hiding under the carpet: a new strategy for cloaking," Physical review letters **101**, 203901 (2008)

[57] Bogdan-Ioan Popa, Lucian Zigoneanu, and Steven A. Cummer, "Experimental acoustic ground cloak in air," Phys. Rev. Lett. **106**, 253901 (Jun 2011), `http://link.aps.org/doi/10.1103/PhysRevLett.106.253901`

[58] Robert Schittny, Muamer Kadic, Tiemo Bückmann, and Martin Wegener, "Invisibility cloaking in a diffusive light scattering medium," Science **345**, 427–429 (2014), ISSN 0036-8075,

http://science.sciencemag.org/content/345/6195/427.full.pdf, http://science.sciencemag.org/content/345/6195/427

[59] Romain Fleury, Francesco Monticone, and Andrea Alù, "Invisibility and cloaking: Origins, present, and future perspectives," Phys. Rev. Applied **4**, 037001 (Sep 2015), http://link.aps.org/doi/10.1103/PhysRevApplied.4.037001

[60] Alison Gopnik, "Scientific thinking in young children: Theoretical advances, empirical research, and policy implications," Science **337**, 1623–1627 (2012)

[61] E. Kreyszig, *Advanced Engineering Mathematics* (John Wiley & Sons, 2010) ISBN 9780470458365, https://books.google.ie/books?id=UnN8DpXI74EC

[62] Eric W. Weisstein, ""analytic function" from mathworld–a wolfram web resource," http://mathworld.wolfram.com/AnalyticFunction.html

[63] O. V. Dolgov, D. A. Kirzhnits, and E. G. Maksimov, "On an admissible sign of the static dielectric function of matter," Rev. Mod. Phys. **53**, 81–93 (Jan 1981), http://link.aps.org/doi/10.1103/RevModPhys.53.81

[64] L.D. Landau, J.S. Bell, J. Kearsley, L.P. Pitaevskii, E.M. Lifshitz, and J.B. Sykes, *Electrodynamics of Continuous Media* (Elsevier Science, 1984) ISBN 9781483293752, http://www.google.no/books?id=jedbAwAAQBAJ

[65] Andrea Alù, Arthur D. Yaghjian, Robert A. Shore, and Mário G. Silveirinha, "Causality relations in the homogenization of metamaterials," Phys. Rev. B **84**, 054305 (Aug 2011), http://link.aps.org/doi/10.1103/PhysRevB.84.054305

[66] Christopher A. Dirdal and Johannes Skaar, "Superpositions of lorentzians as the class of causal functions," Phys. Rev. A **88**, 033834 (Sep 2013), http://link.aps.org/doi/10.1103/PhysRevA.88.033834

[67] Jon A Schuller, Rashid Zia, Thomas Taubner, and Mark L Brongersma, "Dielectric metamaterials based on electric and magnetic resonances of silicon carbide particles," Physical review letters **99**, 107401 (2007)

[68] A. P. Vinogradov and A. V. Aivazyan, "Scaling theory for homogenization of the maxwell equations," Phys. Rev. E **60**, 987–993 (Jul 1999), http://link.aps.org/doi/10.1103/PhysRevE.60.987

[69] David J. Cho, Feng Wang, Xiang Zhang, and Y. Ron Shen, "Contribution of the electric quadrupole resonance in optical metamaterials," Phys. Rev. B

78, 121101 (Sep 2008), http://link.aps.org/doi/10.1103/PhysRevB.78.121101

[70] J. Petschulat, C. Menzel, A. Chipouline, C. Rockstuhl, A. Tünnermann, F. Lederer, and T. Pertsch, "Multipole approach to metamaterials," Phys. Rev. A **78**, 043811 (Oct 2008), http://link.aps.org/doi/10.1103/PhysRevA.78.043811

[71] Constantin Simovski and Sergei Tretyakov, "Material parameters and field energy in reciprocal composite media," in *Metamaterials Handbook: Theory and Phenomena of Metamaterials*, edited by Filippo Capolino (CRC Press, London, 2009) Chap. 2, ISBN 978-1-4200-5425-5

[72] Andrea Alù, "Restoring the physical meaning of metamaterial constitutive parameters," Phys. Rev. B **83**, 081102 (Feb 2011), http://link.aps.org/doi/10.1103/PhysRevB.83.081102

[73] Arthur D Yaghjian, Andrea Alù, and Mário G Silveirinha, "Homogenization of spatially dispersive metamaterial arrays in terms of generalized electric and magnetic polarizations," Photonics and Nanostructures-Fundamentals and Applications **11**, 374–396 (2013)

[74] L. P. Pitaevskii, "On analytical properties of the diamagnetic permeability in the presence of the spatial dispersion," International Journal of Quantum Chemistry **112**, 2998–3001 (2012), ISSN 1097-461X, http://dx.doi.org/10.1002/qua.24185

[75] Mário G. Silveirinha, "Examining the validity of kramers-kronig relations for the magnetic permeability," Phys. Rev. B **83**, 165119 (Apr 2011), http://link.aps.org/doi/10.1103/PhysRevB.83.165119

Paper I

Negative refraction in causal media by evaluating polar paths for rational functions

Published in Journal of the Optical Society of America B

Is not included due to copyright

Paper II

Superpositions of Lorentzians as the class of causal functions

Published in Physical Review A

DOI: 10.1103/PhysRevA.88.033834

Superpositions of Lorentzians as the class of causal functions

Christopher A. Dirdal and Johannes Skaar*

Department of Electronics and Telecommunications, Norwegian University of Science and Technology, NO-7491 Trondheim, Norway

(Received 22 June 2013; published 20 September 2013)

We prove that all functions obeying the Kramers-Kronig relations can be approximated as superpositions of Lorentzian functions, to any precision. As a result, the typical textbook analysis of dielectric dispersion response functions in terms of Lorentzians may be viewed as encompassing the whole class of causal functions. A further consequence is that Lorentzian resonances may be viewed as possible building blocks for engineering any desired metamaterial response, for example, by use of split-ring resonators of different parameters. Two example functions, far from typical Lorentzian resonance behavior, are expressed in terms of Lorentzian superpositions: a steep dispersion medium that achieves large negative susceptibility with arbitrarily low loss or gain and an optimal realization of a perfect lens over a bandwidth. Error bounds are derived for the approximation.

DOI: 10.1103/PhysRevA.88.033834 PACS number(s): 42.70.−a, 81.05.Xj, 78.67.Pt, 41.20.−q

I. INTRODUCTION

When considering the dispersion of dielectric media, textbook analysis typically concerns itself with sums of Lorentzian functions [1–3]. While it can be argued that sums of Lorentzians are physically reasonable response functions for a number of systems, in particular those described by the Lorentz model [1–4], it is well known that the only restrictions imposed by causality are those implied by the Kramers-Kronig relations [1–3,5]. In light of the variety in the electromagnetic responses offered by natural media and metamaterials, it is of interest to consider the possible gap between the function space consisting of sums of Lorentzians and the space consisting of functions satisfying the Kramers-Kronig relations. To this end, it is here demonstrated that any complex-valued function satisfying the Kramers-Kronig relations can be approximated as a superposition of Lorentzian functions, to any desired accuracy. It therefore follows that the typical analysis of causal behavior in terms of Lorentzian functions for dielectric or magnetic media encompasses the whole space of functions obeying the Kramers-Kronig relations. These results therefore serve to strengthen the generality of the typical analysis of causality.

Two examples where the response functions do not resemble typical Lorentzian resonance behavior will here be expressed as Lorentzian superpositions in order to demonstrate the above findings. Section III A considers a steep response function which results in a susceptibility $\mathrm{Re}\chi(\omega) \leqslant -2$ for arbitrarily low loss or gain [6,7], and Sec. III B considers an optimal perfect lens response over a bandwidth [8]. The precisions in both superpositions are shown to become arbitrarily accurate as the parameters are chosen appropriately. A natural consequence of such superpositioning is that Lorentzian functions can be viewed as general building blocks for engineering causal susceptibilities in metamaterials. Considering that systems such as the pioneering split-ring resonator implementation [9] and others [4,10–12] have demonstrated several ways of realizing and tailoring Lorentzian responses, this may prove to be a promising approach.

While the literature has so far tended to focus on specific metamaterial designs, a number of desired responses have emerged for which few physically viable systems are known [4,6,8]. One such set of response functions consists of those that have desired dispersion properties [4], which are relevant for applications such as dispersion compensation [11,13], couplers [14], antenna design [15,16], filters [17], broadband absorption [18], and broadband ultralow-refractive-index media [19]. This leads to the following question: Starting with a target response, how can one realize an approximation of it? Towards this end, it has been proposed to use layered metamaterials [20]. Our article considers more generally the possibility of engineering artificial response functions through the realization of a finite number of Lorentzians, a method which may be applicable to a variety of metamaterials. On this note Sec. IV A addresses how Lorentzian superposition responses can be realized through the arrangement of split-ring cylinders of different radii and material parameters. Finally, Sec. IV B derives an estimate of the error that arises when a target response is approximated by a finite sum of Lorentzian functions.

The following section will set out the main results of this article while leaving detailed calculations to later sections and appendices.

II. SUPERPOSITION OF LORENTZIANS

A Lorentzian function can be written in the form

$$L(\omega) = \frac{2}{\pi}\frac{\omega_0}{\omega_0^2 - \omega^2 - i\omega\Gamma}, \tag{1}$$

where $\omega_0 \geqslant 0$ is the resonance frequency, ω is the frequency, and $\Gamma \geqslant 0$ is the bandwidth. It may be demonstrated that the imaginary part of $L(\omega)$ approaches a sum of two Dirac δ functions with odd symmetry as

$$\mathrm{Im}L(\omega) \longrightarrow \delta(\omega - \omega_0) - \delta(\omega + \omega_0) \tag{2}$$

when $\Gamma \to 0$. This is exemplified in Fig. 1 and proven in Appendix A. A goal function, such as the imaginary part of a susceptibility $\mathrm{Im}\chi(\omega)$, may therefore be expressed as

$$\mathrm{Im}\chi(\omega) = \frac{2}{\pi}\lim_{\Gamma\to 0}\int_0^\infty \mathrm{Im}\chi(\omega_0)\mathrm{Im}\left\{\frac{\omega_0}{\omega_0^2 - \omega^2 - i\omega\Gamma}\right\}d\omega_0. \tag{3}$$

*johannes.skaar@ntnu.no

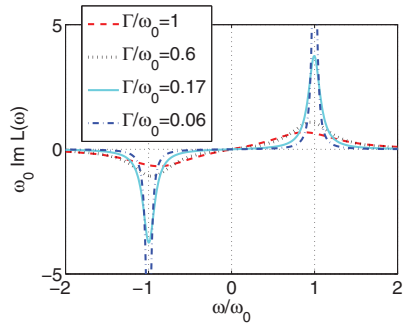

FIG. 1. (Color online) Imaginary part of the Lorentzian function $L(\omega)$ (1) approaching a sum of two δ functions for decreasing values of Γ.

This limit integral expression may then be approximated by the sum

$$\mathrm{Im}\chi(\omega) \approx \frac{2}{\pi}\sum_{m=0}^{M-1}\mathrm{Im}\chi(\omega_m)\mathrm{Im}\left\{\frac{\omega_m\Delta}{\omega_m^2-\omega^2-i\omega\Gamma}\right\}, \quad (4)$$

where $\omega_m = \Delta/2 + m\Delta$, Δ is the resolution along the integration variable ω_0, and M is a large integer. This sum, which shall be designated $\mathrm{Im}\chi_{\Gamma,\Delta}(\omega)$, can be made to approximate $\mathrm{Im}\chi(\omega)$ to any desired degree of accuracy. More precisely, the involved error is shown to converge to zero in both L^∞ and L^2:

$$\|\mathrm{Im}\chi_{\Gamma,\Delta}(\omega) - \mathrm{Im}\chi(\omega)\| \to 0 \quad \text{as} \quad \Gamma \to 0, \quad (5)$$

where Δ is chosen suitably, e.g., $\Delta = \Gamma/\sqrt{M}$ (Appendix B). Considering (4), one may define a function

$$\chi_{\Gamma,\Delta}(\omega) = \frac{2}{\pi}\sum_{m=0}^{M-1}\mathrm{Im}\chi(\omega_m)\frac{\omega_m\Delta}{\omega_m^2-\omega^2-i\omega\Gamma}, \quad (6)$$

where now both real and imaginary parts of the Lorentzians are superposed. From the Kramers-Kronig relations one then has

$$-\mathscr{H}[\mathrm{Im}\chi(\omega) - \mathrm{Im}\chi_{\Gamma,\Delta}(\omega)] = \mathrm{Re}\chi(\omega) - \mathrm{Re}\chi_{\Gamma,\Delta}(\omega), \quad (7)$$

where $\mathscr{H}$ represents the Hilbert transform and $\mathrm{Re}\chi_{\Delta,\Gamma}(\omega)$ is the real part of (6). Since the Hilbert transform preserves the energy, or L^2 norm, it therefore follows that

$$\|\mathrm{Re}\chi_{\Gamma,\Delta}(\omega) - \mathrm{Re}\chi(\omega)\| \to 0 \quad \text{as} \quad \Gamma \to 0 \quad (8)$$

when given (5). On the basis of this, it follows that

$$\chi(\omega) \approx \chi_{\Gamma,\Delta}(\omega), \quad (9)$$

meaning that both the real and imaginary parts of $\chi(\omega)$ are approximated by the summation of Lorentzians. The terms are weighted by $\mathrm{Im}\chi(\omega)$ at each resonance frequency according to (6). Equation (9) combined with (6) therefore becomes the central result of this article. Noting that (6) is itself a Riemann sum, it follows that the limit integral expression

$$\chi(\omega) = \frac{2}{\pi}\lim_{\Gamma\to 0}\int_0^\infty \mathrm{Im}\chi(\omega_0)\frac{\omega_0}{\omega_0^2-\omega^2-i\omega\Gamma}d\omega_0 \quad (10)$$

may be written on the basis of the preceding arguments. Equations (6) and (10) therefore approximate the space of functions satisfying the Kramers-Kronig relations as superpositions of Lorentzians to any degree of precision. In the following section this result shall be demonstrated with two examples.

The validity of (5) requires that $\chi(\omega)$ is analytic on the real axis (not only in the upper half plane). In the event of nonanalytic susceptibilities on the real axis, however, all problems are bypassed by instead evaluating $\mathrm{Im}\chi(\omega)$ along the line $\omega + i\delta$ before approximating by Lorentzians. Here $\delta > 0$ is an arbitrarily small parameter. Since $\chi(\omega)$ is analytic there, (5) is valid. Furthermore, since $\mathrm{Im}\chi(\omega + i\delta) \to \mathrm{Im}\chi(\omega)$ almost everywhere as $\delta \to 0$, the representation can be made arbitrarily accurate, meaning that any $\mathrm{Im}\chi(\omega)$ can be approximated to any precision. In fact, this also includes media that do not strictly obey the Kramers-Kronig relationship due to singularities on the real axis, such as the ideal plasma.

III. EXAMPLES

A. Susceptibility where $\mathrm{Re}\chi \leqslant -2$ through a steep response

It is possible to achieve $\mathrm{Re}\chi \leqslant -2$ with arbitrarily low loss or gain [6,7]. Consider a susceptibility with

$$\mathrm{Im}\chi(\omega) = \begin{cases} \omega/\omega_c & \text{if} \quad |\omega| < \omega_c, \\ 0 & \text{elsewhere.} \end{cases} \quad (11)$$

As a result of the infinite steepness at $\omega = \omega_c$, the Hilbert transform gives $\mathrm{Re}\chi(\omega_c) = -\infty$. It follows that it is possible to scale (11) to make the magnitude $|\mathrm{Im}\chi(\omega)|$ arbitrarily small for all frequencies while maintaining $\mathrm{Re}\chi(\omega_c) \leqslant -2$.

Inserting (11) as $\mathrm{Im}\chi(\omega_0)$ in (10) gives

$$\chi(\omega) = \frac{2}{\pi}\lim_{\Gamma\to 0}\left[1 - i\sqrt{\left(\frac{\omega}{\omega_c}\right)^2 + i\frac{\omega\Gamma}{\omega_c^2}} \times \arctan\left(\frac{1}{i\sqrt{(\omega/\omega_c)^2 + i\left(\omega\Gamma/\omega_c^2\right)}}\right)\right]. \quad (12)$$

One can show that as $\Gamma \to 0$, the imaginary part of (12) yields (11). Using (6), one may likewise approximate the response (11) as a finite sum of Lorentzians: Fig. 2(a) plots the real and imaginary parts of $\chi(\omega)$ as approximated by both sum and integral expressions, (6) and (10), respectively, where Γ/ω_c is chosen equal to 0.1, 0.01, and 0.001 and where $\Delta = \Gamma/2$. One observes that the sum (6) falls in line with the integral result (12). For $\Gamma/\omega_c = 0.001$ one has $\mathrm{Re}\chi(\omega_c) = -2$. As $\Gamma \to 0$, meaning that the drop in the approximated curves of $\mathrm{Im}\chi(\omega)$ at $\omega/\omega_c = 1$ becomes infinitely steep, one has that $\mathrm{Re}\chi(\omega_c) \to -\infty$ in both cases.

The imaginary parts for one out of every five Lorentzians in the sum (6) are displayed in Fig. 2(b) for $\Gamma/\omega_c = 0.01$.

B. Perfect lens

It has been shown in [8,21] that the resolution r for a metamaterial lens of thickness d surrounded by vacuum is

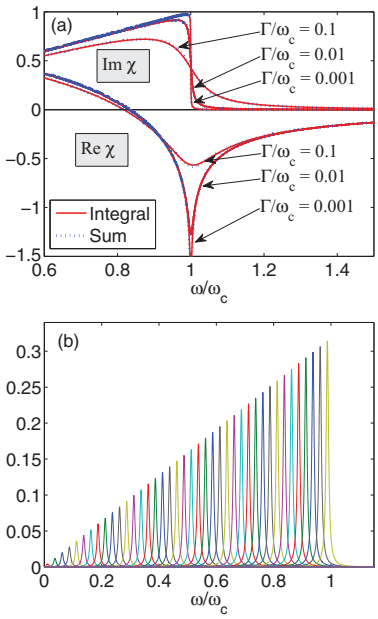

FIG. 2. (Color online) (a) Real and imaginary parts of the integral and sum approximations by (10) and (6), respectively. The drops above the frequency axis correspond to the imaginary parts, whereas the dips below the frequency axis correspond to the real parts. (b) The imaginary parts for one out of every five Lorentzians in the sum (6), where $\Gamma/\omega_c = 0.01$ and $\Delta/\omega_c = 0.005$.

given by

$$r = \frac{-2\pi d}{\ln[|\chi(\omega) + 2|/2]} \tag{13}$$

for a one-dimensional image object. Here, $\chi(\omega)$ is either the electric or magnetic susceptibility depending on the polarization of the incident field. It follows that any perfect lens should approximate $|\chi + 2| = 0$ over a bandwidth. A system approaching such an optimal is displayed in Fig. 3(a) [8]. A strong Lorentzian resonance has been placed at $\omega = \omega_L$ (out of view), and a weak, slowly varying function has been placed around $\omega/\omega_L \sim 2.05$. Taking the absolute value gives the black dashed curve in Fig. 3(c), which reveals that $|\chi + 2|$ remains small and constant over the bandwidth.

Figure 3(b) represents the sum (6) of Lorentzians over the interval $\omega/\omega_L \in (1.95, 2.15)$, where $\Gamma/\omega_L = 0.001$ and $\Delta/\omega_L = 5 \times 10^{-4}$. The goal function for (6) has been found by subtracting the strong resonance situated at $\omega = \omega_L$ from $\mathrm{Im}\chi(\omega)$ in Fig. 3(a). The strong resonance was then later added to the sum of Lorentzians (6). The absolute value of the real and imaginary parts in Fig. 3(b) corresponds to the green solid curve in Fig. 3(c), which neatly follows the dashed curve of $|\chi + 2|$. Also observed in Fig. 3(c) is the corresponding result of another sum approximation where the Lorentzians are wider. Hence one observes the trend that as Γ decreases the Lorentzian sum (6) approximates $|\chi + 2|$ increasingly well.

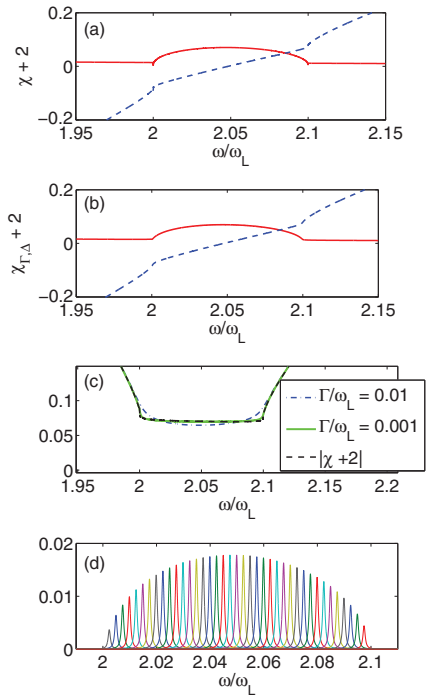

FIG. 3. (Color online) Perfect lens. (a) System designed to minimize $|\chi + 2|$ over a bandwidth. The red solid curve represents $\mathrm{Im}\chi$, whereas the blue dashed curve represents $\mathrm{Re}\chi$. (b) Sum (6) of Lorentzians over the interval $\omega/\omega_L \in (1.95, 2.15)$, where $\Gamma/\omega_L = 0.001$ and $\Delta/\omega_L = 5 \times 10^{-4}$. (c) Plot of $|\chi + 2|$ for both the system in (a) (dashed black curve) and two sum approximations. The solid curve corresponds to the absolute value of (b). (d) The imaginary parts for one out of every five Lorentzians in the sum displayed in (b).

Figure 3(d) displays the imaginary parts for one out of every five Lorentzians in the sum corresponding to Fig. 3(b).

IV. LORENTZIAN FUNCTIONS AS BUILDING BLOCKS FOR TAILORING CAUSAL SUSCEPTIBILITIES

A. Tailoring responses in split-ring resonators

Sections III A and III B have demonstrated that useful responses which do not arise in any natural system can nevertheless be approximated as a superposition of ordinary Lorentzian resonances to any desired precision. Considering that Lorentzian resonances can be realized and tailored for both permittivities ϵ and permeabilities μ in numerous metamaterial realizations [4,9,10,12], this is of particular interest for the prospect of engineering desired metamaterial responses. For instance, in the case of an array of split-ring cylinders one may find for the effective permeability [9]

$$\mu_{\mathrm{eff}} - 1 = \frac{\omega^2 F}{\frac{2}{\pi^2 \mu_0 C r^3} - \omega^2 - i\omega\frac{2\rho}{r\mu_0}}, \tag{14}$$

where C is the capacitance per m^2 in the split-ring cylinder, r is its radius, ρ is the resistance per circumference-length ratio,

and F is the fractional volume of the unit cell occupied by the interior of the cylinder. For small bandwidths the presence of ω^2 in the numerator is not significant, and (14) approximates a Lorentzian response. By comparing it with (1) one may determine the Lorentzian parameters as

$$\omega_0^2 = \frac{2}{\pi^2 \mu_0 C r^3}, \tag{15}$$

$$\Gamma = \frac{2\rho}{r\mu_0}. \tag{16}$$

The resonator strength F is expressed as

$$F = \frac{\pi r^2}{a^2}, \tag{17}$$

where a is the dimension of the unit cell. Hence the resonance frequencies, widths, and strengths can be tailored by varying r, ρ, and C. It may be noted that split-ring cylinders display large resistivity in the optical regime, making it difficult to achieve narrow Lorentzian responses there. For this reason other systems, such as metamolecules of nanoparticles, have been proposed for optical purposes [12].

In order to realize a sum of Lorentzian resonances such as those leading to Figs. 2(b) and 3(d) by means of split-ring cylinders, one could propose to place different cylinders in each unit cell. The idea would be to realize and superpose a number of different Lorentzian resonances of the form (14) corresponding to different values of r, ρ, and C. The density of each type of split-ring cylinder can then be thought to give the appropriate resonance strength. However, as it is known that two dipoles in close vicinity influence each other's dipole moments, it is not intuitively clear that the total response will be as simple as a superposition of the individual responses. The remainder of this section will therefore be used to demonstrate this. Towards this end, the procedure outlined in [9] will be modified to calculate the effective permeability μ_{eff} of a split-ring cylinder metamaterial when every unit cell contains two split-ring cylinders of different radii (Fig. 4).

The effective permittivity μ_{eff} is expressed by finding the effective macroscopic fields B_{ave} and H_{ave} over the array from the corresponding actual fields B and H in each unit cell:

$$\mu_{\text{eff}} = B_{\text{ave}}/\mu_0 H_{\text{ave}}. \tag{18}$$

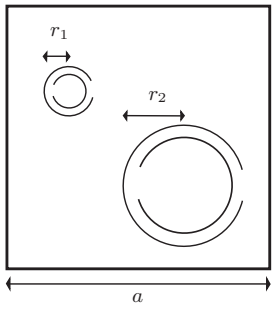

FIG. 4. Base of a unit cell with height l containing two different cylinders.

One may show that

$$B_{\text{ave}} = \mu_0 H_0, \tag{19}$$

$$H_{\text{ave}} = H_0 - \frac{1}{a^2}\left(\pi r_1^2 j_1 + \pi r_2^2 j_2\right), \tag{20}$$

where $j_{1,2}$ is the surface current per unit length along the circumference of the cylinders with radii r_1 and r_2, respectively. When finding an expression for the field inside each cylinder H_1 and H_2, (20) is used to express

$$H_{1,2} = H_{\text{ave}} + j_{1,2}. \tag{21}$$

Since both split-ring cylinders observe the same interaction field contained in H_{ave}, application of Faraday's law to each cylinder leads to two equations that may be solved individually for j_1 and j_2:

$$j_{1,2} = \frac{-H_{\text{ave}}}{1 + \frac{i2\rho_{1,2}}{\omega r_{1,2}\mu_0} - \frac{2}{\mu_0 \omega^2 \pi^2 r_{1,2}^3 C_{1,2}}}. \tag{22}$$

In order to evaluate (18), one may now rearrange (20) to find an expression for H_0 in terms of j_1 and j_2, for which one in turn can use (22) to find

$$\mu_{\text{eff}} - 1 = \sum_k \frac{\omega^2 F_k}{\frac{2}{\pi^2 \mu_0 C_k r_k^3} - \omega^2 - i\omega \frac{2\rho_k}{r_k \mu_0}}. \tag{23}$$

Here $k = \{1,2\}$ and $F_k = \pi r_k^2/a^2$ is the volume fraction occupied by each split-ring cylinder. By comparison with (14) one observes that the resulting $\mu_{\text{eff}} - 1$ here is simply the superposition of the individual split-ring cylinder responses as found in [9]. This comes as a consequence of the interaction field sensed by both split-ring cylinders being uniform. This description of the interaction is valid as long as the cylinders are long, for which the returning field lines at the end of each cylinder are spread uniformly over the unit cell.

Finally, the analysis presented here is easily generalized for unit cells with many different split-ring cylinders, for which (23) remains valid and k labels the different split-ring cylinders in the unit cell.

B. Error estimate

Towards the goal of engineering a desired response $\chi(\omega)$ by use of a finite number of Lorentzians with nonzero widths ($\Gamma > 0$), it is of interest to quantify the precision of such an approximation. An error estimate can be found by considering the combined error introduced in both the δ-function approximation (3) of $\text{Im}\chi(\omega)$ for finite Γ and the Riemann sum approximation (4) of the integral (3). The total error may therefore be bounded according to

$$\begin{aligned}|\text{Im}\chi(\omega) - \text{Im}\chi_{\Gamma,\Delta}(\omega)| \leqslant\ & |\text{Im}\chi_\Gamma(\omega) - \text{Im}\chi(\omega)| \\ & + |\text{Im}\chi_{\Gamma,\Delta}(\omega) - \text{Im}\chi_\Gamma(\omega)|,\end{aligned} \tag{24}$$

where $\text{Im}\chi_\Gamma(\omega)$ represents (3) without the limit and $\text{Im}\chi_{\Gamma,\Delta}(\omega)$ represents the sum (4). In what follows, bounds for the Riemann sum approximation error $|\text{Im}\chi_{\Gamma,\Delta}(\omega) - \text{Im}\chi_\Gamma(\omega)|$ and δ-convergence error $|\text{Im}\chi_\Gamma(\omega) - \text{Im}\chi(\omega)|$ shall be derived in turn.

1. Riemann sum approximation error

Defining $\omega_M = M\Delta$ and naming the integrand in (3) f_{int}, one may find an upper bound on the Riemann approximation error to be

$$\begin{aligned}|\text{Im}\chi_\Gamma(\omega) - \text{Im}\chi_{\Gamma,\Delta}(\omega)| &\leqslant \max|f''_{\text{int}}|\frac{\omega_M^3}{24M^2} + |\chi_{\text{err}}(\omega)| \\ &< |\text{Im}\chi(\omega)|\frac{\omega_M\Delta^2}{3\Gamma^3} \\ &\times\left[1 + O\left(\frac{\Gamma^2}{\omega^2}\right)\right] + |\chi_{\text{err}}(\omega)|,\end{aligned} \tag{25}$$

where

$$\chi_{\text{err}}(\omega) = \frac{2}{\pi}\int_{\omega_M}^{\infty}\text{Im}\chi(\omega_0)\text{Im}\left\{\frac{\omega_0}{\omega_0^2 - \omega^2 - i\omega\Gamma}\right\}d\omega_0. \tag{26}$$

In obtaining the last inequality in (25), we have used the fact that f''_{int} is dominated by the curvature of the Lorentzian for sufficiently small Γ. After some algebra one finds $|f''_{\text{int}}| \leqslant |\text{Im}\chi(\omega)|8/\Gamma^3[1 + O(\Gamma^2/\omega^2)]$ when assuming that $\Gamma/\omega \ll 1$. Note that (26) can be rewritten as

$$\begin{aligned}\chi_{\text{err}}(\omega) = \frac{2}{\pi}\int_0^{\infty}&\left[1 - \text{rect}\left(\frac{\omega_0}{\omega_M}\right)\right]\text{Im}\chi(\omega_0) \\ &\times\text{Im}\left\{\frac{\omega_0}{\omega_0^2 - \omega^2 - i\omega\Gamma}\right\}d\omega_0.\end{aligned} \tag{27}$$

By taking the limit $\Gamma \to 0$ this expression becomes of the form (3), and hence the definition of δ convergence can be used to find the limit of $\chi_{\text{err}}(\omega)$:

$$\lim_{\Gamma\to 0}\chi_{\text{err}}(\omega) = \left[1 - \text{rect}\left(\frac{\omega}{\omega_M}\right)\right]\text{Im}\chi(\omega). \tag{28}$$

It is observed that $|\chi_{\text{err}}(\omega)|$ vanishes as $\omega_M \to \infty$. For $\omega_M/\Gamma \gg 1$ the error involved in replacing $\chi_{\text{err}}(\omega)$ by its limiting value (28) becomes small. Therefore, for most goal functions $\text{Im}\chi(\omega)$, where the sum (6) covers the frequency interval of interest, the error described by $|\chi_{\text{err}}(\omega)|$ is roughly as small as $|\text{Im}\chi(\omega)|$ outside of this interval.

2. δ-convergence approximation error

The δ-convergence approximation error

$$\psi_{\text{err}}(\omega) = |\text{Im}\chi_\Gamma(\omega) - \text{Im}\chi(\omega)|, \tag{29}$$

which arises when using Lorentzians of finite width ($\Gamma > 0$) rather than δ functions in (3), will now be evaluated. Consider Fig. 5: The imaginary part of an arbitrary response $\chi(\omega)$ is to be approximated according to (3) with finite Γ, and the positive frequency peak of the imaginary part of a Lorentzian $\text{Im}L_+(\omega,\omega_0)$ is displayed. The Lorentzian (1) can be expanded in terms of partial fractions as

$$\frac{2}{\pi}\text{Im}\left\{\frac{\omega_0}{\omega_0^2 - \omega^2 - i\omega\Gamma}\right\} = \text{Im}L_+(\omega,\omega_0) - \text{Im}L_-(\omega,\omega_0), \tag{30}$$

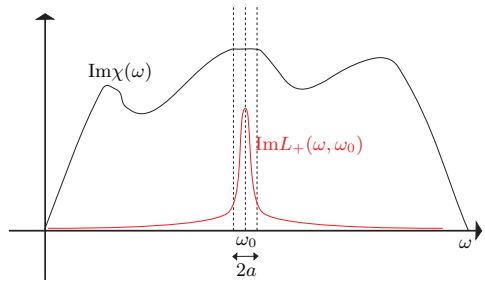

FIG. 5. (Color online) An arbitrary response $\text{Im}\chi(\omega)$ to be expressed as a superposition of finite-sized Lorentzians.

where $\text{Im}L_\pm(\omega,\omega_0)$ corresponds to positive and negative frequency peaks of the Lorentzian, respectively, according to

$$\begin{aligned}&\text{Im}L_\pm(\omega,\omega_0) \\ &= \frac{1}{\pi}\frac{1}{\sqrt{1 - (\Gamma/2\omega_0)^2}}\frac{\frac{1}{2}\Gamma}{[\omega \mp \omega_0\sqrt{1 - (\Gamma/2\omega_0)^2}\,]^2 + \left(\frac{\Gamma}{2}\right)^2}.\end{aligned} \tag{31}$$

Introducing (30) into (3) (without the limit) then allows the δ-convergence error $\psi_{\text{err}}(\omega)$ to be expressed as

$$\begin{aligned}\psi_{\text{err}}(\omega) &= \left|\int_{-\infty}^{\infty}\text{Im}\chi(\omega_0)\text{Im}L_+(\omega,\omega_0)d\omega_0 - \text{Im}\chi(\omega)\right| \\ &= \Bigg|\int_{-\infty}^{\infty}\underbrace{\text{Im}\chi\left(\omega_0\sqrt{1 + \frac{\Gamma^2}{4\omega_0^2}}\right)}_{=\text{Im}\chi_F(\omega_0)}F_\Gamma(\omega_0 - \omega)d\omega_0 \\ &\quad - \text{Im}\chi(\omega)\Bigg|.\end{aligned} \tag{32}$$

Here, by having made an appropriate substitution, it is observed in the last equality that the integral can be written in terms of the Lorentz-Cauchy function $F_\Gamma(\omega_0 - \omega)$:

$$F_\Gamma(\omega_0 - \omega) = \frac{1}{\pi}\frac{\frac{1}{2}\Gamma}{(\omega_0 - \omega)^2 + \left(\frac{\Gamma}{2}\right)^2}. \tag{33}$$

As a consequence of the substitution, a new function $\text{Im}\chi_F(\omega_0)$ is defined in (32) which essentially represents a shifted version of $\text{Im}\chi(\omega_0)$.

The integration interval in (32) may be divided into three intervals corresponding to the intervals designated in Fig. 5, which shall then be evaluated separately:

$$\begin{aligned}&\int_{-\infty}^{\infty}\text{Im}\chi_F(\omega_0)F_\Gamma(\omega_0 - \omega)d\omega_0 \\ &= \Bigg(\underbrace{\int_{-\infty}^{\omega-a}}_{A} + \underbrace{\int_{\omega-a}^{\omega+a}}_{B} + \underbrace{\int_{\omega+a}^{\infty}}_{C}\Bigg)\text{Im}\chi_F(\omega_0)F_\Gamma(\omega_0 - \omega)d\omega_0.\end{aligned} \tag{34}$$

Here the parameter a is, in principle, arbitrary, but can be thought to represent the region around $\omega = \omega_0$ where $\text{Im}\chi_F(\omega)$ is assumed to be Taylor expandable in the lowest orders. Evaluating integrals A and C in (34) together, an upper bound

on their sum may be found:

$$\max_{\omega'} |\mathrm{Im}\chi_F(\omega')| \left(\int_{-\infty}^{\omega-a} + \int_{\omega+a}^{\infty} \right) F_\Gamma(\omega_0 - \omega) d\omega_0 = \max_{\omega'} |\mathrm{Im}\chi(\omega')| \left[1 - \frac{2}{\pi} \arctan\left(\frac{2a}{\Gamma} \right) \right]. \quad (35)$$

Here the fact that $\max_{\omega'} |\mathrm{Im}\chi_F(\omega')| = \max_{\omega'} |\mathrm{Im}\chi(\omega')|$ has been used. One observes that as $\Gamma \ll a$ the arctangent term can be expanded, allowing (35) to be reexpressed as

$$\frac{\Gamma}{\pi a} \max_{\omega'} |\mathrm{Im}\chi(\omega')|, \quad (36)$$

which evidently converges to zero when $\Gamma \to 0$ as long as $\mathrm{Im}\chi(\omega)$ is bounded. In order to calculate integral B, $\mathrm{Im}\chi_F(\omega_0)$ is expanded around $\omega_0 = \omega$:

$$\mathrm{Im}\chi_F(\omega_0) = \mathrm{Im}\chi_F(\omega) + \mathrm{Im}\chi_F'(\omega)(\omega_0 - \omega) + \tfrac{1}{2}\mathrm{Im}\chi_F''(\omega)(\omega_0 - \omega)^2 + O[(\omega_0 - \omega)^3]. \quad (37)$$

Due to the parity when inserting this into integral B only even-order terms remain, giving

$$\int_{\omega-a}^{\omega+a} \mathrm{Im}\chi_F(\omega_0) F_\Gamma(\omega_0 - \omega) d\omega_0 = \frac{2}{\pi} \mathrm{Im}\chi_F(\omega) \arctan\left(\frac{2a}{\Gamma} \right) + \frac{\Gamma a}{2\pi} \mathrm{Im}\chi_F''(\omega) + O\left(\frac{\Gamma}{a} \right). \quad (38)$$

Only Γ terms to the first order have been kept in arriving at this expression. The term $O(\Gamma/a)$ corresponds to terms containing higher-order derivatives of $\mathrm{Im}\chi_F(\omega)$, which will be assumed to be negligible. In the event that there exist significant higher-order derivatives (e.g., as will be the case in Fig. 2 near the steep drop), one may keep more terms in going from (37) to (38) until the next even-ordered derivative is negligible. The same steps that follow hereafter may then be applied in order to find the relevant error estimate.

In order to arrive at an expression for $\psi_{\mathrm{err}}(\omega)$ in terms of the goal function $\mathrm{Im}\chi(\omega)$ and its derivatives, the shifted function $\mathrm{Im}\chi_F(\omega) = \mathrm{Im}\chi(\omega\sqrt{1 + \Gamma^2/4\omega^2})$ is expanded under the assumption that $\Gamma/\omega \ll 1$ and is then inserted for $\mathrm{Im}\chi_F(\omega)$ and its second derivative in (38). Expanding the arctangent under the assumption that $\Gamma \ll a$ permits further simplification. Combining the resulting expression with (36) yields an upper bound on the δ-convergence error:

$$\psi_{\mathrm{err}}(\omega) \leqslant \frac{\Gamma}{\pi} \left(\max_{\omega'} |\mathrm{Im}\chi(\omega')| \frac{2}{a} + |\mathrm{Im}\chi''(\omega)| \frac{a}{2} \right) + O(\Gamma^2), \quad (39)$$

where $O(\Gamma^2)$ arises after having expanded and replaced $\mathrm{Im}\chi_F(\omega)$ and its second derivative. Minimizing the upper bound with respect to a then gives

$$a^2 = \frac{4 \max_{\omega'} |\mathrm{Im}\chi(\omega')|}{|\mathrm{Im}\chi''(\omega)|}. \quad (40)$$

An inverse relationship between a^2 and $|\mathrm{Im}\chi''(\omega)|$ is intuitive given that a must be small when $\mathrm{Im}\chi(\omega)$ varies steeply.

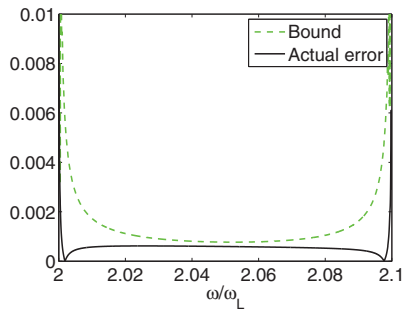

FIG. 6. (Color online) The error in approximating the perfect lens response described in Sec. III B with a Lorentzian superposition is shown to be bounded by (41).

Inserting (40) into (39) while neglecting $O(\Gamma^2)$ gives

$$\psi_{\mathrm{err}}(\omega) \leqslant \frac{2\Gamma}{\pi} (|\mathrm{Im}\chi''(\omega)| \max_{\omega'} |\mathrm{Im}\chi(\omega')|)^{\frac{1}{2}}. \quad (41)$$

Hence the δ-convergence error $\psi_{\mathrm{err}}(\omega)$ is proportional to $\Gamma\sqrt{|\mathrm{Im}\chi''(\omega)|}$ under the assumption that $\Gamma \ll a \propto 1/\sqrt{|\mathrm{Im}\chi''(\omega)|}$, the higher-order derivatives are negligible, and $\Gamma/\omega \ll 1$. Figure 6 shows (41) applied to the imaginary part of the perfect lens response displayed in Fig. 3(b), where one observes that the actual error (black curve) is bounded by (41) (dashed curve). The displayed error is actually taken to be the total error $|\mathrm{Im}\chi(\omega) - \mathrm{Im}\chi_{\Delta,\Gamma}(\omega)|$ of the superposition, rather than the difference between $\mathrm{Im}\chi(\omega)$ and $\mathrm{Im}\chi_\Gamma(\omega)$. However, here Δ/ω_L in the sum (6) has been reduced by a factor of 2 compared to that in Fig. 3(b) in order to reduce the significance of the Riemann sum error (25) in comparison to the δ-convergence approximation error (32).

V. CONCLUSION

It has been demonstrated that superpositions of Lorentzian functions are capable of approximating all complex-valued functions satisfying the Kramers-Kronig relations, to any desired precision. The typical textbook analysis of dielectric or magnetic dispersion response functions in terms of Lorentzians is thereby extended to cover the whole class of causal functions. The discussion started by approximating the imaginary part of an arbitrary susceptibility $\chi(\omega)$ by a superposition of imaginary parts of Lorentzian functions. The error $|\mathrm{Im}\chi(\omega) - \mathrm{Im}\chi_{\Gamma,\Delta}(\omega)|$ was then shown to become arbitrarily small as $\Gamma \to 0, \omega_M \to \infty$, and $\Delta = \Gamma^2/\omega_M$. Since this error was shown to vanish in L^2, it was known that $\mathrm{Re}\chi_{\Gamma,\Delta}(\omega) \to \mathrm{Re}\chi(\omega)$. From this the superposition $\chi_{\Gamma,\Delta}(\omega)$ was found, which approximates $\chi(\omega)$ to any desired precision.

The superposition $\chi_{\Gamma,\Delta}(\omega)$ has been demonstrated to reconstruct two response functions that obey the Kramers-Kronig relations while not resembling typical Lorentzian resonance behavior. The first response is known to lead to significant negative real values of the susceptibility $\chi(\omega)$ in a narrow bandwidth with arbitrarily low gain or loss, while the other response represents the optimal realization of a perfect lens on a bandwidth. These examples demonstrate the possibility of viewing Lorentzians as useful building blocks for

manufacturing desired responses that are not found in conventional materials. To this end, the ability to realize Lorentzian sums using split-ring cylinders with varying parameters was shown. In order to quantify the precision of a superposition approximation, error estimates have been derived.

APPENDIX A: δ CONVERGENCE OF LORENTZIANS

This section will prove (2) and, equivalently, (3). In doing so, observe that an implicit definition of the δ function is

$$\begin{aligned}\mathrm{Im}\chi(\omega) &= \int_{-\infty}^{\infty} \mathrm{Im}\chi(\omega_0)\delta(\omega_0-\omega)d\omega_0 \\ &= \int_0^{\infty} \mathrm{Im}\chi(\omega_0)[\delta(\omega_0-\omega)-\delta(\omega_0+\omega)]d\omega_0.\end{aligned} \tag{A1}$$

Note that the last line holds only insofar as the goal function obeys odd symmetry $\mathrm{Im}\chi(-\omega_0) = -\mathrm{Im}\chi(\omega_0)$. By inserting (30) into (3) and using the symmetry $L_-(\omega,-\omega_0) = L_+(\omega,\omega_0)$, one observes that the goal of this section becomes demonstrating that

$$\lim_{\Gamma\to 0}\int_{-\infty}^{\infty} \mathrm{Im}\chi(\omega_0)\mathrm{Im}L_+(\omega,\omega_0)d\omega_0 = \mathrm{Im}\chi(\omega). \tag{A2}$$

Inserting for $\mathrm{Im}L_+(\omega,\omega_0)$ in the integral and making the appropriate substitution lead to

$$\lim_{\Gamma\to 0}\frac{1}{\pi}\int_{-\infty}^{\infty}\frac{\mathrm{Im}\chi\left[\frac{\Gamma}{2}\sqrt{(2\omega/\Gamma-u)^2+1}\right]}{u^2+1}du. \tag{A3}$$

One may then move the limit inside the integral under the criteria of Lebesgue's dominated convergence theorem. As $\Gamma\to 0$, the function $\mathrm{Im}\chi[\frac{\Gamma}{2}\sqrt{(2\omega/\Gamma-u)^2+1}]$ converges pointwise to $\mathrm{Im}\chi(\omega)$. Furthermore, it is clear that an integrable function that bounds the integrand for all values of Γ exists under the condition that $\mathrm{Im}\chi(\omega)$ is bounded. Hence (A3) gives

$$\frac{1}{\pi}\mathrm{Im}\chi(\omega)\int_{-\infty}^{\infty}\frac{1}{u^2+1}du = \mathrm{Im}\chi(\omega), \tag{A4}$$

which concludes the proof.

APPENDIX B: L^2 CONVERGENCE

This section considers the conditions upon Γ, Δ, and ω_M needed in order to obtain the L^2 convergence expressed in (5). From the discussion in Sec. IV B, one may express

$$\begin{aligned}&|\mathrm{Im}\chi(\omega)-\mathrm{Im}\chi_{\Gamma,\Delta}(\omega)| \\ &\leqslant \left|\mathrm{Im}\chi(\omega)\frac{\omega_M\Delta^2}{3\Gamma^3}\left[1+O\left(\frac{\Gamma^2}{\omega^2}\right)\right]\right| && \text{(B1)} \\ &\quad+\left|\frac{2}{\pi}\int_{\omega_M}^{\infty}\mathrm{Im}\chi(\omega_0)\mathrm{Im}\left\{\frac{\omega_0}{\omega_0^2-\omega^2-i\omega\Gamma}\right\}d\omega_0\right| && \text{(B2)} \\ &\quad+\left|\left[\frac{2}{\pi}\arctan\left(\frac{2a}{\Gamma}\right)-1\right]\mathrm{Im}\chi(\omega)\right| && \text{(B3)} \\ &\quad+\left|\frac{\Gamma a}{2\pi}\mathrm{Im}\chi''(\omega)+O(\Gamma^2)\right| && \text{(B4)} \\ &\quad+\left|\left(\int_{-\infty}^{\omega-a}+\int_{\omega+a}^{\infty}\right)\mathrm{Im}\chi_F(\omega_0)F_\Gamma(\omega_0-\omega)d\omega_0\right|. && \text{(B5)}\end{aligned}$$

The Riemann sum error (25) is expressed through (B1) and (B2), and the δ-convergence error from (34) and (38) is expressed in (B3), (B4), and (B5). The term $O(\Gamma^2)$ in (B4) is included because $\mathrm{Im}\chi_F(\omega)$ and its second derivative have been expanded and replaced so as to express (38) in terms of $\mathrm{Im}\chi(\omega)$ and its second derivative.

The bound given by (B1)–(B5) has been derived under the assumption that $\omega \gg \Gamma$. Before proceeding to evaluating the L^2 norm by this bound, one must therefore demonstrate that $|\mathrm{Im}\chi(\omega)-\mathrm{Im}\chi_{\Gamma,\Delta}(\omega)|$ is bounded in a region $|\omega|\in(0,\beta)$ where $\beta\gg\Gamma$ [representing the region not accounted for by (B1)–(B5)], so that as $\Gamma\to 0$ and then $\beta\to 0$, it is known that the L^2 norm converges to zero also here. A detailed proof of this will not be given here, but its result can be understood by noting that (3), when without its limit, is bounded by an integral of $\mathrm{Im}L(\omega)$ on the interval $\omega_0\in(0,\infty)$ multiplied with $\max_{\omega'}|\mathrm{Im}\chi(\omega')|$. Since the integral is finite and $\chi(\omega)$ is analytic, it follows that (3) is bounded. Furthermore, since the sum (4) can be made arbitrarily close to (3), it is intuitive that it also remains bounded for all ω. Since $\mathrm{Im}\chi(\omega)$ and $\mathrm{Im}\chi_{\Gamma,\Delta}(\omega)$ are bounded, it follows that $|\mathrm{Im}\chi(\omega)-\mathrm{Im}\chi_{\Gamma,\Delta}(\omega)|$ is finite for all ω.

Proceeding now to evaluate the L^2 norm from (B1)–(B5), convergence for (B1) is achieved by setting $\Delta=\Gamma^2/\omega_M$ and taking the limit $\Gamma\to 0$ since $\mathrm{Im}\chi(\omega)$ is in L^2 [the presence of the term $O(\Gamma^2/\omega^2)$ will be discussed below]. The same convergence occurs in (B3) as $\Gamma\to 0$. The L^2 norm arising for (B4),

$$\frac{\Gamma a}{2\pi}\|\mathrm{Im}\chi''(\omega)\|, \tag{B6}$$

converges provided that $\mathrm{Im}\chi''(\omega)$ is in L^2. Since it, however, is conceivable for a function $\chi(\omega)$ in L^2 to have derivatives not in L^2, one may instead consider $\chi(\omega)$ along the line $\omega+i\delta$, where $\delta>0$ is an arbitrarily small parameter. One then finds through the Fourier transform

$$\begin{aligned}\chi(\omega+i\delta) &= \int_0^{\infty}x(t)e^{i(\omega+i\delta)}dt \\ &= \int_0^{\infty}[x(t)e^{-\delta t}]e^{i\omega t}dt,\end{aligned} \tag{B7}$$

given that $x(t)$ is the time-domain response associated with $\chi(\omega)$. Equation (B7) reveals that one may express

$$\begin{aligned}\chi(\omega+i\delta) &\xrightarrow{\mathscr{F}^{-1}} x(t)e^{-\delta t}, \\ \chi''(\omega+i\delta) &\xrightarrow{\mathscr{F}^{-1}} (it)^2x(t)e^{-\delta t}.\end{aligned} \tag{B8}$$

Since $x(t)$ is in L^2, one observes that $(it)^2x(t)e^{-\delta t}$ is in L^2 for $\delta>0$. Knowing that the Fourier transform preserves the L^2 norm, it follows that $\chi''(\omega+i\delta)$ is in L^2.

The terms $O(\Gamma^2/\omega^2)$ and $O(\Gamma^2)$ in (B1) and (B4) involve multiples of either $\mathrm{Im}\chi(\omega)$ or its derivatives. From (B8) it is clear that derivatives of all orders are assured to be in L^2 by the above procedure. Hence these terms vanish as $\Gamma\to 0$. Note that in the derivation of (B4), derivatives greater than the second order of $\mathrm{Im}\chi(\omega)$ have been neglected, as discussed with regards to (38). If these were to be included here, they would lead to terms of the same form as (B6) and would converge in the same manner.

Considering now (B2), one observes that by using (30) one may write its expression as

$$\left|\left(\int_{-\infty}^{-\omega_M}+\int_{\omega_M}^{\infty}\right)\mathrm{Im}\chi(\omega_0)\mathrm{Im}L_+(\omega,\omega_0)d\omega_0\right|. \tag{B9}$$

To find the limit of the L^2 norm, the task here is therefore to evaluate

$$\lim_{\Gamma\to 0}\int_{-\infty}^{\infty}\left|\left(\int_{-\infty}^{-\omega_M}+\int_{\omega_M}^{\infty}\right)\mathrm{Im}\chi(\omega_0)\mathrm{Im}L_+(\omega,\omega_0)d\omega_0\right|^2 d\omega. \tag{B10}$$

Moving the limit inside the outermost integral is permitted through Lebesgue's dominated convergence theorem under the condition that $\mathrm{Im}\chi(\omega_0)$ is bounded. In the event that $\mathrm{Im}\chi(\omega_0)$ is singular on the real axis, one may instead use $\mathrm{Im}\chi(\omega_0+i\delta)$ (where $\delta>0$ is an arbitrarily small parameter) for which any divergence is quenched, as discussed in the Introduction. This gives

$$\begin{aligned}&\int_{-\infty}^{\infty}\left|\lim_{\Gamma\to 0}\left(\int_{-\infty}^{-\omega_M}+\int_{\omega_M}^{\infty}\right)\mathrm{Im}\chi(\omega_0)\mathrm{Im}L_+(\omega,\omega_0)d\omega_0\right|^2 d\omega\\ &\quad=\left(\int_{-\infty}^{-\omega_M}+\int_{\omega_M}^{\infty}\right)|\mathrm{Im}\chi(\omega)|^2 d\omega\end{aligned} \tag{B11}$$

when having used (A2). The final result (B11) reveals that the norm is finite and that one, however, must demand $\omega_M\to\infty$ in order that (B2) converges to zero.

The remaining task is to evaluate (B5) through the limit

$$\lim_{\Gamma\to 0}\int_{-\infty}^{\infty}\left|\left(\int_{-\infty}^{\omega-a}+\int_{\omega+a}^{\infty}\right)\mathrm{Im}\chi_F(\omega_0)F_\Gamma(\omega_0-\omega)d\omega_0\right|^2 d\omega. \tag{B12}$$

Under the same condition as before one may move the limit inside the outermost integral through Lebesgue's dominated convergence theorem:

$$\begin{aligned}&\int_{-\infty}^{\infty}\left|\lim_{\Gamma\to 0}\left(\int_{-\infty}^{\omega-a}+\int_{\omega+a}^{\infty}\right)\mathrm{Im}\chi_F(\omega_0)\right.\\ &\qquad\left.\times F_\Gamma(\omega_0-\omega)d\omega_0\right|^2 d\omega=0.\end{aligned} \tag{B13}$$

Here the δ-convergence property of the Lorentz-Cauchy function $F_\Gamma(\omega_0-\omega)$ has been used.

Hence it has been demonstrated that the L^2 convergence expressed in (5) is achieved by setting $\Gamma\to 0$, $\omega_M\to\infty$, and $\Delta=\Gamma^2/\omega_M$.

[1] B. E. Saleh and M. C. Teich, *Fundamentals of Photonics*, 2nd ed. (Wiley, Hoboken, NJ, 2007).
[2] J. Jackson, *Classical Electrodynamics* (Wiley, New York, 1999).
[3] M. Dressel and G. Grüner, *Electrodynamics of Solids: Optical Properties of Electrons in Matter* (Cambridge University Press, Cambridge, 2002).
[4] C. Caloz, Proc. IEEE **99**, 1711 (2011).
[5] L. D. Landau and E. M. Lifshitz, *Electrodynamics of Continuous Media* (Pergamon, New York, 1960), Chap. 9.
[6] B. Nistad and J. Skaar, Phys. Rev. E **78**, 036603 (2008).
[7] C. A. Dirdal and J. Skaar, J. Opt. Soc. Am. B **30**, 370 (2013).
[8] Ø. Lind-Johansen, K. Seip, and J. Skaar, J. Math. Phys. **50**, 012908 (2009).
[9] J. B. Pendry, A. J. Holden, D. J. Robbins, and W. J. Stewart, IEEE Trans. Microwave Theory Tech. **47**, 2075 (1999).
[10] J. A. Schuller, R. Zia, T. Taubner, and M. L. Brongersma, Phys. Rev. Lett. **99**, 107401 (2007).
[11] C.-Y. Cheng and R. Ziolkowski, IEEE Trans. Microwave Theory Tech. **51**, 2306 (2003).
[12] F. Shafiei, F. Monticone, K. Q. Le, X.-X. Liu, T. Hartsfield, A. Alù, and X. Li, Nat. Nanotechnol. **8**, 95 (2013).
[13] N. Engheta and R. Ziolkowski, IEEE Trans. Microwave Theory Tech. **53**, 1535 (2005).
[14] C. Caloz, A. Sanada, and T. Itoh, IEEE Trans. Microwave Theory Tech. **52**, 980 (2004).
[15] W. Rotman, IEEE Trans. Antennas Prop. **10**, 82 (1962).
[16] E. Lier, D. H. Werner, C. P. Scarborough, Q. Wu, and J. A. Bossard, Nat. Mater. **10**, 216 (2011).
[17] M. Gil, J. Bonache, and F. Martín, Metamaterials **2**, 186 (2008).
[18] Q. Feng, M. Pu, C. Hu, and X. Luo, Opt. Lett. **37**, 2133 (2012).
[19] B. T. Schwartz and R. Piestun, J. Opt. Soc. Am. B **20**, 2448 (2003).
[20] A. V. Goncharenko, V. U. Nazarov, and K.-R. Chen, Appl. Phys. Lett. **101**, 071907 (2012).
[21] S. A. Ramakrishna, J. B. Pendry, D. Schurig, D. R. Smith, and S. Schultz, J. Mod. Opt. **49**, 1747 (2002).

Paper III

Superposing Lorentzian resonance functions towards engineering target responses

Published in Proceedings of META'14 – Singapore, The 5th International Conference on Metamaterials, Photonic Crystals and Plasmonics

ISBN: 978-2-9545460-4-9

Superposing Lorentzian resonance functions towards engineering target responses

Christopher A. Dirdal and Johannes Skaar

Department of Electronics and Telecommunications,
Norwegian University of Science and Technology, NO-7491 Trondheim, Norway
*corresponding author, E-mail: christopher.dirdal@iet.ntnu.no

Abstract

We prove that all complex valued response functions obeying the Kramers-Kronig relations can be approximated as superpositions of Lorentzian resonance functions, to any precision. A practical consequence is that arbitrary target response functions can be engineered in terms of common resonant metamaterial responses. A basic dispersion engineering methodology outlining these possibilities is presented, along with relevant metamaterial systems.

1. Introduction

The prospect of engineering metamaterials with tailor-made dispersion properties, rather than being limited to the dispersions of conventional media, is becoming a reality. Such dispersion engineering finds interesting applications within dispersion compensation [1, 2] broadband absorption [3], broadband ultra-low refractive index media [4], couplers [5], antenna design [6, 7], and filters [8], to mention but a few. The rapid developments made in metamaterial design and manufacturing towards this goal, allow us to speculate on what classes of dispersion behavior will be ultimately realizable as further progress is made. Important restrictions in this respect are for instance compliance with the Kramers-Kronig relations, which characterize the class of causal functions, and considerations such as whether the medium in question is to be passive or active. Since both of these conditions can be seen as somewhat lenient (the space of passive/active and causal functions is large), it seems natural to expect a significant degree of freedom for prospective metamaterial dispersions.

Contrary to this intuition, however, most treatments of dispersion phenomena commonly model dielectric media as superpositions of a single causal response function, the Lorentzian resonance, owing to its generality in describing a wide range of resonance phenomena and its simplicity [9–11]. It is natural to ask whether or not typical textbook discussions on dispersion therefore leave a significant number of possibilities out of view, and how large the possible gap in the function space between causal functions and Lorentzian superpositions is. With these considerations at hand, it comes as somewhat of a surprise that superpositions of Lorentzian functions can be shown to approximate any causal function obeying the Kramers-Kronig relations to any precision, as we have recently demonstrated [12]. In other words, there exists no gap in the function space between complex valued functions fulfilling the Kramers-Kronig relations and the superpositions of Lorentzian resonance functions commonly used in textbook treatments. The typical textbook approach to dispersion is therefore shown to encompass all responses fulfilling the Kramers Kronig relations.

In the context of this paper, the above results also demonstrate interesting practical consequences to the prospects of engineering desired dispersions. Since a number of metamaterial systems capable of realizing Lorentzian superpositions exist in literature [12–14], it seems possible to realize a given target response function, for which no physical system is known, by a metamaterial realization of its corresponding Lorentzian resonance superposition.

This paper will derive expressions for the relevant superpositions of Lorentzian resonance function, as well as outline a basic design methodology for the realization of arbitrary target response functions. With relation to our former discussions on Lorentzian resonance superpositions [12], this paper complements earlier results by providing a simpler proof, while expanding on inherent possibilities for realizing arbitrary target dispersions in metamaterials.

2. Identifying the superposition of Lorentzian resonance functions

A Lorentzian resonance function may be written in the form

$$L(\omega) = \frac{\omega_0}{\omega_0^2 - \omega^2 - i\omega\Gamma}, \tag{1}$$

where ω is the frequency and ω_0 and Γ are the resonance frequency and bandwidth, respectively. Fig. 1 displays its characteristic plot. For an arbitrary susceptibility function $\chi(\omega)$ that is analytic in the upper complex frequency plane, we shall now demonstrate that

$$\chi(\omega) = \frac{2}{\pi} \lim_{\Gamma \to 0} \int_0^\infty \mathrm{Im}\chi(\omega_0) \frac{\omega_0}{\omega_0^2 - \omega^2 - i\omega\Gamma} \mathrm{d}\omega_0, \tag{2}$$

which constitutes the main result of this paper. Eq. (2) shows that the susceptibility $\chi(\omega)$ can be expressed as a superposition of Lorentzian resonance functions weighted by $\mathrm{Im}\chi(\omega)$ under the limit $\Gamma \to 0$. This can be understood intuitively by noting that the imaginary part of (1) approaches

a δ-function as a distribution under the limit $\Gamma \to 0$, and that $\mathrm{Re}\chi(\omega)$ and $\mathrm{Im}\chi(\omega)$ are Hilbert transforms of each other, as discussed at length in [12]. However, this result is in fact simply a consequence of the analytic properties of $\chi(\omega)$ in the upper complex half plane. To show this, we first separate (1) into partial fractions

$$L(\omega) = \frac{1}{2(\omega_0 - \omega_p)} + \frac{1}{2(\omega_0 + \omega_p)}, \tag{3}$$

where $\omega_p = \sqrt{\omega^2 + i\omega\Gamma}$. The pole positions of (3) are displayed in Fig. 2 along with a semicircle contour curve C in the upper half-plane for ω_0. Note that despite being analytic in the upper complex ω-plane, (3) is not required to be analytic in the upper complex ω_0-plane, as observed in Fig. 2. Multiplying with the susceptibility function $\chi(\omega_0)$ and using Cauchy's Integral Formula and Cauchy's Integral Theorem over the contour C on each of the terms in (3), respectively, give

$$\frac{1}{2}\int_{-\infty}^{\infty} \frac{\chi(\omega_0)}{\omega_0 - \omega_p} \mathrm{d}\omega_0 = i\pi\chi(\omega_p) \tag{4}$$

$$\frac{1}{2}\int_{-\infty}^{\infty} \frac{\chi(\omega_0)}{\omega_0 + \omega_p} \mathrm{d}\omega_0 = 0, \tag{5}$$

when having assumed that the radius of the contour semicircle tends to infinity. Adding (4) and (5) together then gives

$$\int_{-\infty}^{\infty} \frac{\omega_0\chi(\omega_0)}{\omega_0^2 - \omega^2 - i\omega\Gamma} \mathrm{d}\omega_0 = i\pi\chi(\omega_p). \tag{6}$$

The reality of the time domain fields requires that $\chi(-\omega_0) = \chi^*(\omega_0)$ along the real ω_0 axis. This symmetry property allows us to re-express the integral and obtain

$$\chi(\omega_p) = \frac{2}{\pi}\int_0^{\infty} \mathrm{Im}\chi(\omega_0) \frac{\omega_0}{\omega_0^2 - \omega^2 - i\omega\Gamma} \mathrm{d}\omega_0. \tag{7}$$

Taking the limit $\lim_{\Gamma\to 0}\chi(\omega_p) = \chi(\omega)$ gives (2) and concludes this proof.

The superposition (2) corresponds to an infinite number of Lorentzian resonances with zero widths. We will

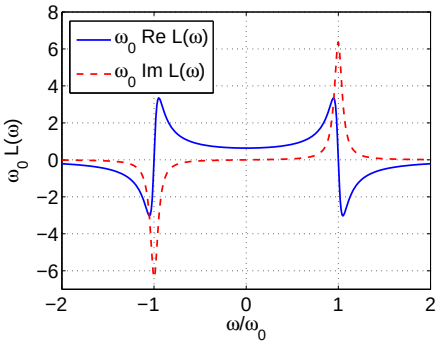

Figure 1: A Lorentzian resonance function.

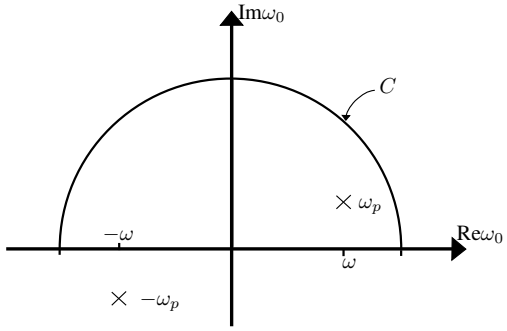

Figure 2: The complex plane of the resonance frequency ω_0. Note that the function (3) is not analytic in the upper complex half plane of ω_0, despite analyticity being ensured in the upper half plane for ω.

now show that $\chi(\omega)$ can be approximated by a finite sum of finite-width Lorentzian resonance functions to any degree of precision. As a first step, we therefore remove the limit $\Gamma \to 0$ from (2), thereby giving the right hand side of (7), which we rename $\chi_\Gamma(\omega)$. Since $\lim_{\Gamma\to 0}\chi_\Gamma(\omega) = \chi(\omega)$, it follows that $\chi_\Gamma(\omega)$ approximates $\chi(\omega)$ to any desired degree of precision. The next step is to approximate the integral in $\chi_\Gamma(\omega)$, as expressed in (7), by a finite sum of finite-width resonances giving

$$\chi_{\Gamma,\Delta}(\omega) = \frac{2}{\pi}\sum_{m=0}^{M-1} \mathrm{Im}\chi(\omega_m) \frac{\omega_m\Delta}{\omega_m^2 - \omega^2 - i\omega\Gamma}. \tag{8}$$

Here Δ is the spacing between the resonance frequencies, $\omega_m = \Delta/2 + m\Delta$, and M is a large integer. Intuitively a sufficient condition for $\chi_{\Gamma,\Delta}(\omega)$ to converge to $\chi(\omega)$ is to e.g. set $M = 1/\Delta$ and take the limit $\Delta \to 0$ before taking the limit $\Gamma \to 0$. This condition is however not practical as we desire to use a finite number of Lorentzian resonance functions. It can be shown that if we for instance set $\Delta = \Gamma^2/\sqrt{M}$ the error $|\chi_{\Gamma,\Delta}(\omega) - \chi(\omega)|$ converges in L^2 as $\Gamma \to 0$, and vanishes if we also let $M\Delta \to \infty$ [12]. This demonstrates that $\chi_{\Gamma,\Delta}(\omega)$, a finite sum of finite width Lorentzians, can approximate any $\chi(\omega)$ to any desired accuracy.

3. Engineering target dispersions by metamaterials

Owing to the generality of resonance phenomena in physical systems a number of material realizations exist for the response (1), and a number of metamaterial systems have demonstrated that it is possible to tailor its resonance strengths, widths and positions [13, 14]. This seems to suggest that it is possible to engineer desired responses $\chi(\omega)$ by use of superpositions of Lorentzian resonance functions

in the manner of (8). Here a basic design methodology shall be outlined.

3.1. Reducing the number of resonances

To facilitate the discussion, a simple target response $\chi(\omega)$ is chosen with the imaginary part

$$\mathrm{Im}\chi(\omega) = \begin{cases} \omega/\omega_c & \text{if } |\omega| < \omega_c \\ 0 & \text{elsewhere .} \end{cases} \tag{9}$$

Inserting this target function into (8) and choosing $\Gamma/\omega_c = 0.001$ and $\Delta/\omega_c = 0.0005$ yields the sum plotted in Fig. 3a. In order to accurately approximate the steep drop at $\omega/\omega_c = 1$, this sum contains 2000 narrow Lorentzian resonance functions. An interesting feature of this target $\chi(\omega)$ is that it leads to $\mathrm{Re}\chi(\omega) = -2$ in a narrow frequency region around ω_c. As a side remark we note that the Kramers-Kronig relations can be used to show that if the edge of $\mathrm{Im}\chi(\omega)$ is made infinitely steep at $\omega = \omega_c$ then one can achieve $\mathrm{Re}\chi(\omega_c) = -2$ with negligible loss for all frequencies [15]. Here we can at best hope to approximate this effect, since an infinitely steep drop would require using infinitely many Lorentzian resonance functions of zero width.

The high number of resonances in the sum (8) displayed in Fig. 3a may present a challenge towards metamaterial realization. Forty out of a total of 2000 are shown individually in Fig. 3b. However, making use of the observation that the bandwidth Γ and density of resonances do not have to be equal everywhere, it is possible to reduce the number of needed resonances dramatically. For $\mathrm{Im}\chi(\omega)$ defined by (9) we can for instance imagine placing many narrow resonances close to $\omega = \omega_c$, and few, though wider, resonances at lower frequencies. To help illustrate the process of placing resonances with varying widths in a systematic manner, it can be helpful to define two functions for the target characterized by (9):

1. **Placement function:** We set $\omega_m/\omega_c = 1-(m/N)^\nu$, where ω_m is the mth resonance out of a total of N resonances, and ν is a parameter one may vary. Setting $\nu = 1$ gives linear spacing between the resonances, while increasing ν concentrates them towards $\omega = \omega_c$. For our purpose we choose $\nu = 4$ and $N = 20$.

2. **Width function:** We simply choose $\Gamma/\omega_c = 1 - (\omega_m/\omega_c)^\gamma$, where γ is a parameter we shall vary. Setting $\gamma = 1$ makes the widths decrease linearly over the bandwidth, while we set $\gamma = 0.5$.

Figure 4 displays the resonance placements and widths for our chosen functions and parameters, leading to the superposition displayed in Fig. 5. This superposition is a Riemann sum similar to (8), but differs due to the fact that both Γ and Δ vary with respect to frequency. This superposition approximates the shape of Fig. 3a with only 20 Lorentzian resonance functions instead of the 2000 needed earlier, and

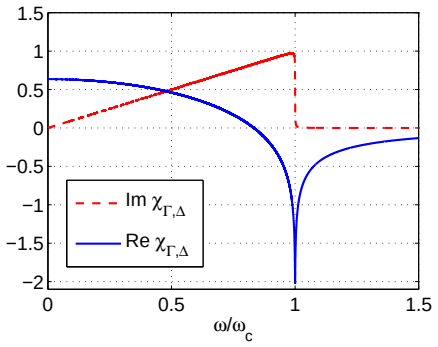

(a) Real and imaginary parts of the sum approximations by (8) for $\Gamma/\omega_c = 0.001$ and $\Delta/\omega_c = 0.0005$. There are 2000 Lorentzian resonance functions included in the sum. The red and blue curves correspond to $\mathrm{Im}\chi_{\Gamma,\Delta}$ and $\mathrm{Re}\chi_{\Gamma,\Delta}$, respectively.

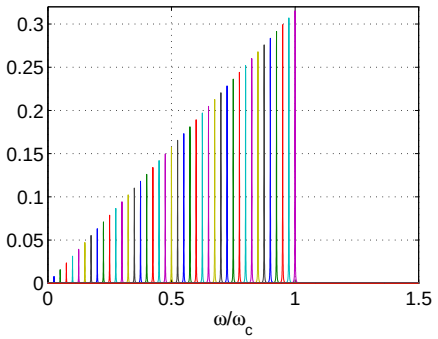

(b) The imaginary parts for one out of every fifty Lorentzians in the sum (8), when $\Gamma/\omega_c = 0.001$ and $\Delta/\omega_c = 0.0005$.

Figure 3

maintains $\mathrm{Re}\chi(\omega_c) \approx -2$ without any significant change in the amount of loss below ω_c.

Having found an approximation of the target function $\chi(\omega)$ by a superposition of Lorentzian resonance functions where the tradeoff between the needed accuracy and the maximum number of resonances has been satisfactory negotiated, the next step is to find a suitable metamaterial realization. Continuing with the target response characterized by (9), we shall consider two possible metamaterials in which the sum displayed in Fig. 5 can be realized.

3.2. Metamaterial realization 1: Network of loaded RLC transmission lines

Homogeneous dielectric or magnetic media can be given a network equivalent in the low frequency limit. A network of lumped circuit elements with unit cells much smaller than the operating wavelength results in effective parameters $\mu(\omega)$ and $\epsilon(\omega)$ for the magnetic permeability and the electric permittivity, respectively. These may be derived

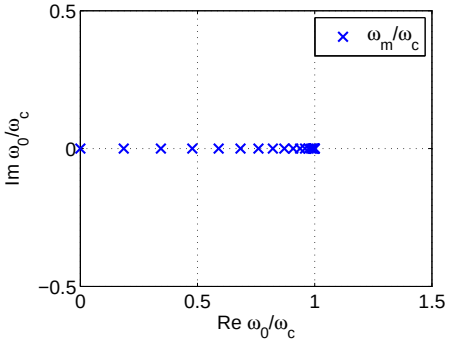

(a) Positioning of the resonance frequencies according to the placement function $\omega_m/\omega_c = 1 - (m/20)^4$ where ω_m is the mth resonance where $m = \{1, ..., 20\}$.

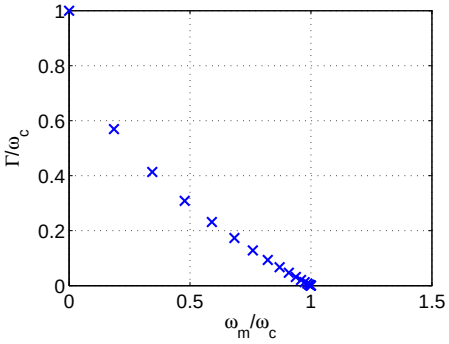

(b) Designation of the width $\Gamma(\omega_m)$ of each Lorentzian resonance function at each resonance frequency ω_m in (a), according to the width function $\Gamma/\omega_c = 1 - (\omega_m/\omega_c)^{0.5}$.

Figure 4

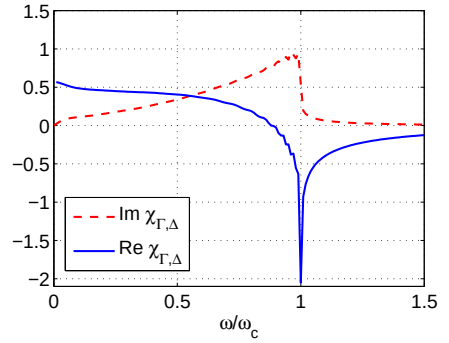

(a) Real and imaginary parts of a sum approximation of (2) where the resonances ω_m are placed according to Fig. 4a, and the widths Γ of each resonance are given by Fig. 4b. By varying the placements and widths of the resonances, a similar response to that displayed in Fig. 3a is achieved with only 20 resonances.

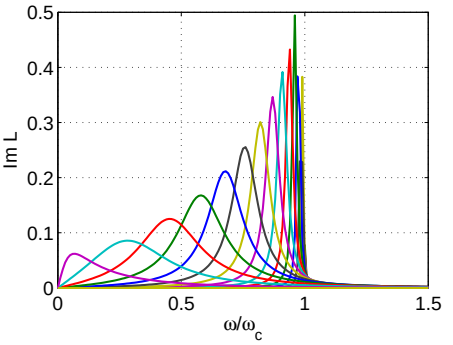

(b) Imaginary parts of the Lorentzian resonance functions constituting the sum displayed in (a). The widths Γ and resonance frequencies are varied according to the width- and placement functions displayed in Fig. 4.

Figure 5

through the use of the telegrapher's and Maxwell equations after having related the current and voltage in each unit cell to the magnetic and electric fields [16, 17]. In terms of the series impedance $Z(\omega)$ per unit length and the shunt admittance $Y(\omega)$ per unit length in a 1D unit cell displayed in Fig. 6a, one has

$$\mu(\omega) = -\frac{1}{i\omega\mu_0} Z(\omega) \tag{10}$$

$$\epsilon(\omega) = -\frac{1}{i\omega\epsilon_0} Y(\omega). \tag{11}$$

In order to realize Lorentzian resonance functions of the form $L(\omega)$ from (1), we must synthesize circuits that give the necessary impedance and/or admittance in (10) and (11) to achieve $\mu(\omega) - 1 = L(\omega)$ and/or $\epsilon(\omega) - 1 = L(\omega)$. This may for instance be achieved through straightforward application of Brune synthesis [18] leading to the circuits displayed in Fig. 6b. The impedance circuit leads to

$$\mu(\omega) = 1 + \frac{F}{\omega_0^2 - \omega^2 - i\omega\Gamma}, \tag{12}$$

where $F = 1/\mu_0 C$, $\Gamma = \mu_0 F/R$ and $\omega_0^2 = \mu_0 F/L$. Similarly, the admittance circuit gives the same form as (12) for $\epsilon(\omega)$ with $F = 1/\epsilon_0 L$, $\Gamma = \epsilon_0 FR$, and $\omega_0^2 = \epsilon_0 F/C$. The circuit elements with parameters L' and C' correspond to the inductance and capacitance per unit length of the transmission line, which we have set equal to μ_0 and ϵ_0, respectively. We observe that the resonator strength, width and resonance frequency of the resonances may be tailored by altering the values of the lumped elements in Fig. 6b for both $\mu(\omega)$ and $\epsilon(\omega)$. In order to realize the sum displayed in Fig. 5 for $\mu(\omega)$ and/or $\epsilon(\omega)$ we must construct a unit cell consisting of the circuit in (6b) repeated twenty times (apart from the elements corresponding to L' and C') for different values of R, L, C.

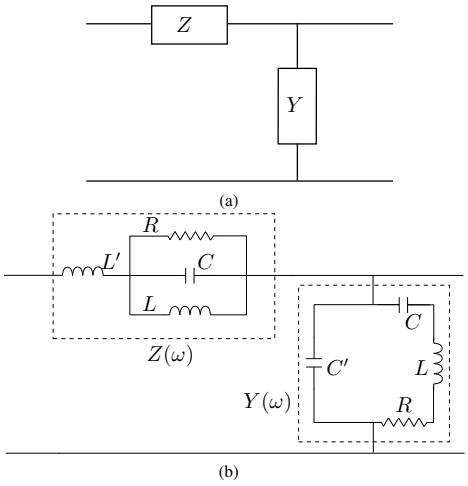

Figure 6

3.3. Metamaterial realization 2: Split ring cylinders of varying parameters

Split ring cylinder metamaterials are known to lead to resonances similar to that of the Lorentzian resonance function (1) [13]. We have recently shown elsewhere that a superposition of Lorentzian resonance functions with different resonance frequencies, widths and strengths can be realized in terms of split ring cylinders of differing radii r, capacitance C per m^2, resistance ρ per circumference-length ratio, and fractional volume F of the unit cell occupied by the interior of the cylinders [12]. The effective parameter in the case of N split ring cylinders per unit cell then becomes

$$\mu(\omega) - 1 = \sum_{k}^{N} \frac{\omega^2 F_k}{\frac{2}{\pi^2 \mu_0 C_k r_k^3} - \omega^2 - i\omega \frac{2\rho_k}{r_k \mu_0}}. \qquad (13)$$

where k represents the kth split ring cylinder in the unit cell. This expression becomes exact as the cylinder heights tend toward infinity. It is observed that the expression within the sum is similar to that of the Lorentzian resonance function (1), with the discrepancy in the numerator becoming negligible as the width of each resonance becomes small relative to the resonance frequency. The task of realizing the sum displayed in Fig. 5 therefore amounts to tailoring the geometry, material composition and density of a given split ring cylinder with parameters r_k, C_k, ρ_k, F_k so that its response approximates one of the resonances displayed in Fig. 5b.

4. Conclusion

It has been proven that causal susceptibility functions obeying the Kramers-Kronig relations can be approximated by superpositions of Lorentzian resonance functions, to any precision. Making use of the practical implications that follow from this result, a basic metamaterial design methodology for the realization of arbitrary target responses has been outlined. This consists in reducing the number of needed Lorentzian resonance functions by varying their widths and resonance frequencies, and then finding a suitable metamaterial system for their realization. Two metamaterial systems were identified: A network of RLC-loaded transmission lines, and split ring cylinder arrays.

References

[1] C.-Y. Cheng and R. Ziolkowski, "Tailoring double-negative metamaterial responses to achieve anomalous propagation effects along microstrip transmission lines," *IEEE Trans. Microw. Theory Tech.*, vol. 51, pp. 2306 – 2314, dec. 2003.

[2] N. Engheta and R. Ziolkowski, "A positive future for double-negative metamaterials," *IEEE Trans. Microw. Theory Tech.*, vol. 53, pp. 1535 – 1556, april 2005.

[3] Q. Feng, M. Pu, C. Hu, and X. Luo, "Engineering the dispersion of metamaterial surface for broadband infrared absorption," *Opt. Lett.*, vol. 37, no. 11, pp. 2133–2135, 2012.

[4] B. T. Schwartz and R. Piestun, "Total external reflection from metamaterials with ultralow refractive index," *J. Opt. Soc. Am. B*, vol. 20, pp. 2448–2453, Dec 2003.

[5] C. Caloz, A. Sanada, and T. Itoh, "A novel composite right-/left-handed coupled-line directional coupler with arbitrary coupling level and broad bandwidth," *IEEE Trans. Microw. Theory Tech.*, vol. 52, pp. 980 – 992, march 2004.

[6] W. Rotman, "Plasma simulation by artificial dielectrics and parallel-plate media," *IEEE Trans. Antennas Prop.*, vol. 10, pp. 82–95, january 1962.

[7] E. Lier, D. H. Werner, C. P. Scarborough, Q. Wu, and J. A. Bossard, "An octave-bandwidth negligible-loss radiofrequency metamaterial," *Nature Materials*, vol. 10, no. 3, pp. 216–222, 2011.

[8] M. Gil, J. Bonache, and F. Martín, "Metamaterial filters: A review," *Metamaterials*, vol. 2, no. 4, pp. 186 – 197, 2008.

[9] B. E. Saleh and M. C. Teich, *Fundamentals of photonics, 2nd ed.* John Wiley & Sons, Inc., 2007.

[10] J. Jackson, *Classical Electrodynamics*. Wiley, 1999.

[11] M. Dressel and G. Grüner, *Electrodynamics of Solids: Optical Properties of Electrons in Matter*. Cambridge University Press, 2002.

[12] C. A. Dirdal and J. Skaar, "Superpositions of lorentzians as the class of causal functions," *Phys. Rev. A*, vol. 88, p. 033834, Sep 2013.

[13] J. B. Pendry, A. J. Holden, D. J. Robbins, and W. J. Stewart, "Magnetism from conductors and enhanced nonlinear phenomena," *IEEE Trans. Microwave Theory and Tech.*, vol. 47, pp. 2075–2084, November 1999.

[14] J. A. Schuller, R. Zia, T. Taubner, and M. L. Brongersma, "Dielectric metamaterials based on electric and magnetic resonances of silicon carbide particles," *Phys. Rev. Lett.*, vol. 99, p. 107401, Sep 2007.

[15] C. A. Dirdal and J. Skaar, "Negative refraction in causal media by evaluating polar paths for rational functions," *J. Opt. Soc. Am. B*, vol. 30, pp. 370–376, Feb 2013.

[16] G. Eleftheriades, A. Iyer, and P. Kremer, "Planar negative refractive index media using periodically l-c loaded transmission lines," *Microwave Theory and Techniques, IEEE Transactions on*, vol. 50, pp. 2702–2712, Dec 2002.

[17] B. Nistad and J. Skaar, "Simulations and realizations of active right-handed metamaterials with negative refractive index," *Opt. Express*, vol. 15, pp. 10935–10946, 2007.

[18] O. Wing, *Classical Circuit Theory*. Springer US, 2009.

Paper IV

Relaxed dispersion constraints and metamaterial effective parameters with physical meaning for all frequencies

Published in Physical Review B

DOI: 10.1103/PhysRevB.91.134102

Relaxed dispersion constraints and metamaterial effective parameters with physical meaning for all frequencies

Christopher A. Dirdal, Tarjei Bondevik, and Johannes Skaar*

Department of Electronics and Telecommunications, Norwegian University of Science and Technology, NO-7491 Trondheim, Norway

(Received 27 October 2014; revised manuscript received 26 March 2015; published 10 April 2015)

Metamaterial effective parameters may exhibit freedom from typical dispersion constraints. For instance, the emergence of a magnetic response in arrays of split ring resonators for long wavelengths cannot be attained in a passive continuous system obeying the Kramers-Kronig relations. We characterize such freedom by identifying the three possible asymptotes which effective parameters can approach when analytically continued. Apart from their dispersion freedom, we also demonstrate that the effective parameters may be redefined in such a way that they have a certain physical meaning for all frequencies. There exist several possible definitions for the effective permittivity and permeability whereby this is achieved, thereby giving several possible frequency variations for high frequencies, while nevertheless converging to the same dispersion for long wavelengths.

DOI: 10.1103/PhysRevB.91.134102 PACS number(s): 78.67.Pt, 78.20.Ci, 42.25.Bs

I. INTRODUCTION

The concept of a metamaterial is a powerful one. Complex electromagnetic systems are treated as simple, effectively continuous media with effective homogeneous fields, for which electromagnetic properties unlike those found in any conventional media may emerge. These properties are described by effective parameters $\mu_{\text{eff}}(\omega)$ and $\epsilon_{\text{eff}}(\omega)$, which represent the effective permeability and permittivity, respectively, as seen by macroscopic fields in the long-wave limit. Analytic expressions of such parameters have been derived for several systems, including arrays of split ring cylinders [1] in which magnetism is realized from nonmagnetic conductors, and L-C loaded transmission lines [2], which realize a left-handed medium.

In order to examine dispersion properties of metamaterial systems it is natural to consider their effective parameters in relationship with the Kramers-Kronig (KK) relations. For the permittivity one has

$$\text{Re}\,\epsilon(\omega) = 1 + \frac{2\mathcal{P}}{\pi}\int_0^\infty \frac{x\,\text{Im}\,\epsilon(x)}{x^2-\omega^2}dx, \tag{1a}$$

$$\text{Im}\,\epsilon(\omega) = -\frac{2\omega\mathcal{P}}{\pi}\int_0^\infty \frac{\text{Re}\,\epsilon(x)-1}{x^2-\omega^2}dx, \tag{1b}$$

where $\mathcal{P}$ represents the principle value. These are derived under the conditions that the permittivity $\epsilon(\omega)\to 1$ as $\omega\to\infty$ and that $\epsilon(\omega)$ must be analytic for $\text{Im}\,\omega \geqslant 0$. On the basis of causality and other physically reasonable assumptions, the permittivity of common media is generally assumed to fulfill these requirements [3] (pp. 332 and 333), and hence Eq. (1). However, in, for example, metamaterials consisting of L-C loaded transmission lines this is not necessarily the case. The effective parameters for the particular arrangement of the one-dimensional (1D) unit cell displayed in Fig. 1 with series impedance $Z'(\omega)$ and the shunt admittance $Y'(\omega)$ per unit length are [2]

$$\epsilon_{\text{eff}}(\omega) = -\frac{Y'}{i\omega}, \tag{2a}$$

$$\mu_{\text{eff}}(\omega) = -\frac{Z'}{i\omega}. \tag{2b}$$

If the impedance and admittance of the transmission line are taken to represent common lumped circuit elements such as inductors $Y_L = -i\omega L$, resistors $Y_R = R$, or capacitors $Y_C = -1/i\omega C$, then it is clear from Eq. (2a) that the asymptotic forms $O[\epsilon_{\text{eff}}(\omega)] = 1$, ω^{-1}, and ω^{-2} follow upon analytic continuation for $\omega\to\infty$. The latter two of these cases clearly violate the premisses for Eq. (1) and hence do not fulfill the Kramers-Kronig relations.

Equivalent remarks regarding the effective permeability of a metamaterial system can be made. It is evident that Eq. (2b) will not obey the Kramers-Kronig relations for impedances $Z_R = R$ and $Z_C = -1/i\omega C$. This is also the case for the effective permeability in another well-known metamaterial system: an array of the split ring cylinders. The effective parameter as derived by Pendry *et al.* [1] takes the form

$$\mu_{\text{eff}}(\omega) = 1 + \frac{\omega^2 F}{\omega_0^2 - \omega^2 - i\omega\Gamma}. \tag{3}$$

Here F is the volume fraction of the interior of the cylinder in the unit cell, ω_0 is the resonance frequency determined by the cylinder radius and capacitance, and Γ is the response width determined by the conductivity and cylinder radius [4]. On account of the deviation from unity of the asymptote of this parameter's analytic continuation

$$\mu_{\text{eff}}(\omega) \to 1 - F, \quad \text{as } \omega\to\infty, \tag{4}$$

the parameter (3) will not obey the Kramers-Kronig relations. As a side remark, the bianisotropy of the split ring cylinder [5] is avoided while yielding the same response [Eq. (3)] by a slight modification of the resonator design [6,7] (Sec. 16.2). This ensures that the parameter (3) is local under the constraints discussed further below.

At first glance it might not seem clear that the parameter asymptotes of Eqs. (2) and (3) being unequal to unity carries any significant practical consequences. However, on account of their analyticity the behavior at all frequencies, even for high frequencies (where the parameters may no longer even be physical; see Sec. II B), is important for how the parameter behaves *in the long-wavelength regime*. By violating the assumptions of Eq. (1) or the KK relation for the permeability function, which are generally taken to describe the class of

*johannes.skaar@ntnu.no

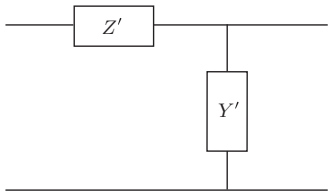

FIG. 1. Unit cell of a 1D transmission line with series impedance $Z'(\omega)$ and shunt admittance $Y'(\omega)$ per unit length.

possible dispersions in ordinary media, these metamaterial cases serve as tell-tale signs of some additional dispersion freedom from ordinary dispersion constraints. For instance, it will be shown in the next section that the characteristic occurrence of a magnetic response [Eq. (3)] in an array of split ring cylinders made from nonmagnetic metals is not possible in a passive continuous medium obeying the Kramers-Kronig relations. Hence, questions naturally arise as to what degree dispersion freedom can be attained in general, and what interesting consequences there may be in metamaterials. The purpose of this paper is to characterize this freedom of the effective parameters in relation to the constraints set by the Kramers-Kronig relations, and to explain the origin of their deviation from these. To this end, the following section deduces the possible asymptotic forms which are attainable for passive metamaterial systems. These are then used to identify the space of possible dispersions. Section II B discusses the origin of the parameter freedom in relation to their possible loss of physical meaning for large frequencies and wave numbers (ω,k). This encourages us to consider alternative definitions of the effective material parameters in Sec. III: As will be shown, we may attribute another physical meaning to the parameters which is kept also for wavelengths outside the long-wave limit, which nevertheless coincides with the usual meaning of effective permeability or permittivity at low frequencies. Finally, case examples will be presented which illustrate the findings of this paper.

This paper considers effective parameters $\mu_{\text{eff}}(\omega)$ and $\epsilon_{\text{eff}}(\omega)$ that locally relate the fields of macroscopic electromagnetism. Since spatially dispersive effects have been shown to be a general property of metamaterials [8] (p. 8) [9], local parameters are only possible for long wavelengths, i.e., $kd \ll 1$, where d represents the characteristic size of the relevant nonbianisotropic inclusions, and the wave number k must be sufficiently small as to render such effects negligible. Note that this implies that the inclusion parameters then must be chosen suitably to ensure that the relevant response features fall within this region: e.g., for the split ring cylinder array described by Eq. (3) the radius r and capacitance per unit area C must be tailored so that the resonance wave number $k_0 = \omega_0/c$ obeys $k_0 r = \sqrt{2/c^2\pi^2\mu_0 C r} \ll 1$.

For simplicity, the effective parameters are assumed to be scalar throughout the paper. We assume an $e^{-i\omega t}$ time dependence, meaning that positive imaginary parts of $\epsilon_{\text{eff}}(\omega)$ and $\mu_{\text{eff}}(\omega)$ correspond to a dissipation of energy [10] (p. 274) (for frequencies ω in the long-wavelength regime).

II. CHARACTERIZING DISPERSION FREEDOM

A. Asymptotic forms

This section will identify the set of possible asymptotic forms which an analytic continuation of the effective parameters can take. When these are known, it is possible to characterize the space of possible dispersions in terms of alternative Kramers-Kronig relations. This space will be shown to be greater than that encompassed by the standard dispersion constraints.

In the doctoral thesis of Otto Brune from 1931 [11] an argument was given which will now be presented here in an adapted form to show that the only three possible asymptotic forms consonant with passivity are

$$O(\mu_{\text{eff}}), O(\epsilon_{\text{eff}}) = 1, \omega^{-1}, \text{ or } \omega^{-2}, \quad \text{as } \omega \to \infty, \tag{5}$$

under the condition that ω remains in the frequency bandwidth where $\mu_{\text{eff}}(\omega)$ and $\epsilon_{\text{eff}}(\omega)$ represent effective permeability and permittivity, respectively. In practical terms, this means that if the long-wavelength regime of the physical model underlying $\mu_{\text{eff}}(\omega)$ or $\epsilon_{\text{eff}}(\omega)$ is extended indefinitely, for instance by reducing the characteristic sizes of the inclusions, then it follows that $\mu_{\text{eff}}(\omega)$ and $\epsilon_{\text{eff}}(\omega)$ must take one of the forms given by Eq. (5).

For a passive system, the passivity condition [as derived in [10] (Sec. 80)] when extended to the upper complex half plane for the permeability of a system becomes $\text{Im}\,\omega\mu \geqslant \text{Im}\,\omega$ [12] (under the assumption of no spatial dispersion [13]). For our present purposes we observe the necessary condition that $\text{Im}\,\omega\mu > 0$. We consider the possible asymptotic forms of $\mu_{\text{eff}}(\omega)$ in general by assuming

$$O(\omega\mu_{\text{eff}}) = \omega^n, \quad \text{as } |\omega| \to \infty, \tag{6}$$

where $n \in \mathbb{Z}$. Then, by expressing $\omega^n = |\omega|^n \exp(in\theta)$, one may write

$$O(\text{Im}\,\omega\mu_{\text{eff}}) = |\omega|^n \sin(n\theta), \quad \text{as } |\omega| \to \infty. \tag{7}$$

Now in order that $\text{Im}\,\omega\mu_{\text{eff}} > 0$ for $\text{Im}\,\omega > 0$, it may be seen from Eq. (7) that the values of n are restricted to $n \in \{-1,0,1\}$, so as to avoid a sign change for $\theta \in [0,\pi]$. Hence, on the basis of passivity the parameter $\mu_{\text{eff}}(\omega)$ can only have one of the asymptotic forms (5). Equivalent considerations on $\epsilon_{\text{eff}}(\omega)$ give the same result.

In order to characterize the space of possible dispersions on the basis of the forms (5), Kramers-Kronig relations generalized to these can be derived by expressing the effective parameter as

$$\mu_{\text{eff}}(\omega) \equiv a + \mu_a(\omega), \tag{8}$$

where $a = \lim_{\omega\to\infty} \mu_{\text{eff}}(\omega)$, $\mu_a(\omega)$ is square integrable, and $\mu_{\text{eff}}(\omega)$ is analytic for $\text{Im}\,\omega > 0$, and then applying Cauchy's integral theorem. From the symmetry property $\mu_{\text{eff}}(-\omega) = \mu^*_{\text{eff}}(\omega^*)$ it follows that the constant a is real. This gives the following expressions:

$$\text{Re}\,\mu_{\text{eff}}(\omega) = a + \frac{2\mathcal{P}}{\pi}\int_0^\infty \frac{x\,\text{Im}\,\mu_a(x)}{x^2-\omega^2}dx, \tag{9a}$$

$$\text{Im}\,\mu_{\text{eff}}(\omega) = -\frac{2\omega\mathcal{P}}{\pi}\int_0^\infty \frac{\text{Re}\,\mu_a(x)}{x^2-\omega^2}dx. \tag{9b}$$

Notice that, in the event that $\lim_{\omega\to\infty}\mu_{\text{eff}}(\omega)=1$, Eqs. (9a) and (9b) reduce to the conventional Kramers-Kronig relations [where $\mu_a(\omega)$ is set equal to the magnetic susceptibility]. Otherwise, they characterize a larger space of dispersions than the conventional Kramers-Kronig relations do. We note also that the KK relation suggested for the magnetic permeability by Landau and Lifshitz becomes equal to Eq. (9a) if the parameter ω_1 in [10] (p. 283) is set equal to infinity.

The additional freedom present in metamaterial systems can be exemplified by applying the generalized Kramers-Kronig relations (9) to Pendry *et al.*'s split ring cylinder metamaterial, where the cylinders are made of a nonmagnetic metal, such as aluminum or copper [1]. Upon applying a time-varying field, induced current flows on the cylinder surfaces and thereby leads to the emergence of a magnetic response, which is described by $\mu_{\text{eff}}(\omega)\neq 1$. At zero frequency, however, only the intrinsic material properties matter, meaning that $\mu_{\text{eff}}(0)=1$. Now, if we were to search for such emergent magnetism in a continuous medium which obeys Eq. (1), it turns out that we would necessarily be looking for a gain medium. This is observed from the analogous KK relation of Eq. (1a) for $\mu(\omega)$ with $\omega=0$:

$$\text{Re}\,\mu(0)=1+\frac{2\mathcal{P}}{\pi}\int_0^\infty\frac{\text{Im}\,\mu(x)}{x}dx. \tag{10}$$

The only way to have $\text{Re}\,\mu(0)=1$ for our system is for the integral to equal zero, thereby implying that $\text{Im}\,\mu(\omega)<0$ for some frequencies. This makes the freedom in the metamaterial arrangement explicit: While a continuous medium would need to display gain in order to have this property of emergent magnetism, Pendry *et al.*'s split ring cylinder metamaterial achieves this while being passive. Equation (3) shows that $\mu_{\text{eff}}(0)=1$ while $\text{Im}\mu_{\text{eff}}(\omega)\geqslant 0$ for all positive frequencies. By use of the generalized Kramers-Kronig relation (9a) where $a=1-F$ according to Eq. (4) we find

$$\text{Re}\,\mu_{\text{eff}}(0)=1-F+\frac{2\mathcal{P}}{\pi}\int_0^\infty\frac{\text{Im}\,\mu_a(x)}{x}dx. \tag{11}$$

Evidently, one need not assume that $\text{Im}\,\mu_{\text{eff}}(\omega)=\text{Im}\mu_a(\omega)<0$ in order that $\mu_{\text{eff}}(0)=1$.

B. Origin of freedom

So far we have characterized the dispersion freedom stemming from the asymptotic forms (5) without giving any explanation of their origin. An important observation in this respect is that the bandwidth of frequencies for which $\mu_{\text{eff}}(\omega)$ and $\epsilon_{\text{eff}}(\omega)$ carry the meaning of effective permeability and effective permittivity, respectively, under eigenmodal propagation is usually narrow in comparison to the range of frequencies for which the constituent materials of the metamaterial have an electromagnetic response [10,14]. This is because we only can define local effective parameters in the long-wavelength regime $kd\ll 1$ [8,9,15]. When assuming eigenmodal propagation this naturally also implies restrictions upon ω. Furthermore, metamaterial models often use the assumption of quasistatic interactions that may become invalid with increasing ω. Hence the subset in which $\epsilon_{\text{eff}}(\omega)$ and $\mu_{\text{eff}}(\omega)$ correspond to the effective permittivity and permeability, respectively, may be classified as $k\leqslant k_{\max}$ and $\omega\leqslant\omega_{\max}$,

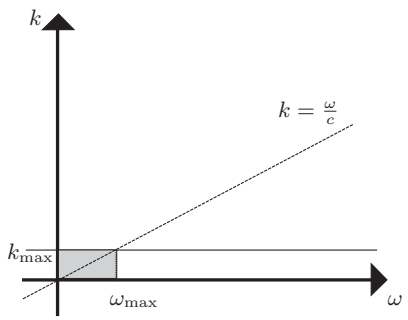

FIG. 2. The subset of (ω,k) for which the effective parameters $\mu_{\text{eff}}(\omega)$ and $\epsilon_{\text{eff}}(\omega)$ represent the effective properties of their corresponding systems according to a suitable homogenization theory (shaded region). The upper eigenmodal frequency $\omega_{\max}$ has here for simplicity been determined from the intersection between $k=k_{\max}$ and the line of eigenmodal propagation in vacuum.

where k dependence in $\mu_{\text{eff}}(\omega)$ and $\epsilon_{\text{eff}}(\omega)$ is for the sake of illustration assumed negligible below $k_{\max}$, and $\omega_{\max}$ is found according to the dispersion relation or according to quasistatic assumptions (see Fig. 2).

Since for $\omega>\omega_{\max}$ the effective parameters $\mu_{\text{eff}}(\omega)$ and $\epsilon_{\text{eff}}(\omega)$ do not have any direct correspondence with the effective permeability and permittivity of the system, these parameters are not necessarily subjected to ordinary dispersion constraints there. In other words, since the parameters cease to represent the effective properties of the medium they need not necessarily comply with the usual Kramers-Kronig relations or even passivity requirements. Since the parameters are analytic, this freedom at large frequencies also leads to dispersion freedom at low frequencies for which interesting physical consequences may occur. This is the origin of the freedom that has been characterized in the previous section.

As a side remark, one should note that source-driven systems do not in general need to adhere to the dispersion relation: Any combination of ω and k is in principle possible provided one is able to supply the necessary arrangement of sources within the medium [8,15]. Physical $\mu_{\text{eff}}(\omega)$ and $\epsilon_{\text{eff}}(\omega)$ may therefore in principle be defined for all ω if the medium is source driven to keep $k<k_{\max}$, and the parameters are obtained from an appropriate homogenization procedure [8].

III. PARAMETER DEFINITIONS THAT GIVE ALTERNATIVE PHYSICAL MEANING FOR ALL (ω,k)

Following the discussions in Sec. II B, it may be argued that the form of the frequency variation in $\mu_{\text{eff}}(\omega)$ given by Eq. (3) for $\omega>\omega_{\max}$ is in some sense arbitrary. What if we therefore were to alter the mathematical expression of $\mu_{\text{eff}}(\omega)$ in such a way that for $\omega>\omega_{\max}$ one instead has $\mu_{\text{eff}}(\omega)\to 1$ as $\omega\to\infty$, while allowing it to (approximately) keep the response shape (3) for $\omega<\omega_{\max}$? According to the discussion in Sec. II A regarding Eq. (10), such a modified $\mu_{\text{eff}}(\omega)$ would obey the conventional KK relations and have $\text{Im}\mu_{\text{eff}}(\omega)<0$ in some region where $\omega>\omega_{\max}$. Thereby, instead of observing dispersion freedom as a violation of the conventional KK

relations, it is now seen in terms of having $\mathrm{Im}\mu_{\mathrm{eff}}(\omega) < 0$ for a passive system. This therefore constitutes an alternative way of visualizing the same dispersion freedom that was discussed in Sec. II A. We shall examine this further in the first of the following case examples.

A second interesting point may be observed from the above illustration. It is possible to construct for the effective parameters $\epsilon_{\mathrm{eff}}(\omega)$ and $\mu_{\mathrm{eff}}(\omega)$ of a given metamaterial system a number of different frequency variations for large ω and k. On this note, we shall in the following show that it is possible and arguably preferable to redefine the parameters $\epsilon_{\mathrm{eff}}(\omega)$ and $\mu_{\mathrm{eff}}(\omega)$ in such a way that their frequency variations have a clear, physical meaning for all (ω,k). Since the concepts of local permittivity and permeability functions are not extendable to the entire space (ω,k), this necessarily implies giving $\epsilon_{\mathrm{eff}}(\omega)$ and $\mu_{\mathrm{eff}}(\omega)$ *other physical meanings* that nevertheless coincide with that of effective permittivity and permeability for $\omega \leqslant \omega_{\mathrm{max}}$ and $k \leqslant k_{\mathrm{max}}$. A general procedure by which this is ensured shall now be presented in the case of the effective permeability function $\mu_{\mathrm{eff}}(\omega)$ [an analogous approach may be employed in the case of $\epsilon_{\mathrm{eff}}(\omega)$], before moving on to two case examples.

We select for the parameter $\mu_{\mathrm{eff}}(\omega)$ of an arbitrary metamaterial the following definition:

$$\mathbf{B}^{\mathrm{d}}_{\mathrm{av}}(\omega) = \mu_0\mu_{\mathrm{eff}}(\omega)\mathbf{H}^{\mathrm{d}}_{\mathrm{av}}(\omega), \tag{12}$$

where

$$\mathbf{B}^{\mathrm{d}}_{\mathrm{av}} = \mu_0\bar{\mathbf{H}} + \frac{1}{V}\int_V \mathbf{M}(\mathbf{r})d^3\mathbf{r}, \tag{13a}$$

$$\mathbf{H}^{\mathrm{d}}_{\mathrm{av}} = \bar{\mathbf{H}} + \frac{i\omega}{V}\int_V \frac{\mathbf{r}\times\mathbf{P}(\mathbf{r})}{2}d^3\mathbf{r}, \tag{13b}$$

$$\bar{\mathbf{H}} = \frac{1}{V}\int_V \mathbf{H}(\mathbf{r})\mathrm{e}^{-i\mathbf{k}\cdot\mathbf{r}}d^3\mathbf{r}. \tag{13c}$$

Here $\mathbf{B}^{\mathrm{d}}_{\mathrm{av}}(\omega)$ and $\mathbf{H}^{\mathrm{d}}_{\mathrm{av}}(\omega)$ generally represent the dominant terms of the averaged field expansions according to the homogenization approach outlined in [8]; $\mathbf{M}(\mathbf{r})$ and $\mathbf{P}(\mathbf{r})$ represent the microscopic induced magnetization and electrical polarization, respectively; and V represents the volume of the unit cell. Even though the physical interpretations of the quantities (13) themselves are not intuitive for $\omega > \omega_{\mathrm{max}}$ and $k > k_{\mathrm{max}}$, the concrete physical meaning of $\mu_{\mathrm{eff}}(\omega)$ by Eq. (12) is kept for all (ω,k). This concrete physical meaning is nothing more than a relationship between $\mathbf{B}^{\mathrm{d}}_{\mathrm{av}}(\omega)$ and $\mathbf{H}^{\mathrm{d}}_{\mathrm{av}}(\omega)$, which is itself without any clear physical interpretation for $\omega > \omega_{\mathrm{max}}$ and $k > k_{\mathrm{max}}$. Nevertheless it is helpful to know exactly what the effective parameter represents there, especially when the parameters display somewhat odd properties such as those discussed in Secs. I and II A. Furthermore, by virtue of Eq. (12) the KK relations of the redefined parameter will now relate an unambiguous quantity. Although the parameter $\mu_{\mathrm{eff}}(\omega)$ no longer represents the effective permeability of the system *in general*, its meaning nevertheless coincides with the *particular* meaning of effective permeability in the long-wave limit $k \to 0$, according to the homogenization procedure [8].

The above procedure by Eqs. (12) and (13) is not unique in its ability to attribute an alternative physical meaning to the parameter $\mu_{\mathrm{eff}}(\omega)$ for all frequencies, however the procedure is quite general.

A. Split ring cylinders

Here the definition (12) will be used to give the parameter $\mu_{\mathrm{eff}}(\omega)$ of an array of split ring cylinders the alternative physical meaning discussed above for all (ω,k). As shall be shown, a consequence of this redefinition under the assumption of eigenmodal propagation is that the analytic continuation of the parameter $\mu_{\mathrm{eff}}(\omega)$ will approach unity, instead of $1-F$ as is the case for Eq. (3). Thus, the redefinition of the parameter by Eq. (12) here succeeds in redefining the parameter in the manner discussed at the introduction of this section. Equation (12) will therefore give a $\mu_{\mathrm{eff}}(\omega)$ with a frequency variation which obeys the conventional KK relations, and will display $\mathrm{Im}\ \mu_{\mathrm{eff}}(\omega) < 0$ for some frequencies while still representing a passive medium.

In the split ring cylinder metamaterial, we consider a polarization where $\mathbf{B}^{\mathrm{d}}_{\mathrm{av}}$ and $\mathbf{H}^{\mathrm{d}}_{\mathrm{av}}$ are parallel to the cylinder axes. Thus $\mu_{\mathrm{eff}}(\omega)$ is a scalar which according to Eq. (12) may be expressed as the ratio of the field quantities:

$$\mu_{\mathrm{eff}}(\omega) = \frac{B^{\mathrm{d}}_{\mathrm{av}}(\omega)}{\mu_0 H^{\mathrm{d}}_{\mathrm{av}}(\omega)} = \frac{1}{1 - M_{\mathrm{net}}/\bar{H}}. \tag{14}$$

Here we have solved for Eqs. (13a) and (13c) and inserted them into Eq. (12) under the assumption that the cylinders have thin walls of a nonmagnetic metal, and defined

$$M_{\mathrm{net}}(\omega) = \frac{F}{2\pi}\int_0^{2\pi} J(r,\phi)|_{r=R}d\phi, \tag{15}$$

which represents the net magnetization density. The constant F represents the volume fraction of the cylinder in a unit cell and J represents the current per cylinder length flowing on the cylinders with radius R. Under the assumption of eigenmodal propagation ($k \to \omega/c$ as $\omega \to \infty$) one has that $M_{\mathrm{net}}/\bar{H} \to 0$ as $\omega \to \infty$ on account of the conductivity of a metal tending to zero here. From Eq. (14) it therefore becomes clear that $\mu_{\mathrm{eff}}(\omega) \to 1$ as $\omega \to \infty$, meaning that it obeys the conventional KK-relations

$$\mathrm{Re}\ \mu_{\mathrm{eff}}(\omega) = 1 + \frac{2\mathcal{P}}{\pi}\int_0^\infty \frac{x\,\mathrm{Im}\ \mu_{\mathrm{eff}}(x)}{x^2-\omega^2}dx, \tag{16a}$$

$$\mathrm{Im}\ \mu_{\mathrm{eff}}(\omega) = -\frac{2\omega\mathcal{P}}{\pi}\int_0^\infty \frac{\mathrm{Re}\ \mu_{\mathrm{eff}}(x) - 1}{x^2-\omega^2}dx, \tag{16b}$$

provided that the resulting $\mu_{\mathrm{eff}}(\omega)$ is analytic.

By Eq. (16a) evaluated at $\omega = 0$ it is clear that one must have $\mathrm{Im}\ \mu_{\mathrm{eff}}(\omega) < 0$ for some frequencies when demanding $\mu_{\mathrm{eff}}(0) = 1$, as discussed in Sec. II A. Thus one observes that the parameter $\mu_{\mathrm{eff}}(\omega)$ found from Eq. (14) by solving for $M_{\mathrm{net}}(\omega)$ is quite different from Eq. (3). Both expressions (3) and (14) must nevertheless coincide in the limit $\omega \to 0$, since they both arise from valid homogenization procedures. In fact Eq. (14) becomes identical to Eq. (3) if $M_{\mathrm{net}}(\omega)$ is solved under the assumption of quasistatic interactions. As a side remark, herein lies the explanation of why different frequency variations are permitted for the effective parameters of a single metamaterial system, despite the existence of a unique continuation of an analytic parameter: There exists

a variety of possible definitions of $\mu_{\text{eff}}(\omega)$ which attain the particular meaning of the effective permeability in the limit $k \to 0$. Since these will generally be approximations of the effective permeability in the long-wavelength regime, each definition of $\mu_{\text{eff}}(\omega)$ may exhibit small, perhaps negligible, deviations from one another here. It follows that each of their respective continuations to higher frequencies, though unique, may nevertheless deviate significantly from one another.

We have demonstrated that the parameter $\mu_{\text{eff}}(\omega)$ for a split ring cylinder metamaterial may both take different frequency variations for large frequencies and obey different KK relations, without actually finding the net magnetization density $M_{\text{net}}(\omega)$ in Eq. (14). Solving $M_{\text{net}}(\omega)$ for all frequencies poses difficulties beyond the scope of this paper. However, in order to illustrate the findings discussed above, we shall now pursue a qualitative and slightly arbitrary approach, while referring the interested reader to the rigorous method presented for determining $\mu_{\text{eff}}(\omega)$ by Eqs. (12) and (13) in [8]. If the interaction between the cylinders is modeled quasistatically, straightforward application of Faraday's law [1,4] gives for the magnetization density

$$M_{\text{net}}^{\text{q.s.}}(\omega) = \frac{\omega^2 \bar{H} F}{\omega_0^2 - \omega^2(1-F) - i\omega\Gamma}, \tag{17}$$

where ω_0 is the resonance frequency determined by the cylinder radius and capacitance, and Γ is the response width determined by the conductivity and cylinder radius. The asymptote of Eq. (17) is erroneous in that it does not approach zero for infinite frequencies. Rather than calculate the exact dynamic $M_{\text{net}}(\omega)$ we instead correct the asymptote of the quasistatic solution by multiplying it with a Lorentzian response function with resonance outside the quasistatic limit $\omega_{\text{r}} \gg \omega_0$ and width Γ_{m}, according to

$$M_{\text{net}}^{\text{arb}}(\omega) = M_{\text{net}}^{\text{q.s.}}(\omega)\frac{\omega_{\text{r}}^2}{\omega_{\text{r}}^2 - \omega^2 - i\omega\Gamma_{\text{m}}}, \tag{18}$$

which therefore ensures that the corrected function is analytic. Although this choice is arbitrary, it nevertheless approximates the correct solution for $M_{\text{net}}(\omega)$ in the quasistatic regime and vacuum limit. Inserting Eq. (18) for $M_{\text{net}}(\omega)$ in Eq. (14) thus yields a $\mu_{\text{eff}}(\omega)$ which can be verified to be analytic, and which obeys Eq. (16).

Figure 3 compares the frequency variations of $\mu_{\text{eff}}(\omega)$ by Eq. (3) in Fig. 3(a) and by Eq. (14) in Fig. 3(b). One observes that both frequency variations are essentially equal for low frequencies, while differing for larger frequencies by having different asymptotes towards the vacuum limit. For the intermediate regime one observes a negative value of Im $\mu_{\text{eff}}(\omega)$ in Fig. 3(b) as predicted by Eq. (16), although the particular plot here does not represent the actual definition of $\mu_{\text{eff}}(\omega)$ by Eq. (14) owing to the arbitrary choice we have made for $M_{\text{net}}(\omega)$ by Eq. (18). The definition of $\mu_{\text{eff}}(\omega)$ according to Eq. (14) allows us to make sense of what a negative Im $\mu_{\text{eff}}(\omega)$ means: Since it does not occur in the long-wave region, it need not be interpreted to indicate gain (which would be nonsensical for a passive system), but represents a phase difference greater than π between the quantities $B_{\text{av}}^{\text{d}}(\omega)$ and $H_{\text{av}}^{\text{d}}(\omega)$.

Figure 3 is interesting in reference to the discussion in Sec. II A regarding the different asymptotic forms (5) that

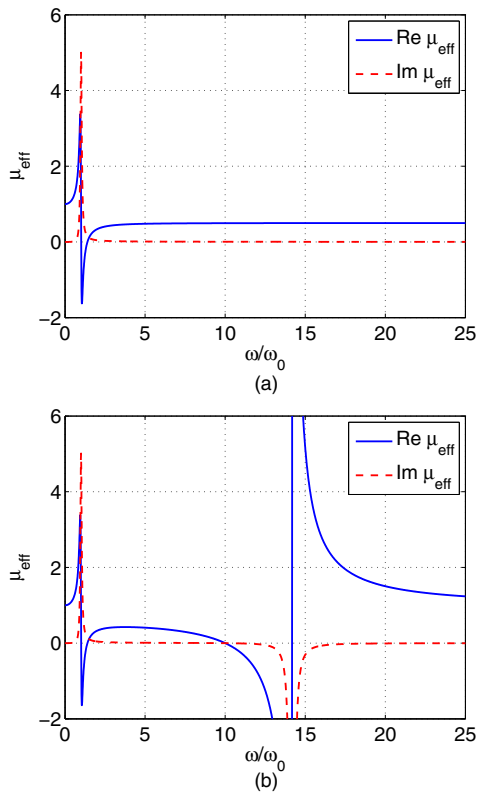

FIG. 3. (Color online) (a) The parameter $\mu_{\text{eff}}(\omega)$ for the split ring cylinder arrangement in [1], for a quasistatic model of the fields where the magnetization is given by Eq. (17). This gives the asymptote $\mu_{\text{eff}}(\omega) \to 1 - F$ when analytically continued to high frequencies, assuming a filling factor $F = 0.5$. Hence $\mu_{\text{eff}}(\omega)$ fulfills the generalized Kramers-Kronig relations (9) with $a = 0.5$. (b) The parameter $\mu_{\text{eff}}(\omega)$ for the same system, now using a modified magnetization density model $M_{\text{net}}^{\text{arb}}(\omega)$ according to Eq. (18). This results in $\mu_{\text{eff}}(\omega) \to 1$ as $\omega \to \infty$, as we expect for a dynamic model under eigenmodal propagation. Hence $\mu_{\text{eff}}(\omega)$ now fulfills the conventional Kramers-Kronig relations (1), and as a result displays Im $\mu_{\text{eff}}(\omega) < 0$ for some frequencies, as implied by Eq. (16).

can be present in a metamaterial. The three asymptotic forms discussed there encompass all possible dispersions for metamaterials *in the long-wave limit*. Contrary to the first impression one might get from Fig. 3, the parameters as given by Eqs. (3) and (14) in this sense have the same asymptotic form $\mu_{\text{eff}}(\omega) \to 1 - F$. Put more precisely, if one assumes that the long-wavelength regime is extended indefinitely by, e.g., reducing inclusion sizes so that $\omega_{\text{max}} \to \infty$ before we let $\omega \to \infty$, both Eqs. (3) and (14) would give $\mu_{\text{eff}}(\omega) \to 1 - F$. Hence, despite the different asymptotes in Figs. 3(a) and 3(b) for fixed ω_{max}, both parameters nevertheless carry the same dispersion freedom as characterized by Eq. (5), which leads to the property of emergent magnetism discussed in Sec. II A. This freedom is, however, manifested differently: In Fig. 3(a)

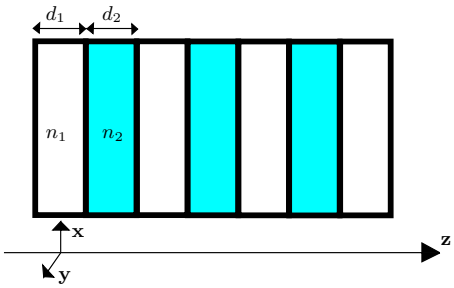

FIG. 4. (Color online) 1D photonic crystal with alternating dielectric layers where $n_1 < n_2$.

one observes a frequency variation which does not obey the conventional KK relations, while in Fig. 3(b) one observes $\mathrm{Im}\mu_{\mathrm{eff}}(\omega) < 0$ even though the metamaterial is passive.

B. 1D Bragg stack

This section presents a simpler approach by which an effective parameter may be redefined to have alternative physical meaning for all frequencies. We shall consider a 1D Bragg stack under eigenmodal propagation, for which the solution is straightforward. We choose as our parameter $n_{\mathrm{eff}}(\omega)$, which will give the effective refractive index in the long-wave limit. As will be shown, this parameter will depend on the z coordinate along the axis of periodicity for frequencies outside the long-wavelength regime. Hence, it will be possible to have a large number of different effective frequency variations for $n_{\mathrm{eff}}(\omega)$ at large frequencies, each corresponding to different values of z, which all nevertheless converge to the same dispersion in the long-wave limit. Some of these may exhibit $\mathrm{Im}\, n_{\mathrm{eff}}(\omega) < 0$ for some ω, while others will have only positive imaginary parts.

Consider the 1D photonic crystal as shown in Fig. 4. We imagine placing a current sheet at $z = 0$ in the layer of lowest refractive index n_1 in which the current alternates as $\mathbf{J}_s = J_0\hat{\mathbf{x}}$ (with the harmonic time variation suppressed). Noting that the resulting fields must be continuous over the interfaces, it follows that for $\omega \to 0$ the magnetic field approaches that of an effective continuous medium

$$\mathbf{H} = -\frac{J_0}{2}\exp(in_{\mathrm{eff}}\omega z/c)\hat{\mathbf{y}} \quad \text{for } 0 < z < \frac{d_1}{2}, \tag{19}$$

in terms of an effective index of refraction n_{eff}. Therefore, as $\omega \to 0$ the transfer function

$$G \equiv \frac{H(z)}{H(0^+)} \tag{20}$$

approaches that of a continuous medium:

$$G = \exp\left(in_{\mathrm{eff}}\frac{\omega}{c}z\right). \tag{21}$$

Motivated by the form of Eq. (21) we obtain our definition:

$$n_{z,\mathrm{eff}}(\omega) \equiv -\frac{ic}{\omega z}\ln G, \tag{22}$$

where G is given by Eq. (20). Now our parameter $n_{z,\mathrm{eff}}(\omega)$ is in general a quantity proportional to the logarithm of the transfer function in the medium: a quantity that has physical meaning for all frequencies. For low frequencies, this physical meaning coincides with that of the effective refractive index. The subscript z indicates that the transfer function evaluated at each value of z yields a different frequency variation. All of these converge to the same $n_{\mathrm{eff}}(0)$ as $\omega \to 0$, for which the analytic value may be calculated to be

$$n_{\mathrm{eff}}(0) = \sqrt{\frac{n_1^2 d_1 + n_2^2 d_2}{d_1 + d_2}}. \tag{23}$$

Provided the transfer function G does not have zeros in the upper complex half plane, our parameter $n_{z,\mathrm{eff}}(\omega)$ is analytic there while having the asymptote $n_{z,\mathrm{eff}}(\omega) \to 1$, and therefore obeys the conventional Kramers-Kronig relations.

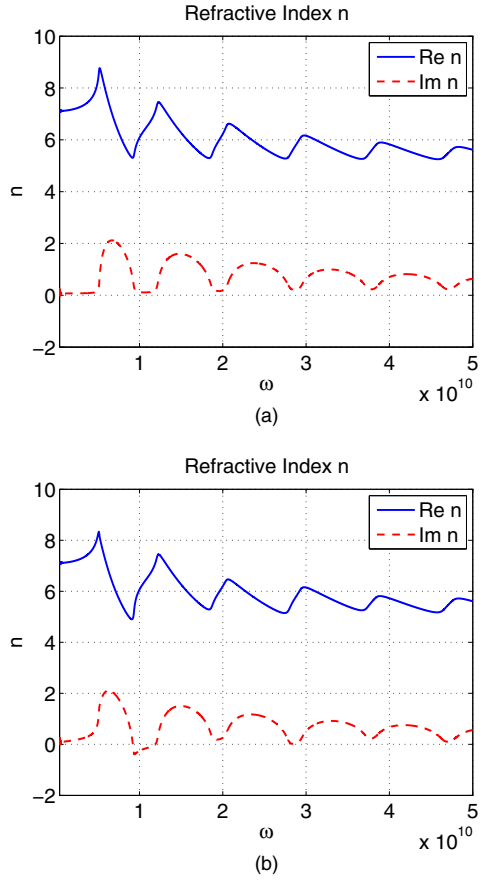

FIG. 5. (Color online) (a) The parameter $n_{z,\mathrm{eff}}(\omega)$ as given by Eq. (22) where $z = 5(d_1 + d_2)$, i.e., z is chosen within a lower index layer with index $n_1 = 1$. The higher index layer has $n_2 = 10 + 0.1i$. (b) The parameter $n_{z,\mathrm{eff}}(\omega)$ as given by Eq. (22) for the same photonic crystal, but where $z = 5.5(d_1 + d_2)$, i.e., z is chosen within a high index layer with index n_2. Notice that $\mathrm{Im}\, n_{\mathrm{eff}} < 0$ for a small bandwidth even though the photonic crystal is passive. This occurs as a result of a transfer function $G > 1$ in Eq. (22) through the accumulation of field in the high index layer.

Figure 5 displays two possible variations as given by Eq. (22) where z is chosen within a layer of the low index $n_1 = 1$ in Fig. 5(a) and where z is chosen within a layer of the higher index $n_2 = 10 + 0.1i$ in Fig. 5(b). The transfer function (20) has been calculated by use of the relevant transfer matrices and boundary conditions. The indices n_1 and n_2 have been assumed constant with respect to frequency for simplicity. This means that for $\omega \to \infty$ one has $n_{z,\mathrm{eff}}(\omega) \to n_\infty \neq 1$. As a side remark, we note that a similar effective parameter definition for the effective refractive index with a similar plot as that in Fig. 5(a) is proposed in [12]. Figures 5(a) and 5(b) give slightly different variations: Fig. 5(a) has $\mathrm{Im}\, n_{z,\mathrm{eff}}(\omega) \geqslant 0$ for all ω, while Fig. 5(b) displays $\mathrm{Im}\, n_{z,\mathrm{eff}}(\omega) < 0$ for a small bandwidth. This demonstrates that the parameter may be redefined to give frequency variations both with and without $\mathrm{Im}\, n_{\mathrm{eff}}(\omega) < 0$. This corresponds to the multiple ways in which one may define a physical quantity that is meaningful for all frequencies, which at the same time approximates the refractive index of the medium for small frequencies.

In light of the physical definition of $n_{z,\mathrm{eff}}(\omega)$, we notice that the negative imaginary part in Fig. 5(b) has nothing to do with gain: A negative value of $\mathrm{Im}\, n_{z,\mathrm{eff}}(\omega)$ in Eq. (22) corresponds to a transfer function greater than unity. This occurs as a result of a Fabry-Perot interference occurring between the low and high index layers, leading to a local accumulation of field in the high index layer where the transfer function is evaluated.

IV. CONCLUSIONS

In this paper we have identified examples of metamaterial effective parameters that do not follow conventional dispersion constraints, as represented by the Kramers-Kronig relations. This freedom in dispersion has been characterized through the identification of the three asymptotes which the analytic continuation of the effective parameters $\mu_{\mathrm{eff}}(\omega)$ and $\epsilon_{\mathrm{eff}}(\omega)$ may approach. The space of possible dispersions in metamaterials have been identified through generalizing the Kramers-Kronig relations for the three possible asymptotes. The possibility of redefining metamaterial parameters so as to achieve a certain physical meaning for all frequencies has also been presented. Such an approach may be both aesthetically and practically motivated. Regarding the former the Kramers-Kronig relations of the redefined parameters generally relate an unambiguous physical quantity. Regarding the latter, it can be useful to have a clear definition of what the effective parameters represent for large frequencies, as in the two case examples considered where the occurrence of negative imaginary parts in the effective parameters of two passive metamaterials has been given an intuitive physical explanation.

[1] J. Pendry, A. Holden, D. Robbins, and W. Stewart, IEEE Trans. Microwave Theory Tech. **47**, 2075 (1999).

[2] G. Eleftheriades, A. Iyer, and P. Kremer, IEEE Trans. Microwave Theory Tech. **50**, 2702 (2002).

[3] J. D. Jackson, *Classical Electrodynamics*, 3rd ed. (Wiley, New York, 1999).

[4] C. A. Dirdal and J. Skaar, Phys. Rev. A **88**, 033834 (2013).

[5] R. Marqués, F. Medina, and R. Rafii-El-Idrissi, Phys. Rev. B **65**, 144440 (2002).

[6] R. Marqués, J. D. Baena, J. Martel, F. Medina, F. Falcone, M. Sorolla, and F. Martín, Proc. ICEAA **3**, 439 (2003).

[7] F. Capolino, *Theory and Phenomena of Metamaterials*, Metamaterials Handbook (CRC, Boca Raton, 2009).

[8] A. Alù, Phys. Rev. B **84**, 075153 (2011).

[9] A. Alù, Phys. Rev. B **83**, 081102 (2011).

[10] L. D. Landau, L. P. Pitaevskii, and E. M. Lifshitz, *Electrodynamics of Continuous Media*, 2nd ed., Course of Theoretical Physics Vol. 8 (Butterworth-Heinemann, Washington, DC, 1984).

[11] O. Brune, http://hdl.handle.net/1721.1/10661 (1931).

[12] Y. Liu, S. Guenneau, and B. Gralak, Phys. Rev. B **88**, 165104 (2013).

[13] L. P. Pitaevskii, Int. J. Quantum Chem. **112**, 2998 (2012).

[14] M. G. Silveirinha, Phys. Rev. B **83**, 165119 (2011).

[15] M. G. Silveirinha, Phys. Rev. B **75**, 115104 (2007).

Paper V

Higher order terms in metamaterial homogenization

Submitted for journal publication

Arxiv: 1701.01708

Higher order terms in metamaterial homogenization

Christopher A. Dirdal,[1] Hans Olaf Hågenvik,[1] Haakon Aamot Haave,[1] and Johannes Skaar[1]
[1] *Department of Electronic Systems, NTNU-Norwegian University of Science and Technology, NO-7491 Trondheim, Norway*
(Dated: March 23, 2017)

The higher order terms in the expansion of the macroscopic polarization, above the electrical quadrupole, are commonly neglected in metamaterial homogenization due to their typically small magnitudes. We show that they nevertheless are generally significant when second order spatial dispersive effects, such as the magnetic response, are considered. In this respect, they are generally equally important as the polarization, magnetization and quadrupole terms, and should not be neglected. The article discussions are facilitated by both analytical approaches and numerical simulations using the plane wave expansion method for the case of a distributed plane wave source.

PACS numbers: 78.67.Pt, 78.20.Ci, 78.20.-e, 42.25.Bs, 41.20.Jb, 42.70.-a,42.70.Qs, 41.20.-q

I. INTRODUCTION

The structural freedom in metamaterials have spurred renewed interest into homogenization theories. These are theories that allow for the formulation of *effective* macroscopic Maxwell's equations in structured media from the *exact* microscopic ones. The macroscopic equations have effective plane wave solutions in materials with complex structures, where dimensions are well below the wavelength. Despite the similarities between conventional and metamaterial homogenization, it has become evident that certain differences need to be taken into consideration [1–9]; in particular, the importance of spatial dispersion. In this paper we would like to add another characteristic feature of metamaterial homogenization to the list: That higher order terms in the expansion of macroscopic polarization, *above the electric quadrupole*, generally have physical significance with respect to the magnetic response of the system, despite often being far smaller in magnitude than the lower orders. Hence, some of the underlying assumptions regarding the non-importance of the electrical quadrupole *and higher order terms* in both classical [10–13] and more recent [2, 3, 8, 9] treatments on homogenization, should in some cases be reconsidered when applied to metamaterials.

Faced with the wide variety of proposed homogenization theories in literature, it seems reasonable to make classical formulations by Landau-Lifshitz, Casimir, Russakoff and Jackson [10–14] our starting point, which have parallels among more recent metamaterial treatments such as [2, 8]. The article is structured in the following manner: In Sec. II we present the needed background on the homogenization procedure and the multipoles of the macroscopic polarization according to Russakoff-Jackson homogenization [12, 13]. Section III then presents the needed background on the constitutive relations between the macroscpic fields and multipole quantities, as well as the effective permeability and permittivity functions of the Casimir and Landau-Lifshitz formulations [11, 14]. Both of these sections lead up to Sec. IV where we demonstrate how the higher order terms, *above the electric quadrupole*, may be of general importance. Analytical results and simulations are shown. Appendix A, as a side-remark, presents an interesting case where the inclusion of the higher order terms leads to increased locality of the effective permittivity and permeability.

II. HOMOGENIZATION AND MULTIPOLES

The microscopic Maxwell's equations are

$$\nabla \times \mathbf{e}(\mathbf{r}) = i\omega \mathbf{b}(\mathbf{r}), \tag{1a}$$

$$\nabla \times \frac{\mathbf{b}(\mathbf{r})}{\mu_0} = -i\omega\epsilon_0 \mathbf{e}(\mathbf{r}) + \mathbf{j}(\mathbf{r}) + \mathbf{J}_{\text{ext}}(\mathbf{r}), \tag{1b}$$

$$\nabla \cdot \mathbf{e}(\mathbf{r}) = \frac{\varrho(\mathbf{r}) + \rho_{\text{ext}}(\mathbf{r})}{\epsilon_0}, \tag{1c}$$

$$\nabla \cdot \mathbf{b}(\mathbf{r}) = 0, \tag{1d}$$

where $\mathbf{e}(\mathbf{r})$ and $\mathbf{b}(\mathbf{r})$ represent the microscopic electric field and magnetic flux density, respectively, $\mathbf{j}(\mathbf{r})$ and $\varrho(\mathbf{r})$ represent the induced current and charge densities, respectively, and $\mathbf{J}_{\text{ext}}(\mathbf{r})$ and $\rho_{\text{ext}}(\mathbf{r})$ represent the source current and charge densities. Harmonic fields with angular frequency ω have been assumed, and the $\mathrm{e}^{-i\omega t}$ dependence is suppressed. For simplicity, we will throughout this article consider structures consisting of non-magnetic inclusions. While generalization is not very complicated, the simplifications lead to more transparent expressions. The medium is assumed to be passive (or in thermal equilibrium in the absence of the field under study [11]), i.e., we exclude gain media.

The homogenization method described in Russakoff [12] and Jackson [13] can be applied relatively straightforwardly to the case of metamaterials, replacing molecules by metamaterial cells. The cells can be those resulting from a partition of the metamaterial into small volumes (compared to the spatial variation of the source). For the special case where the metamaterial is a periodic structure, the cells are chosen to be the smallest unit cells. The Russakoff-Jackson formulation of effective, macroscopic fields relies on an averaging procedure of the form

$$\langle F(\mathbf{r}) \rangle = \int f(\mathbf{r}') F(\mathbf{r} - \mathbf{r}') \mathrm{d}^3 r', \tag{2}$$

where F is the function to be averaged, and $f(\mathbf{r})$ is an arbitrary test function that varies slowly over the size of a cell (and may extend over several such cells) [12, 13]. We now specialize to periodic metamaterials, and consider only a single spatial Fourier component of the source, i.e.,

$$\mathbf{J}_{\text{ext}} = \bar{\mathbf{J}}_{\text{ext}} \mathrm{e}^{i\mathbf{k}\cdot\mathbf{r}}, \tag{3a}$$

$$\rho_{\text{ext}} = \overline{\rho}_{\text{ext}} \mathrm{e}^{i\mathbf{k}\cdot\mathbf{r}}, \tag{3b}$$

where $\bar{\mathbf{J}}_{\text{ext}}$ and $\overline{\rho}_{\text{ext}}$ are constant. Then the averaging procedure (2) can be written

$$\langle F(\mathbf{r})\rangle = \bar{F}\mathrm{e}^{i\mathbf{k}\cdot\mathbf{r}}, \tag{4a}$$

where

$$\bar{F} = \frac{f(\mathbf{k})}{V}\int_V F(\mathbf{r})\mathrm{e}^{-i\mathbf{k}\cdot\mathbf{r}}\mathrm{d}^3r, \tag{4b}$$

and the integral is taken over the volume of a unit cell V of the periodic medium (see for example [3]). In arriving at this expression we have made use of the fact that the microscopic fields are Bloch waves of the form

$$F(\mathbf{r}) = U_F(\mathbf{r})\mathrm{e}^{i\mathbf{k}\cdot\mathbf{r}}, \tag{5}$$

where $U_F(\mathbf{r})$ has the same periodicity as the metamaterial. Moreover, we have assumed that the test function in (2) is band-limited, or more precisely, its Fourier transform $f(\mathbf{k})$ is required to vanish outside the first Brillouin zone. This is approximately the case for any sufficiently smooth function $f(\mathbf{r})$ which extends over several unit cells. The operation (4b) essentially represents the spatial average of the periodic modulation $U_F(\mathbf{r})$. In the remainder of this article, we will consider small $\mathbf{k}$'s, well inside the first Brillouin zone. Moreover, we choose the test function such that $f(\mathbf{k}) \approx 1$ there. Then the averaging procedure (4) corresponds to that utilized in Refs. [2, 8].

Application of the averaging procedure (4) to (1a)-(1b), and using the fact that $\mathbf{e}\mathrm{e}^{-i\mathbf{k}\cdot\mathbf{r}}$ and $\mathbf{b}\mathrm{e}^{-i\mathbf{k}\cdot\mathbf{r}}$ are periodic give macroscopic Maxwell's equations

$$i\mathbf{k}\times\mathbf{E} = i\omega\mathbf{B}, \tag{6a}$$

$$i\mathbf{k}\times\frac{\mathbf{B}}{\mu_{\mathbf{0}}} = -i\omega\epsilon_0\mathbf{E} - i\omega\langle\mathbf{p}\rangle + \mathbf{J}_{\text{ext}}, \tag{6b}$$

having identified $\mathbf{j} = -i\omega\mathbf{p}$ and defined macroscopic fields $\mathbf{E} = \langle\mathbf{e}\rangle$ and $\mathbf{B} = \langle\mathbf{b}\rangle$. The effective electromagnetic response of the system is contained in the induced current $-i\omega\langle\mathbf{p}\rangle$, which we shall now expand into multipoles [8, 15]. With the expansion $\exp(-i\mathbf{k}\cdot\mathbf{r}) \approx 1 - i\mathbf{k}\cdot\mathbf{r} - (\mathbf{k}\cdot\mathbf{r})^2/2 + O(k^3)$ we obtain from (4) (to the second order in k)

$$\langle\mathbf{p}\rangle = \frac{\mathrm{e}^{i\mathbf{k}\cdot\mathbf{r}}}{V}\int_V \mathbf{p}\mathrm{e}^{-i\mathbf{k}\cdot\mathbf{r}}\mathrm{d}^3r \tag{7}$$

$$= \frac{\mathrm{e}^{i\mathbf{k}\cdot\mathbf{r}}}{V}\cdot\left(\int_V \mathbf{p}\mathrm{d}^3r - i\mathbf{k}\cdot\int_V \mathbf{r}\mathbf{p}\mathrm{d}^3r - \frac{1}{2}\int_V(\mathbf{k}\cdot\mathbf{r})^2\mathbf{p}\mathrm{d}^3r\right)$$

$$\equiv \mathbf{P} - \frac{\mathbf{k}\times\mathbf{M}}{\omega} - i\mathbf{k}\cdot\mathbf{Q} + \mathbf{R}, \tag{8}$$

where

$$\mathbf{P} = \frac{\mathrm{e}^{i\mathbf{k}\cdot\mathbf{r}}}{V}\int_V \mathbf{p}\mathrm{d}^3r, \tag{9a}$$

$$\mathbf{M} = -\frac{i\omega}{2}\frac{\mathrm{e}^{i\mathbf{k}\cdot\mathbf{r}}}{V}\int_V \mathbf{r}\times\mathbf{p}\mathrm{d}^3r, \tag{9b}$$

$$\mathbf{Q} = \frac{1}{2}\frac{\mathrm{e}^{i\mathbf{k}\cdot\mathbf{r}}}{V}\int_V (\mathbf{r}\mathbf{p}+\mathbf{p}\mathbf{r})\mathrm{d}^3r, \tag{9c}$$

$$\mathbf{R} = -\frac{1}{2}\frac{\mathrm{e}^{i\mathbf{k}\cdot\mathbf{r}}}{V}\int_V (\mathbf{k}\cdot\mathbf{r})^2\mathbf{p}\mathrm{d}^3r. \tag{9d}$$

and we have decomposed the tensor $\mathbf{rp}$ into its antisymmetric and symmetric parts,

$$\begin{aligned}\mathbf{k}\cdot\mathbf{r}\mathbf{p} &= \mathbf{k}\cdot(\mathbf{r}\mathbf{p}-\mathbf{p}\mathbf{r})/2 + \mathbf{k}\cdot(\mathbf{r}\mathbf{p}+\mathbf{p}\mathbf{r})/2\\ &= -\mathbf{k}\times\mathbf{r}\times\mathbf{p}/2 + \mathbf{k}\cdot(\mathbf{r}\mathbf{p}+\mathbf{p}\mathbf{r})/2.\end{aligned} \tag{10}$$

In addition to the polarization vector $\mathbf{P}$, magnetization vector $\mathbf{M}$, and quadrupole tensor $\mathbf{Q}$, we have included an extra term $\mathbf{R}$ which denotes the so-called *higher order terms* discussed in the introduction, corresponding to electric octupole and magnetic quadrupole. In the following, we will often combine $\mathbf{M}$ and $\mathbf{Q}$ into a combined tensor $\mathbf{Q}^{\text{tot}}$:

$$\mathbf{Q}^{\text{tot}} = \frac{\mathrm{e}^{i\mathbf{k}\cdot\mathbf{r}}}{V}\int_V \mathbf{r}\mathbf{p}\mathrm{d}^3r, \tag{11}$$

such that

$$i\mathbf{k}\cdot\mathbf{Q}^{\text{tot}} = \frac{\mathbf{k}\times\mathbf{M}}{\omega} + i\mathbf{k}\cdot\mathbf{Q}. \tag{12}$$

III. CONSTITUTIVE RELATIONS

The aim of a homogenization procedure is often to arrive at effective parameters or tensors ϵ and μ that describe the effective electromagnetic response of a linear metamaterial. In the so-called Casimir formulation, common among textbook treatments such as [13], the effective parameters are defined

$$\epsilon'(\omega,\mathbf{k})\epsilon_0\mathbf{E} = \epsilon_0\mathbf{E} + \mathbf{P}, \tag{13a}$$

$$[1-\mu'^{-1}(\omega,\mathbf{k})]\mathbf{B} = \mu_0\mathbf{M}. \tag{13b}$$

The Casimir formulation thus places $\langle\mathbf{p}\rangle$ *partially* in a permittivity $\epsilon'(\omega,\mathbf{k})$ and *partially* in $1-\mu'^{-1}(\omega,\mathbf{k})$, where $\mu'(\omega,\mathbf{k})$ is a permeability. Evidently the terms $-i\mathbf{k}\cdot\mathbf{Q}$ and $\mathbf{R}$ in (8) have been excluded in this definition, although sometimes $i\mathbf{k}\cdot\mathbf{Q}$ is included in the permittivity [14].

Another possible effective parameter definition is [11]

$$\epsilon_0\epsilon(\omega,\mathbf{k})\mathbf{E} = \epsilon_0\mathbf{E} + \langle\mathbf{p}\rangle, \tag{14}$$

where *all* of $\langle\mathbf{p}\rangle$, including $\mathbf{Q}$ and $\mathbf{R}$, is described by a total permittivity $\epsilon(\omega,\mathbf{k})$. This is called the Landau-Lifshitz formulation, and was used e.g. by Silveirinha [2].

We shall proceed with the Landau-Lifshitz formulation, and return to the Casimir formulation later on.

In a linear medium, we can express multipole densities (9) with constitutive relations

$$P_i = \epsilon_0\chi_{ij}E_j + \xi_{ikj}k_kE_j + \eta_{iklj}k_kk_lE_j, \tag{15a}$$
$$Q^{\rm tot}_{ik} = i\zeta_{ikj}E_j + i\gamma_{iklj}k_lE_j, \tag{15b}$$
$$R_i = \psi_{iklj}k_kk_lE_j, \tag{15c}$$

where summation over repeated indices is implied. In (15) we have included the necessary orders of k such that $\langle\mathbf{p}\rangle$ is second order in k upon their insertion in (8). Magneto-electric coupling is included in terms of the tensor elements ξ_{ikj} and ζ_{ikj}. From (8), (14) and (15) we obtain

$$\epsilon_{ij}(\omega,\mathbf{k}) - \delta_{ij} = \chi_{ij} + (\xi_{ikj}+\zeta_{ikj})k_k/\epsilon_0 + (\psi_{iklj}+\gamma_{iklj}+\eta_{iklj})k_kk_l/\epsilon_0. \tag{16}$$

While it may be convenient to have only a single constitutive tensor $\epsilon(\omega,\mathbf{k})$, it is often desirable to express the magnetic response more explicitly by introducing a permeability tensor. It is well known that the permeability is related to the second order term in (16) [2, 11]. Observe that the macroscopic quantities $\mathbf{B}$ and $\mathbf{E}$ are left invariant upon the transformation

$$-i\omega\langle\mathbf{p}\rangle \to -i\omega\hat{\mathbf{P}} + i\mathbf{k}\times\hat{\mathbf{M}}, \tag{17}$$

where the new polarization $\hat{\mathbf{P}}$ and magnetization $\hat{\mathbf{M}}$ are arbitrarily chosen. We can express the left hand side in terms of the non-local tensor $\epsilon(\omega,\mathbf{k})$ by (14), and the right hand side in terms of two new tensors ϵ and $1-\mu^{-1}$, in order to obtain

$$\epsilon(\omega,\mathbf{k}) = \epsilon - \frac{c^2}{\omega^2}\mathbf{k}\times[1-\mu^{-1}]\times\mathbf{k}. \tag{18}$$

Here, we have used $\hat{\mathbf{M}} = \mu_0^{-1}(1-\mu^{-1})\mathbf{B}$ and (6a). If we choose the coordinate system such that $\mathbf{k} = k\hat{\mathbf{x}}$, then (18) may be expressed

$$\epsilon(\omega,\mathbf{k}) = \epsilon + \frac{k^2c^2}{\omega^2}\begin{bmatrix}0 & 0 & 0\\ 0 & (1-\mu^{-1})_{33} & -(1-\mu^{-1})_{32}\\ 0 & -(1-\mu^{-1})_{23} & (1-\mu^{-1})_{22}\end{bmatrix}. \tag{19}$$

We now assume a non-gyrotropic medium[1], such that the first order term in (16) vanishes. Comparing (19) with (16) lets us find

$$1-\mu^{-1} = \omega^2\mu_0\cdot \begin{bmatrix}\cdot & \cdot & \cdot\\ \cdot & (\psi_{3113}+\gamma_{3113}+\eta_{3113}) & -(\psi_{3112}+\gamma_{3112}+\eta_{3112})\\ \cdot & -(\psi_{2113}+\gamma_{2113}+\eta_{2113}) & (\psi_{2112}+\gamma_{2112}+\eta_{2112})\end{bmatrix}, \tag{20}$$

if we choose to put $\epsilon_{22} = 1+\chi_{22}$, $\epsilon_{33} = 1+\chi_{33}$, $\epsilon_{23} = \chi_{23}$, and $\epsilon_{32} = \chi_{32}$. The missing entries in (20) are a result of the fact that $\mathbf{B}$ is transverse, $\mathbf{k}\cdot\mathbf{B} = 0$, and that only the transversal part of $\hat{\mathbf{M}}$ contributes to the induced current.

In principle the magnetization and therefore permeability can be defined in an infinite number of ways, by including any given part of the transversal, induced current. However, the above identification is somewhat natural, as the magnetization term includes all transversal, induced current, except a part possibly induced by the longitudinal component of the electric field. Eq. (20) is a generalization of the relation in Ref. [2]. Note that the Casimir permeability is related to part of the γ_{ikjl} tensor, and may therefore also be viewed as a second order spatial dispersion effect.

IV. IMPORTANCE OF HIGHER ORDER TERMS

The tensors ψ, γ and η relate to $\mathbf{R}$, $\mathbf{Q}^{\rm tot}$ and $\mathbf{P}$, respectively, in the manner shown in (15). As seen in (16) these contribute on an equal footing to the second order effects of $\epsilon(\omega,\mathbf{k})$ [6], which may be interpreted as describing the magnetic response of the system according to (20). While it is known that the quadrupole tensor $\mathbf{Q}$ may be significant [4, 5], we shall now show that $\mathbf{R}$ too is generally physically important.

Despite the common practice of neglecting $\mathbf{R}$, and therefore ψ, in the multipole expansion (8), the tensors ψ, $\gamma/2$ and η often turn out to be on the same order of magnitude for metamaterial structures. Before demonstrating this from numerical simulations, we may first gain some further intuition by considering (9) and (11) for a plane-wave dependence of the field[2]

$$\mathbf{e}(\mathbf{r}) = \overline{E}e^{i\mathbf{k}\cdot\mathbf{r}}\hat{\mathbf{y}}, \tag{21}$$

and $\mathbf{k} = k\hat{\mathbf{x}}$. The following relationship may then be observed

$$\frac{2R_2}{k^2E_2} = i\frac{\partial}{\partial k}\left\{\frac{Q^{\rm tot}_{21}}{E_2}\right\} = \frac{\partial^2}{\partial k^2}\left\{\frac{P_2}{E_2}\right\}, \tag{22}$$

which gives

$$\psi_{2112} = -\frac{\gamma_{2112}}{2} = \eta_{2112} \tag{23}$$

[1] For non-gyrotropic media, i.e., when there exists a center of symmetry, we have $\epsilon(\omega,-\mathbf{k}) = \epsilon(\omega,\mathbf{k})$ [10, 11], which implies that odd-order terms in (16) must be zero. Note that there is no way to distinguish between ξ_{ikj} and ζ_{ikj} in the expression for $\epsilon_{ij}(\omega,\mathbf{k})$; only the sum appears. In other words, even though the microscopic physics may be dependent on these tensors separately, only the sum matters for the macroscopic fields $\mathbf{E}$ and $\mathbf{B}$. A similar comment is valid when considering $\psi_{iklj}+\gamma_{iklj}+\eta_{iklj}$; only the sum matters macroscopically. We could for instance therefore choose to put $\psi_{iklj} = \eta_{iklj} = 0$ and include their contribution in γ_{iklj}, without altering $\mathbf{E}$ and $\mathbf{B}$.

[2] The wave equation (25) reveals that this solution is approached for a source $\mathbf{J}_{\rm ext} = \overline{J}_{\rm ext}e^{ikx}\hat{\mathbf{y}}$ in the limit $\omega \ll ck$. Alternatively, the solution is approached for high frequencies where the permittivity tends to unity.

when compared with (15). Here ψ_{2112} is proportional with the quantity R_2/E_2, while γ_{2112} is related to the first order k-dependence of the quantity Q_{21}^{tot}/E_2, and η_{2112} is related with the second order k-dependence of the quantity P_2/E_2. With this in mind we may qualify the physical importance of $\mathbf{R}$. From (8) and (9) it is evident that the magnitude of $\mathbf{R}$ may not be significant in comparison to the terms associated with $\mathbf{P}$, $\mathbf{M}$ and $\mathbf{Q}$, since $\mathbf{R}$ results from a higher order term of the exponential in $\mathbf{k}\cdot\mathbf{r}$. Nevertheless, this does not mean that it is insignificant when the *second order effects* of $\epsilon(\omega,\mathbf{k})$ (i.e. the magnetic response) are concerned, as seen from (22)-(23). Before moving on, note that since $\mathbf{k}\perp\mathbf{p}(\mathbf{r})$ due to (21), one finds using (10) that

$$\frac{\mathbf{k}\times\mathbf{M}}{\omega} = i\mathbf{k}\cdot\mathbf{Q}, \tag{24}$$

revealing that $\mathbf{M}$ and $\mathbf{Q}$ contribute equally to γ_{iklj} in (15b).

Let us now consider ψ_{2112}, γ_{2112} and η_{2112} for a metamaterial consisting of periodically arranged dielectric cylinders in vacuum. These parameters give the component μ_{33} according to (20). The microscopic dielectric function $\varepsilon(\mathbf{r})$ in a unit cell is displayed in Fig. 1a. Solving the multiple unknowns in (15) generally requires multiple equations. We therefore calculate $\mathbf{E}$, $\mathbf{P}$, $\mathbf{Q}^{\text{tot}}$, and $\mathbf{R}$ by solving $\mathbf{p}=\epsilon_0(\varepsilon(\mathbf{r})-1)\mathbf{e}$ for two choices of $\bar{\mathbf{J}}_{\text{ext}}$, perpendicular and parallel to $\mathbf{k}$, respectively. Utilizing the Floquet property of the source (3) and field (5), a plane wave expansion method can be used to solve the wave equation

$$\nabla\times\nabla\times\mathbf{e} - \frac{\omega^2}{c^2}\varepsilon(\mathbf{r})\mathbf{e} = i\omega\mu_0\mathbf{J}_{\text{ext}}, \tag{25}$$

by inserting Fourier series representations of $\mathbf{e}(\mathbf{r})$, $\varepsilon(\mathbf{r})$, and $\mathbf{J}_{\text{ext}}(\mathbf{r})$. Solutions for the microscopic field $\mathbf{e}(\mathbf{r})$ are then readily found numerically for a given number of Fourier coefficients in the series representations. In order to extract the coefficient parameters in (15), the field quantities $\mathbf{E}$, $\mathbf{P}$, $\mathbf{Q}^{\text{tot}}$, and $\mathbf{R}$ are calculated for three values of k so that first and second order derivatives wrt. k of appropriate quantities can be obtained. By application of this method to the dielectric cylinder in Fig. 1a, the parameter values displayed in Table I are obtained. Here we use normalized parameters: Frequency $\omega a/c = 0.2\pi$ and wavevector $\mathbf{k}a = 0.2\hat{\mathbf{x}}$. We have used $91\times91 = 8281$ spatial harmonics. We observe that ψ_{2112}, $\gamma_{2112}/2$ and η_{2112} are all on the same order of magnitude, similar to what was found in (23). Using a finite number of spatial

$\psi_{2112}/\epsilon_0 a^2$	-0.060
$\gamma_{2112}/\epsilon_0 a^2$	0.19
$\eta_{2112}/\epsilon_0 a^2$	-0.048

TABLE I: Parameter values in (15) for dielectric annulus.

harmonics corresponds to performing a *low-pass filtering* of Fig. 1a. The selection of spatial harmonics is performed by a truncation and subsequent application of a Blackman-Harris window in the Fourier domain. Thus, the *actual* structure corresponding to the parameter values in Table I is found by inverse-Fourier transforming the finite coefficient series representation of $\varepsilon(\mathbf{r})$, as given in Fig. 1b: An annulus with slightly rounded edges.

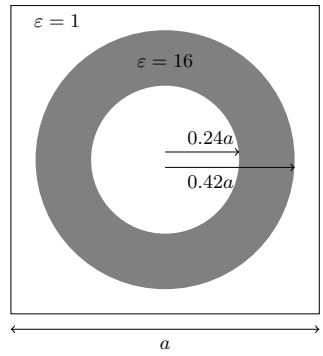

(a)

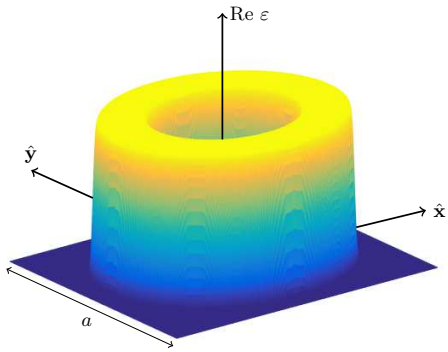

(b)

FIG. 1: (a) Dielectric annulus in vacuum with microscopic permittivity $\varepsilon = 16$. (b) Inverse Fourier transform of finite series representation of $\varepsilon(\mathbf{r})$, having used 91×91 coefficients. As a result of having used a finite number of coefficients, the edges become smoothened, corresponding to low-pass filtering of (a).

Using (20) we may calculate

$$1-\mu_{33}^{-1} = \left(\frac{\omega a}{c}\right)^2\left(\frac{\psi_{2112}}{\epsilon_0 a^2}+\frac{\gamma_{2112}}{\epsilon_0 a^2}+\frac{\eta_{2112}}{\epsilon_0 a^2}\right) = 0.0345, \tag{26}$$

for the periodic cylinder metamaterial having inserted the simulation values. Eq. (26) allows us to observe the physical importance of $\mathbf{R}$: Since the parameter ψ_{2112} is on the same order of magnitude as η_{2112} and $\gamma_{2112}/2$, one cannot neglect $\mathbf{R}$ without incurring significant error.

Also note that the second order term of $\mathbf{P}$ should not be neglected.

Consider Fig. 2, which shows the real and imaginary part of the microscopic polarization $\mathbf{p}(\mathbf{r})$ in the dielectric annulus. We may interpret the imaginary and real parts as originating individually from the first and second terms in the expansion of the source (3) for $ka \ll 1$, respectively:

$$\mathbf{J}_{\text{ext}} \approx \bar{\mathbf{J}}_{\text{ext}} + i\mathbf{k}\cdot\mathbf{r}\bar{\mathbf{J}}_{\text{ext}} + O(k^2). \tag{27}$$

For the values in Table I the source amplitude $\bar{\mathbf{J}}_{\text{ext}}$ has been chosen to be real, and from (25) one observes that if both $\mathbf{J}_{\text{ext}}$ and $\varepsilon(\mathbf{r})$ are real, then $\mathbf{e}(\mathbf{r})$ and $\mathbf{p}(\mathbf{r}) = \epsilon_0(\varepsilon(\mathbf{r}) - 1)\mathbf{e}(\mathbf{r})$ are imaginary. Hence Fig. 2b corresponds with the first, constant source term in the expansion (27). Similarly, the field distribution in Fig. 2a thus arises from the second, nonconstant source term, and is less dominant due to $ka \ll 1$. From (4) and (9) it therefore follows that $\mathbf{E}$ and $\mathbf{P}$ are dominated by their imaginary parts, and it follows from (15) that the parameters $\psi_{2112}, \gamma_{2112}$ and η_{2112} are then dominated by their *real* parts for the dielectric annulus.

In metamaterial applications it is most often of interest to work with inclusions made of conducting materials, rather than purely dielectric structures such as those considered so far. To model this we consider a complex microscopic permittivity

$$\varepsilon = 1 + i16, \tag{28}$$

within the same ring structure as pictured in Fig. 1a. Applying otherwise the same parameters as those leading to Table I, now yields the numerical values of Table II.

$\psi_{2112}/\epsilon_0 a^2$	$-0.066 - i0.048$
$\gamma_{2112}/\epsilon_0 a^2$	$0.011 + i0.17$
$\eta_{2112}/\epsilon_0 a^2$	$-0.055 - i0.023$

TABLE II: Parameter values in (15) for a (poorly) conducting annulus of the same geometry as that pictured in Fig. 1.

Now that ε is complex, the real and imaginary parts of the microscopic polarization $\mathbf{p}(\mathbf{r})$ each arise from a *combination* of the source terms $\bar{\mathbf{J}}_{\text{ext}}$ and $i\mathbf{k}\cdot\mathbf{r}\bar{\mathbf{J}}_{\text{ext}}$, as may be seen from (25). Hence Re $\mathbf{p}(\mathbf{r})$ and Im $\mathbf{p}(\mathbf{r})$ are roughly on the same order of magnitude, and therefore so are the real and imaginary parts of $\psi_{2112}, \gamma_{2112}/2$ and η_{2112}.

Assuming dimensions $a \geq 1\mu$m, the relation $\varepsilon = 1 + i\sigma/\epsilon_0\omega$ reveals that the parameter choice (28) and the given normalized frequency correspond with $\sigma \leq 2.7 \cdot 10^4$ Sm^{-1}. This conductivity is not very large. In the limit that $\sigma \to \infty$, however, we know that the electrostatic field vanishes within the conducting ring, leaving only that part of the field distribution which comes from the nonconstant source term $i\mathbf{k}\cdot\mathbf{r}\bar{\mathbf{J}}_{\text{ext}}$; i.e. a polarization resembling that of Fig. 2a. Such a cylinder-symmetric

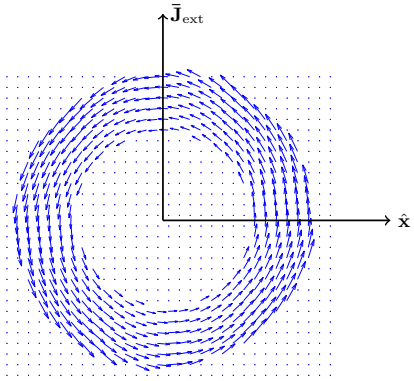

(a) Re $\mathbf{p}(\mathbf{r})$

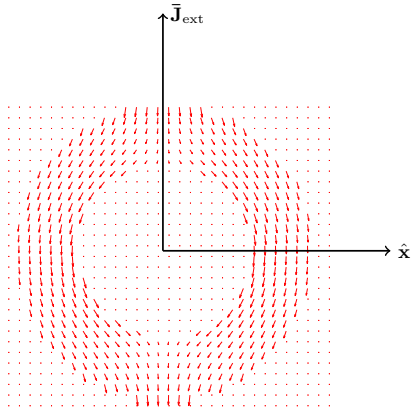

(b) Im $\mathbf{p}(\mathbf{r})$

FIG. 2: Real and imaginary parts of the microscopic polarization $\mathbf{p}(\mathbf{r})$ in the dielectric annulus in Fig. 1. The vectors in (b) have been minimized by a factor 50 for comparison with (a); i.e. the imaginary part of $\mathbf{p}(\mathbf{r})$ dominates.

distribution of $\mathbf{p}(\mathbf{r})$ yields $\mathbf{R} = 0$ in (9d), and hence we expect $\psi_{2112} = 0$. More generally, for ideal conductors and $\mathbf{k} = k\hat{\mathbf{x}}$, we expect that the $\mathbf{R}$-term generally remains important, but that it looses importance as the degree of mirror-symmetry about the yz-plane increases.

Having considered the general importance of the higher order term $\mathbf{R}$, Appendix A considers a special case where the inclusion of the higher order terms leads to effective Casimir permittivity and permeability parameters which are in some sense maximally local.

V. CONCLUSION

When concerned with spatial dispersive effects of the second order in k (i.e. magnetic response), it has been shown that the higher order multipoles *above* the electrical quadrupole are significant. They generally contribute with the same magnitude as do the polarization, magnetization and electrical quadrupole multipoles, and should therefore not be neglected, despite the higher order multipoles themselves generally being of smaller magnitude. This has been demonstrated in simulations on metamaterials consisting of periodic arrays of dielectric or conducting cylinders, and analytical findings have been provided in the special case where plane wave fields can be assumed. The plane wave expansion method in the case of a distributed plane wave source has been used to provide the relevant simulation results.

To facilitate our discussions we have utilized the classical scheme of Russakoff-Jackson homogenization, and effective parameter formulations by Landau-Lifshitz, and Casimir.

Appendix A: Increased locality for Casimir formulation

Here some side remarks regarding the influence of the higher order terms on the locality of the effective parameters shall be made. Local parameters ϵ and μ are desirable, since they enable the use of Fresnel equations to describe the behavior of finite samples or layered samples. The permittivity and permeability resulting from the Landau-Lifshitz formulation are therefore appealing, since they in some sense are maximally local[3]. In the Casimir formulation, however, the parameters ϵ' and μ' according to (13) are generally highly nonlocal. In this section, we will examine a special case where *modified* Casimir parameters can nevertheless be made equally local by including the higher order terms $\mathbf{Q}$ and $\mathbf{R}$ in ϵ' and μ', and choosing an appropriate coordinate origin.

A coordinate transformation $\mathbf{r} \rightarrow \tilde{\mathbf{r}} = \mathbf{r} - \mathbf{r}_0$, causes the multipole quantities in (8) to mix: Considering for instance the polarization and magnetization vectors, they mix according to

$$\tilde{\mathbf{P}} = [1 - i\mathbf{k}\cdot\mathbf{r}_0 - \frac{1}{2}(\mathbf{k}\cdot\mathbf{r}_0)^2]\mathbf{P}, \tag{A1a}$$

$$\tilde{\mathbf{M}} = [1 - i\mathbf{k}\cdot\mathbf{r}_0][\mathbf{M} + i\omega\frac{\mathbf{r}_0\times\mathbf{P}}{2}], \tag{A1b}$$

where we have kept necessary orders of k such that $\langle\mathbf{p}\rangle$ is second order in k upon their insertion in (8). By combining (13a) and (A1a), and noting that $\mathbf{E}$ is invariant under the coordinate transformation, the Casimir permittivity elements, *after* coordinate transformation, is expressed

$$\tilde{\epsilon}'_{ij} - \delta_{ij} = [1 - ik_l r_{0l} - \frac{1}{2}(k_l r_{0l})^2](\epsilon'_{ij} - \delta_{ij}). \tag{A2}$$

Analogous steps lead to an expression for a coordinate-shifted Casimir permeability $1 - \tilde{\mu}'^{-1}_{ij}$. Since the parameters $\tilde{\epsilon}'_{ij}$ and $1 - \tilde{\mu}'^{-1}_{ij}$ vary with the coordinate shift $\mathbf{r_0}$ as seen in (A2), it is in some cases possible to choose a coordinate origin in which the first order k-dependence, if any, is cancelled. Coordinate shifts may therefore help in making the parameters more local, as will be observed in the example below.

A special case for which the Casimir parameters can be made maximally local, in the sense mentioned earlier, is obtained by including $\mathbf{Q}$ and $\mathbf{R}$ in modified versions of (13) of the following manner[4]

$$\epsilon_0(\epsilon' - 1)\mathbf{E} = \mathbf{P} - i\mathbf{k}\cdot\mathbf{Q}, \tag{A3a}$$

$$\frac{\mathbf{k}\times(1 - \mu'^{-1})\mathbf{B}}{\mu_0\omega} = \frac{\mathbf{k}\times\mathbf{M}}{\omega} - \mathbf{R}, \tag{A3b}$$

while assuming the plane wave solution of the microscopic field considered in (21) with $\mathbf{k} = k\hat{\mathbf{x}}$ (realistic fields will be considered below in a simulation). We then find

$$\epsilon'_{22} = 1 + \chi_{22} + \frac{k}{\epsilon_0}\left(\xi_{212} + \frac{\zeta_{212}}{2}\right) + \frac{k^2}{\epsilon_0}\left(\eta_{2112} + \frac{\gamma_{2112}}{2}\right), \tag{A4a}$$

$$(1 - \mu'^{-1}_{33}) = \mu_0\omega^2\left(\frac{\zeta_{212}}{2k} + \psi_{2112} + \frac{\gamma_{2112}}{2}\right), \tag{A4b}$$

where we have used (12) and (24) in (15b) to express $\mathbf{Q}$ and $\mathbf{M}$ in terms of the parameters ζ_{212} and γ_{2112}. If we assume $\xi_{212} = -\zeta_{212} = 0$ (no magnetoelectric coupling), and make use of (23), we obtain $\mathbf{k}$-independent parameters within the frame of second order dispersion treated in this article: $\epsilon'_{22} = 1 + \chi_{22}$ and $1 - \mu'^{-1}_{33} = 0$. In other words, the Casimir parameters have become even more local due to the inclusion of contributions from $\mathbf{Q}$ and $\mathbf{R}$ in the definitions (A3).

Let us now apply the modified Casimir parameters (A3) to a realistic system: Consider a 1D metamaterial consisting of periodically alternating layers (a unit cell of which is displayed in Fig. 3) for frequency $\omega a/c = 0.009$, wavevector $\mathbf{k}a = 0.01\hat{\mathbf{x}}$, and equal layer thicknesses. The source $\mathbf{J}_{\text{ext}}$ and field $\mathbf{e}(\mathbf{r})$ point along $\hat{\mathbf{y}}$, and thus $\mathbf{M}$ and $\mathbf{Q}$ contribute equally to γ_{iklj} since $\mathbf{k} \perp \mathbf{p}$, in accordance

[3] In particular, for non-gyrotropic, weakly spatially dispersive media, where $\epsilon(\omega, \mathbf{k})$ only contains zeroth and second order terms in k, as much as possible of the induced current are represented by a local μ (20). Under certain circumstances (if the second order term of $\langle\mathbf{p}\rangle$ is perpendicular to $\mathbf{k}$, and this term is independent of the longitudinal part of $\mathbf{E}$), all induced current is described by the permeability. This will e.g. be the case for the 1D example below.

[4] Note that these expressions apply to the case where $\mathbf{R} \perp \mathbf{k}$, i.e., when it is possible to describe the entire $\mathbf{R}$-contribution in terms of $1 - \mu'^{-1}$.

with (24). Instead of the plane wave expansion method described earlier, the simplicity of the system allows us to find an exact solution to the wave equation (25) in terms of a matrix approach making use of the boundary conditions and the Bloch property of the fields. The results of the simulation are presented in Table III, where we observe that ψ_{2112}, $\gamma_{2112}/2$ and η_{2112} follow (23). In terms of the scaled parameters we may express (A4) as

$$\epsilon'_{22} = 1 + \chi_{22} + (ka)\left(\frac{\xi_{212}}{a\epsilon_0} + \frac{\zeta_{212}}{2a\epsilon_0}\right) + (ka)^2\left(\frac{\eta_{2112}}{\epsilon_0 a^2} + \frac{\gamma_{2112}}{2\epsilon_0 a^2}\right),$$
$$(1 - {\mu'_{33}}^{-1}) = \left(\frac{\omega a}{c}\right)^2\left(\frac{\zeta_{212}}{2(ka)\epsilon_0 a} + \frac{\psi_{2112}}{\epsilon_0 a^2} + \frac{\gamma_{2112}}{2\epsilon_0 a^2}\right) \quad \text{(A5)}$$

Inserting the simulation values in the above relation reveals that the magnitudes of ξ_{212} and ζ_{212} are negligible. This is due to the choice of coordinate origin in the unit cell (Fig. 3): It corresponds to that r_0 which gives a zero first order derivative of (A2) for $k = 0$, when assuming (21). A slight shift of the coordinate origin away from $r_0 = 0.75a$ renders $\xi_{212} = -\zeta_{212}$ significant (e.g. if the coordinate origin is located at $0.76a$ one obtains $\xi_{212} = -\zeta_{212} = -0.075i$).

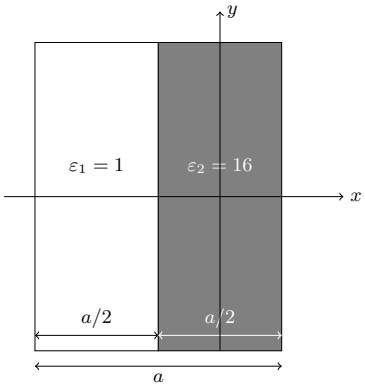

FIG. 3: Unit cell of a layered medium (1D metamaterial) which extends infinitely to the left and right

Comparing the modified Casimir parameters (A4) with the Landau-Lifshitz parameters ϵ_{22} and $1 - \mu_{33}^{-1}$ defined by (20),

$$\epsilon_{22} = 1 + \chi_{22}, \quad \text{(A6a)}$$
$$(1 - \mu_{33}^{-1}) = \mu_0\omega^2(\psi_{2112} + \gamma_{2112} + \eta_{2112}), \quad \text{(A6b)}$$

reveals that $\epsilon'_{22} = \epsilon_{22}$ and $\mu'^{-1}_{33} = \mu^{-1}_{33}$ when (23) and $\xi_{212} = -\zeta_{212} = 0$ apply. In other words, when we evaluate the Landau-Lifshitz and modified Casimir permeabilities they give identical values in this case (*almost identical* in the case of the layered metamaterial of Fig. 3). If we consider the Landau-Lifshitz parameter as the benchmark for local parameters, the modified Casimir parameter has in this sense become maximally local.

χ	7.50
$\xi/\varepsilon_0 a$	$i4.75 \cdot 10^{-9}$
$\zeta/\varepsilon_0 a$	$-i3.76 \cdot 10^{-17}$
$\psi/\varepsilon_0 a^2$	-0.0782
$\gamma/\varepsilon_0 a^2$	0.1563
$\eta/\varepsilon_0 a^2$	-0.0782

TABLE III: Parameter values in (15) for the 1D metamaterial displayed in Fig. 3.

Although (A4) and (A6) yield identical results in the above case, they have different expressions. This indicates that the manner in which we have included **Q** and **R** into modified Casimir parameters is not unique.

[1] A. P. Vinogradov and A. V. Aivazyan, Phys. Rev. E **60**, 987 (1999).
[2] M. G. Silveirinha, Phys. Rev. B **75**, 115104 (2007).
[3] M. G. Silveirinha, in *Metamaterials Handbook: Theory and phenomena of metamaterials*, edited by F. Capolino (CRC Press, London, 2009) Chap. 10.
[4] D. J. Cho, F. Wang, X. Zhang, and Y. R. Shen, Phys. Rev. B **78**, 121101 (2008).

[5] J. Petschulat, C. Menzel, A. Chipouline, C. Rockstuhl, A. Tünnermann, F. Lederer, and T. Pertsch, Phys. Rev. A **78**, 043811 (2008).
[6] C. Simovski and S. Tretyakov, in *Metamaterials Handbook: Theory and Phenomena of Metamaterials*, edited by F. Capolino (CRC Press, London, 2009) Chap. 2.
[7] A. Alù, Phys. Rev. B **83**, 081102 (2011).
[8] A. Alù, Phys. Rev. B **84**, 075153 (2011).
[9] A. D. Yaghjian, A. Alù, and M. G. Silveirinha, Photonics and Nanostructures - Fundamentals and Applications **11**, 374 (2013).
[10] V. Agranovich and V. Ginzburg, *Crystal optics with spatial dispersion, and excitons:*, Springer series in solid-state sciences (Springer-Verlag, 1984).
[11] L. D. Landau, E. M. Lifshitz, and L. P. Pitaevskii, *Electrodynamics of continuous media* (Pergamon Press, Oxford, 1984).
[12] G. Russakoff, Am. J. Phys. **38**, 1188 (1970).
[13] J. D. Jackson, *Classical electrodynamics*, 3rd ed. (Wiley, New York, 1999).
[14] A. P. Vinogradov, Physics-Uspekhi **45**, 331 (2002).
[15] J. van Bladel, *Electromagnetic fields* (IEEE Press, Hoobken, NJ, 2007).

Paper VI

Diamagnetism and the dispersion of the magnetic permeability

Submitted for journal publication

Arxiv: 1410.5999

Diamagnetism and the dispersion of the magnetic permeability

Christopher A. Dirdal[1] and Johannes Skaar[1]

[1] *Department of Electronic Systems, NTNU – Norwegian University of Science and Technology, NO-7491 Trondheim, Norway*

(Dated: March 24, 2017)

In the presence of spatial dispersion it is possible to have an analytic permeability function $\mu(\omega, \mathbf{k})$ that does not tend to 1 for high frequencies ω and fixed wavenumber $\mathbf{k}$. This fact explains that diamagnetism can be compatible with causality and a positive imaginary part of permeability, while possessing negligible spatial dispersion in the low wavenumber spectrum.

PACS numbers: 78.20.Ci,42.70.-a,41.20.-q,42.25.Bs

I. INTRODUCTION

With recent advances in metamaterial research, there is a renewed interest in the properties of the magnetic permeability function. The permeability function extracted by homogenization methods may show peculiar properties, such as a negative imaginary part, anomalous dispersion effects, and diamagnetism [1, 2]. This has lead to investigations on the properties of the magnetic permeability [1–7].

A related problem is the well known paradox that diamagnetism is not compatible with a permeability function that satisfies the Kramers–Kronig relations and has a positive imaginary part. Letting $\mu(\omega)$ be the relative permeability, and considering zero frequency in the Kramers–Kronig relation, one has

$$\mu(0) - 1 = \frac{2}{\pi} \int_0^\infty \frac{\operatorname{Im} \mu(\omega) \mathrm{d}\omega}{\omega}. \tag{1}$$

Apparently, (1) predicts that $\mu(0) < 1$ is not possible for media with $\operatorname{Im} \mu(\omega) > 0$. It has been argued that the Kramers–Kronig relations should be modified [2, 8] to avoid this problem. It has also been argued that the magnetic permeability can have a negative imaginary part, at least for high frequencies [2, 6, 7, 9, 10].

In this article we show that Maxwell's equations and the fundamental principle of causality do not require the magnetic permeability to approach unity for high frequencies and fixed wavenumbers (Sec. II). Causality is not violated, as the requirement $\mu \to 1$ for high frequencies is only necessary under eigenmodal propagation (in the absence of sources in the medium), where k and ω are connected by the dispersion relation $k = \sqrt{\epsilon\mu}\omega/c$. Here ϵ is the relative permittivity, $c = 1/\sqrt{\epsilon_0\mu_0}$ is the vacuum light velocity, and ϵ_0 and μ_0 are the vacuum permittivity and permeability, respectively. We consider the ambiguity in associating induced currents with the electric polarization or magnetization, and describe a simple homogeneous conductor or superconductor as concrete examples of media possessing diamagnetism (Sec. III). We find that their permeabilities do not tend to unity for high frequencies and fixed wavenumbers. Finally, we evaluate the permeability of 1d and 2d metamaterial examples with conducting inclusions, and demonstrate analytically and numerically that the permeability does not tend to unity for high frequencies (Sec. IV).

It turns out that diamagnetism is possible while μ has a positive imaginary part and is analytic in the upper half-plane. Spatial dispersion is central in the description of diamagnetism; however, it is seen that the medium may behave spatially nondispersive over a wide wavenumber spectrum. To compare with previous literature, we prove that the polarization–magnetization ambiguity means that for the same diamagnetic medium, other analytic μ's can be defined, that tend to 1 for high frequencies. However these functions get negative imaginary parts for some frequencies, while not violating the passivity requirement. Our findings therefore do not contradict previous results [2, 6, 8, 9].

II. ELECTROMAGNETIC PARAMETERS

Following the classic treatments [8, 11], we consider a passive and time-shift invariant medium, and formulate electromagnetism in frequency–wavenumber space. The Ampere–Maxwell's law and Faraday's law can be written

$$\frac{1}{\mu_0} i\mathbf{k} \times \mathbf{B} = -i\omega\epsilon_0 \mathbf{E} + \mathbf{J}_{\text{ind}} + \mathbf{J}_{\text{ext}}, \tag{2a}$$

$$i\mathbf{k} \times \mathbf{E} = i\omega \mathbf{B}. \tag{2b}$$

Here $\mathbf{J}_{\text{ext}}$ is the external source, and $\mathbf{J}_{\text{ind}}$ is the induced current density. We consider a single spatial Fourier component of the source, i.e., $\mathbf{J}_{\text{ext}} = \bar{\mathbf{J}}_{\text{ext}} \exp(i\mathbf{k} \cdot \mathbf{r})$ with constant $\bar{\mathbf{J}}_{\text{ext}}$. In a homogeneous medium, $\mathbf{E}$ and $\mathbf{B}$ are the electric field and magnetic flux density, respectively. In a periodic metamaterial, the Maxwell equations (2) result from an averaging of the corresponding microscopic equations [4, 5, 7, 12]. The macroscopic electric and magnetic fields $\mathbf{E}$ and $\mathbf{B}$ are then averaged microscopic fields $\mathbf{e}$ and $\mathbf{b}$ according to

$$\mathbf{E}(\mathbf{r}) = \int f(\mathbf{r}') \mathbf{e}(\mathbf{r} - \mathbf{r}') \mathrm{d}^3 r', \tag{3}$$

and similarly for $\mathbf{B}$. Here $f(\mathbf{r})$ is a test function whose Fourier transform vanishes outside the first Brilloin zone, and normalized to unity for $\mathbf{k} = 0$. When using the single Fourier component source, the averaging operation can

be rewritten to [4]

$$\mathbf{E}(\mathbf{r}) = \frac{\mathrm{e}^{i\mathbf{k}\cdot\mathbf{r}}}{V}\int_V \mathbf{e}(\mathbf{r})\mathrm{e}^{-i\mathbf{k}\cdot\mathbf{r}}\mathrm{d}^3r, \tag{4}$$

where integration is over a unit cell volume V.

The induced current can be decomposed in several ways. One option is to decompose it in terms of polarization and magnetization terms,

$$\mathbf{J}_{\mathrm{ind}} = -i\omega\mathbf{P} + i\mathbf{k}\times\mathbf{M}. \tag{5}$$

In (5) the two terms do not have to be defined from a multipole expansion, but of course, the second term can only contain transverse parts of the induced current. Assuming a linear medium, a permittivity and a permeability are defined from

$$\mathbf{P} = \epsilon_0(\epsilon - 1)\mathbf{E}, \tag{6a}$$

$$\mu_0\mathbf{M} = (1-\mu^{-1})\mathbf{B}, \tag{6b}$$

respectively. In general, both ϵ and μ are dependent on ω and $\mathbf{k}$, i.e., they are temporally and spatially dispersive.

By introducing auxillary fields $\mathbf{D} = \epsilon_0\mathbf{E} + \mathbf{P} = \epsilon\epsilon_0\mathbf{E}$ and $\mathbf{H} = \mathbf{B}/\mu_0 - \mathbf{M}$, we obtain from (2) the Maxwell equations

$$i\mathbf{k}\times\mathbf{H} = -i\omega\epsilon\epsilon_0\mathbf{E} + \mathbf{J}_{\mathrm{ext}}, \tag{7a}$$

$$i\mathbf{k}\times\mathbf{E} = i\omega\mu\mu_0\mathbf{H}. \tag{7b}$$

For simplicity, assume that μ is scalar, and write ϵ in the form [8]

$$\epsilon = \begin{bmatrix} \epsilon_\parallel & 0 & 0 \\ 0 & \epsilon_\perp & 0 \\ 0 & 0 & \epsilon_\perp \end{bmatrix}, \tag{8}$$

expressed in an orthogonal basis where the first unit vector is $\mathbf{k}/k$. By combining the two Maxwell equations (7), we obtain the solutions

$$\mathbf{B} = \frac{i\mu\mu_0\mathbf{k}\times\mathbf{J}_{\mathrm{ext}\perp}}{k^2 - \frac{\omega^2}{c^2}\epsilon_\perp\mu}, \tag{9a}$$

$$\mathbf{E}_\perp = \frac{i\omega\mu\mu_0\mathbf{J}_{\mathrm{ext}\perp}}{k^2 - \frac{\omega^2}{c^2}\epsilon_\perp\mu}, \tag{9b}$$

$$\mathbf{E}_\parallel = \frac{\mathbf{J}_{\mathrm{ext}\parallel}}{i\omega\epsilon_\parallel\epsilon_0}. \tag{9c}$$

In (9) the source $\mathbf{J}_{\mathrm{ext}}$ and field $\mathbf{E}$ are decomposed into their components parallel $\parallel$ and perpendicular $\perp$ to $\mathbf{k}$.

As $\omega\to\infty$ the fields do not feel the presence of the medium, so the solutions (9) must be the same as if we set ϵ and μ equal to unity in the expressions. Considering (9c) this immediately gives that $\epsilon_\parallel\to 1$. Also, for fixed k, (9b) means $\epsilon_\perp\to 1$ (excluding the possibility $\epsilon_\perp\mu\to 0$). Remarkably, we do not get any condition for the asymptotic behavior of μ. Indeed, for fixed k, the expressions become independent of μ in the limit $\omega\to\infty$. Thus the permeability is not required to approach unity for high frequencies.

Nevertheless, even though μ does not necessarily approach unity, the magnetization $\mathbf{M}$ vanishes in the limit $\omega\to\infty$. This is a result of the fact that according to (9a), the magnetic field vanishes in this limit.

For eigenmodal propagation, $k^2 = \epsilon_\perp\mu\omega^2/c^2$, the situation is different. To see this, let a current source plane be located somewhere in the infinite medium. In the limit $\omega\to\infty$ the generated waves must have the same amplitude and the same phase velocity as if the medium were not present. In other words, the impedance and phase velocity must take their vacuum values, which means that $\epsilon\to 1$ and $\mu\to 1$ under eigenmodal propagation. This ensures relativistic causality, i.e., the front of a wave packet propagates at the speed of light in vacuum.

Apparently, any transformation $\mathbf{P}\to\mathbf{P}'$ and $\mathbf{M}\to\mathbf{M}'$ satisfying

$$-i\omega\mathbf{P}' + i\mathbf{k}\times\mathbf{M}' = -i\omega\mathbf{P} + i\mathbf{k}\times\mathbf{M} \tag{10}$$

will leave $\mathbf{J}_{\mathrm{ind}}$ and the fundamental fields $\mathbf{E}$ and $\mathbf{B}$ unchanged. This means that the permittivity and permeability are not uniquely defined by (5)-(6). Substituting (6) into (10), and eliminating $\mathbf{B}$ with (2b),

$$\begin{aligned}&(\omega^2/c^2)(\epsilon'-1)\mathbf{E} - \mathbf{k}\times(1-\mu'^{-1})\mathbf{k}\times\mathbf{E}\\ &= (\omega^2/c^2)(\epsilon-1)\mathbf{E} - \mathbf{k}\times(1-\mu^{-1})\mathbf{k}\times\mathbf{E},\end{aligned} \tag{11}$$

where we have defined primed permittivity and permeability similarly to (6). Imagine now that a certain set ϵ and μ of a medium is known. Then (11) predicts the existence of another set of parameters ϵ' and μ', which is equivalent to the first set. We find

$$\epsilon'_\parallel = \epsilon_\parallel, \tag{12a}$$

$$\epsilon'_\perp + \frac{k^2c^2}{\omega^2}(1-\mu'^{-1}) = \epsilon_\perp + \frac{k^2c^2}{\omega^2}(1-\mu^{-1}). \tag{12b}$$

The relation (12) is well known in literature, although it is usually specialized to the case $\mu' = 1$. This case, which is called the Landau–Lifshitz formulation, is particularly useful in the presence of spatial dispersion, where there is no set of local (independent of $\mathbf{k}$) parameters ϵ and μ [8, 11]. Then it is convenient to specify the medium properties by a single (but nonlocal) quantity ϵ'. For spatially nondispersive media where ϵ and μ are independent of $\mathbf{k}$, it is often more convenient to retain these two parameters, as they are much simpler to use in practical situations formulated in the spatial domain. Since there is not always a set ϵ and μ such that the parameters are independent of $\mathbf{k}$, we allow all parameters in (12), ϵ, μ, ϵ', and μ', to depend on $(\omega,\mathbf{k})$ although not explicitly specified.

Apparently, a medium described by a given set of parameters ϵ and μ is equally well described by any other set of parameters, ϵ' and μ', that satisfies (12). Physically this can be understood as follows: Circulating currents can be described as magnetization, or alternatively as

time-dependent polarization. The choice of parameters determines how much of the total induced current $\mathbf{J}_{\rm ind}$ is described by the magnetization vector and how much remains in the polarization. Clearly, only the transversal ($\perp$) part of the induced current can be associated with magnetization; the parallel ($\parallel$) part must remain in the polarization.

For the situation where the induced current is described solely by the permittivity (i.e., where $\mu' = 1$), we can prove that for passive media, $\mathrm{Im}\,\epsilon' > 0$ for $\omega > 0$ [8]. Using (12b) this means that [6]

$$\mathrm{Im}\,\epsilon'_\perp = \mathrm{Im}\,\epsilon_\perp - \frac{k^2c^2}{\omega^2}\mathrm{Im}\,\mu^{-1} > 0. \tag{13}$$

Thus

$$\mathrm{Im}\,\mu > -\mathrm{Im}\,\epsilon_\perp \frac{\omega^2|\mu|^2}{k^2c^2}. \tag{14}$$

In other words, the ambiguity for $\epsilon_\perp$ and μ makes it possible to define permeabilities or transverse permittivities with negative imaginary parts, even for passive media, as long as (14) is satisfied.

III. HOMOGENEOUS CONDUCTORS AS DIAMAGNETIC MEDIA

Inspired by the split-ring resonator metamaterial [13], we realize that it is not always obvious which choice of parameters that is most "physical". One may take the view that a split-ring resonator metamaterial, made of nonmagnetic constituents, should be described by parameters $\epsilon' \neq 1$ and $\mu' = 1$. This is a perfectly valid and natural choice [4], given that there is no microscopic magnetization in the medium. However, metamaterial research has shown that it is convenient to describe the circulating currents using a macroscopic magnetization vector. This amounts to using a set of parameters ϵ and μ, where $\mu \neq 1$.

As another well known example, we may consider a superconductor. Here there are two extremes [14, 15]: Either the induced current is described explicitly, or the transverse current is described in the form of an effective magnetization. In the latter case, it is argued that one has diamagnetism.

We now consider the superconductor example in more detail. If the induced current is described by the permittivity, the permeability is $\mu' = 1$, and the superconductor can be modeled by a two-fluid model in which the conductivity has two terms. The permittivity is [15]

$$\epsilon' = 1 - \frac{c^2}{\lambda^2\omega^2} - \frac{\omega_{\rm p}^2}{\omega^2 + i\omega\Gamma}. \tag{15}$$

Here the second term describes the supercurrent, λ being the London penetration depth. The third term describes the normal current due to the Drude model, with plasma frequency $\omega_{\rm p}$ and a positive parameter Γ. For a (non-super) conductor, we can set $\lambda = \infty$.

It is also common to refer to a superconductor as diamagnetic. In this alternative picture, circulating currents in the superconductor is described by a magnetization. Then $\epsilon_\perp = 1$, and μ is obtained from

$$1 - \mu^{-1} = -\frac{1}{\lambda^2k^2} - \frac{\omega_{\rm p}^2}{c^2k^2}\cdot\frac{\omega^2}{\omega^2 + i\omega\Gamma}. \tag{16}$$

The equivalence with the first set of parameters ϵ' and μ' is seen by substitution into (12).

We observe from (16) that the superconductor acts as a perfect diamagnet in the limit $k \to 0$; however for spatially varying fields the diamagnetism is not perfect due to the London penetration depth λ.

By inspection we find that $\mu^{-1} = \mu^{-1}(\omega, \mathbf{k})$, as given by (16), is analytic in the upper half-plane $\mathrm{Im}\,\omega > 0$, for any fixed k. Also note that the permeability from (16) is defined and has meaning even for high frequencies, as long as the original ϵ' has meaning. However, we observe that $\mu(\omega, \mathbf{k})$ does not tend to unity as $\omega \to \infty$, but rather tends to a real number $\mu(\infty, \mathbf{k})$ between 0 and 1:

$$\mu^{-1}(\infty, \mathbf{k}) = 1 + \frac{1}{\lambda^2k^2} + \frac{\omega_{\rm p}^2}{c^2k^2}. \tag{17}$$

Therefore, μ^{-1} satisfies a Kramers–Kronig relation of the type

$$\mathrm{Re}\,\mu^{-1}(\omega, \mathbf{k}) - \mu^{-1}(\infty, \mathbf{k}) = \frac{2}{\pi}\mathrm{P}\int_0^\infty \frac{\mathrm{Im}\,\mu^{-1}(x, \mathbf{k})x\mathrm{d}x}{x^2 - \omega^2}, \tag{18}$$

where P denotes the Cauchy principal value.

It is perhaps surprising that $\mu(\omega, \mathbf{k})$ does not tend to unity for high frequencies. Here it is important to remember that in the presence of sources, ω and $\mathbf{k}$ are generally not connected. For eigenmodal propagation where ω and $\mathbf{k}$ are connected by the dispersion relation, the permeability will indeed tend to unity for high frequencies (see Sec. II). We also recall that despite $\mu \not\to 1$, the magnetization vector will tend to zero even for a fixed $\mathbf{k}$.

Setting $\omega = 0$ in (18) we see that for our example, diamagnetism is indeed compatible with causality and $\mathrm{Im}\,\mu(\omega, \mathbf{k}) > 0$. The only requirement from (18) is that

$$\mu(0, \mathbf{k}) > \mu(\infty, \mathbf{k}). \tag{19}$$

Spatial dispersion is central to the understanding of diamagnetism. For the medium described by (16), the permeability depends on the wavenumber k; significant diamagnetism is only present for small k's. Nevertheless, the medium appears spatially nondispersive for excitations with wavenumber spectra in the region $k \ll \lambda^{-1}$. For a conventional conductor with $\lambda = \infty$, the medium remains spatially nondispersive under the condition $k \ll \omega_{\rm p}/c$ and $\omega \gtrsim \Gamma$.

Given the flexibility of the division into $\epsilon_\perp$ and μ, it is interesting to see if it is possible to achieve $\mu \to 1$ for

fixed k, even for a diamagnetic medium. It turns out that it is indeed possible, at the expense of obtaining $\operatorname{Im}\mu < 0$ e.g. in the high-frequency region (while still describing a passive medium) [6, 9]. The idea is to let the division into $\epsilon_\perp$ and μ be frequency-dependent, so that the medium is described solely by a permittivity for high frequencies. From the parameter ϵ' (in the Landau–Lifshitz formulation where $\mu' = 1$), we define a new (equivalent) set of parameters:

$$\epsilon_\perp = 1 + (1-\alpha)(\epsilon'_\perp - 1), \tag{20a}$$

$$1 - \mu^{-1} = \alpha \frac{\omega^2}{k^2 c^2}(\epsilon'_\perp - 1). \tag{20b}$$

The parameter α is a weight factor describing the amount of transversal permittivity placed into μ. It is natural to require $0 \le \alpha \le 1$; however, in principle, α may be a completely arbitrary complex-valued function of ω and $\mathbf{k}$. Taking an ideal plasma response $\epsilon' = 1 - \omega_{\mathrm{p}}^2/\omega^2$ as a simple example, we obtain

$$\epsilon_\perp = 1 - (1-\alpha)\frac{\omega_{\mathrm{p}}^2}{\omega^2}, \tag{21a}$$

$$1 - \mu^{-1} = -\alpha \frac{\omega_{\mathrm{p}}^2}{k^2 c^2}. \tag{21b}$$

Now, provided $\alpha = \alpha(\omega) \to 0$ for $\omega \to \infty$, we will get the asymptote $\mu \to 1$. To describe diamagnetism at low frequencies, we require that $\alpha(0) = 1$. We want μ^{-1} to be analytic, so $\alpha(\omega)$ needs to be analytic. This involves making it complex-valued. From the Kramers–Kronig relations, or in particular (18), we know that the resulting function μ must have a negative imaginary part somewhere in the spectrum. This imaginary part must satisfy (14). Clearly, since the new set $\epsilon_\perp$ and μ is equivalent to the passive original set $\epsilon'_\perp$ and $\mu' = 1$, the negative imaginary part does not contradict passivity.

IV. METAMATERIAL EXAMPLES

We will now consider periodic metamaterials made from nonmagnetic constituents, i.e., dielectrics and conductors. If the metamaterial inclusions are described by a position dependent microscopic permittivity $\varepsilon(\mathbf{r})$, it is known that $\varepsilon(\mathbf{r}) \to 1$ as $\omega \to \infty$. Therefore, as $\omega \to \infty$ the electromagnetic field will tend to the solution we would have if the metamaterial is replaced by vacuum. With a source $\mathbf{J}_{\mathrm{ext}} = \bar{\mathbf{J}}_{\mathrm{ext}} \exp(i\mathbf{k}\cdot\mathbf{r})$, where $\bar{\mathbf{J}}_{\mathrm{ext}} \perp \mathbf{k}$, we obtain from (9):

$$\mathbf{B} = \frac{i\mu_0 \mathbf{k} \times \mathbf{J}_{\mathrm{ext}}}{k^2 - \frac{\omega^2}{c^2}}, \tag{22a}$$

$$\mathbf{E} = \frac{i\omega\mu_0 \mathbf{J}_{\mathrm{ext}}}{k^2 - \frac{\omega^2}{c^2}}. \tag{22b}$$

Thus, in the limit $\omega \to \infty$, we can express the microscopic current $\mathbf{j} = -i\omega(\varepsilon(\mathbf{r}) - 1)\epsilon_0 \mathbf{E}$ as

$$\mathbf{j} = \frac{\bar{\mathbf{J}}_{\mathrm{ext}} \frac{\omega^2}{c^2}}{k^2 - \frac{\omega^2}{c^2}} (\varepsilon(\mathbf{r}) - 1) \exp(i\mathbf{k}\cdot\mathbf{r}). \tag{23}$$

As discussed in Sec. II, the magnetic permability can be defined in several ways. A natural alternative in the so-called Casimir formulation [8, 12, 16] is to define the magnetization from the magnetic moment density:

$$\mathbf{M} = \frac{\mathrm{e}^{i\mathbf{k}\cdot\mathbf{r}}}{2V} \int_V \mathbf{r} \times \mathbf{j}\, \mathrm{d}^3 r, \tag{24}$$

where we can e.g. choose the origin in the center of the unit cell. Compared to e.g. [5] we have included an extra factor $\mathrm{e}^{i\mathbf{k}\cdot\mathbf{r}}$ to be consistent with the definition of the macroscopic fields (4). From (6b) we now have a definition of a permeability, which we in principle can use for all frequencies.

We first consider a 2d metamaterial consisting of quadratic unit cells of area a^2. In the unit cell, there is a conducting ring of inner and outer radius b_1 and b_2, respectively, see Fig. 1. In the high-frequency range the relative permittivity of the conductor is approximated by a plasma response

$$\varepsilon(\omega) = 1 - \frac{\omega_{\mathrm{p}}^2}{\omega^2}. \tag{25}$$

By calculating the integral (24) under the assumption $ka \ll 1$, and using (6b), we find that in the high-frequency regime

$$1 - \mu^{-1}(\infty) = -\frac{\pi\omega_{\mathrm{p}}^2}{8c^2} \frac{b_2^4 - b_1^4}{a^2}. \tag{26}$$

When the ring is seen as a cylinder in 3d, we must interpret $1 - \mu^{-1}$ as the (z, z) element of corresponding tensor. Eq. (26) shows that the permeability tends to a value between 0 and 1 as $\omega \to \infty$ while ka is fixed ($ka \ll 1$).

As proved in the Appendix, the function $\mu^{-1}(\omega, \mathbf{k})$ resulting from (6b) with (24) is analytic in the upper half-plane of complex frequency ($\operatorname{Im}\omega > 0$), for fixed $\mathbf{k}$. Thus μ^{-1} satisfies a Kramers–Kronig relation of the form (18).

We next consider a 1d metamaterial consisting of alternating layers of vacuum and copper. The microscopic permittivity of copper is described by a Drude model:

$$\varepsilon(\omega) = 1 - \frac{\omega_{\mathrm{p}}^2}{\omega^2 + i\omega\Gamma}, \tag{27}$$

where $\omega_{\mathrm{p}} = 1.20 \cdot 10^{16}$ s^{-1} and $\Gamma = 5.24 \cdot 10^{13}$ s^{-1} [17]. Making use of boundary conditions and the Bloch property of the fields, the microscopic fields can be found by use of transfer matrices, thereby allowing for straightforward calculation of the parameter $1 - \mu^{-1}$. Fig. 2 displays a plot of $1 - \mu^{-1}$ vs. scaled frequency, having chosen the structural dimension $a = 100$ nm. Repeated

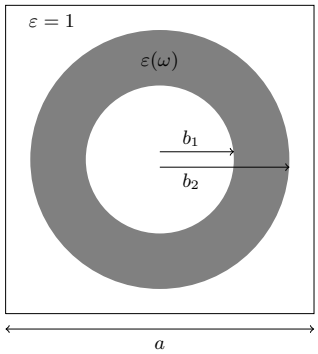

FIG. 1: The metamaterial unit cell consists of a cylinder of inner radius b_1 and outer radius b_2. The cylinder has permittivity $\varepsilon(\omega)$ and is surrounded by vacuum.

resonances are observed, which become narrower with increasing frequency. Except these resonances, $1-\mu^{-1}$ is observed to approach an asymptote unequal to zero. Similarly to (26), the asymptote for this 1d structure can be calculated to be

$$1-\mu^{-1}(\infty) = -\frac{1}{192}\frac{\omega_{\rm p}^2}{c^2}a^2 \qquad (28)$$
$$= -0.084.$$

This asymptote corresponds well with the dispersion of $1-\mu^{-1}$ shown in Fig. 2b.

V. CONCLUSION

It is well known that diamagnetism is an effect related to spatial dispersion, although the medium can behave spatially nondispersive for restricted wavenumber spectra. It turns out that diamagnetism at zero frequency is compatible with Kramers–Kronig relations and a positive $\mathrm{Im}\,\mu$ for all frequencies, as the asymptote of the permeability for high frequencies and fixed $\mathbf{k}$ can be different from 1. We point out that such an asymptote is permitted by Maxwell's equations and causality, and provide analytical and numerical examples of associated diamagnetic media or metamaterials.

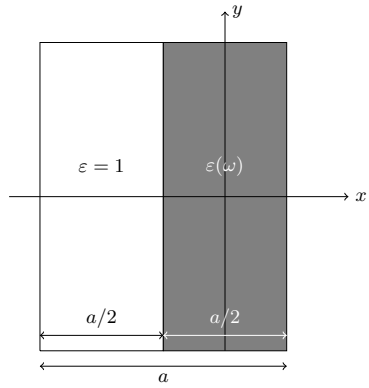

(a)

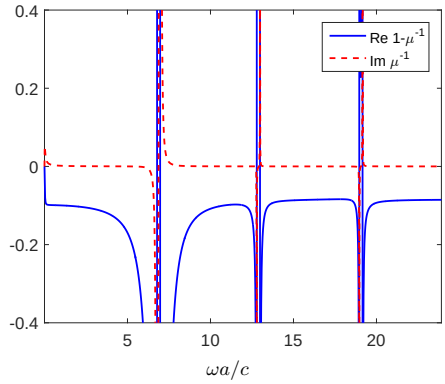

(b)

FIG. 2: (a) Unit cell of a layered medium (1d metamaterial) which extends infinitely to the left and right. (b) Calculated plot of $1-\mu^{-1}$ vs. frequency for $a = 100$ nm. The plasma frequency of copper corresponds with $\omega_{\rm p}a/c = 4.01$. Outside the long wavelength regime, and above the plasma frequency, $1-\mu^{-1}$ approaches the asymptote given by (28): $1-\mu^{-1} = -0.086$ is observed for $\omega a/c = 24$. Several resonances are observed which become narrower with increasing frequency. Notice also that $1-\mu^{-1}$ approaches zero as $\omega \to 0$.

Appendix A: Analyticity and Kramers–Kronig relations

It is interesting to explore the analytic properties of the electromagnetic parameters [8, 11, 18, 19]. If we use the Landau–Lifshitz formulation in which the medium is described solely by a permittivity ϵ', it is usually assumed that ϵ' is an analytic function of ω [8, 11]. This follows by regarding the electric field as the excitation and the displacement field as the response. However, as pointed out in [18], such an argument is not compelling since the electric field includes the response of the medium.

In (9) the fields are expressed from the sources, which means that it is straightforward to identify the response functions. Treating the source $\mathbf{J}_{\rm ext}$ as the excitation, and the electric field as the response, it follows from (9c) that $1/\epsilon'_{\parallel}(\omega,\mathbf{k})$ is analytic in the upper half-plane $\mathrm{Im}\,\omega > 0$

for fixed $\mathbf{k}$. Moreover, from (9b)

$$R(\omega) \equiv \frac{i\omega\mu_0}{k^2 - \frac{\omega^2}{c^2}\epsilon'_\perp} \tag{A1}$$

must be analytic in the upper half-plane. Even though $R(\omega)$ is analytic, it is not entirely obvious that $\epsilon'_\perp$ is. Since $R(\omega)$ is analytic there, any zero of $R(\omega)$ is of finite order. We can write

$$\epsilon'_\perp(\omega, \mathbf{k}) = \frac{R(\omega)k^2 - i\omega\mu_0}{R(\omega)\omega^2/c^2}, \tag{A2}$$

and thus $\epsilon'_\perp(\omega, \mathbf{k})$ is analytic except possibly of poles. In [19] it is proved that $\epsilon'(\omega, \mathbf{k})$ does not contain any poles in the upper half-plane, for a metamaterial made of causal constituents with analytic permittivities in the upper half-plane. With the additional property $\epsilon' \to 1$ as $\omega \to \infty$, the Kramers–Kronig relations are established.

We now leave the Landau–Lifshitz formulation and describe the medium with both ϵ and μ. Due to the presence of both functions $\epsilon_\perp(\omega, \mathbf{k})$ and $\mu(\omega, \mathbf{k})$ in (9a)-(9b), they are not necessarily analytic functions separately. For example, we may choose to describe the transversal current by the permeability up to a given frequency, and abruptly describe it using the permittivity for higher frequencies. Although a somewhat artificial choice, it demonstrates that an extra condition is required to establish analyticity for $\epsilon_\perp$ and μ.

For the permeability resulting from the magnetization (24), we can prove analyticity for μ^{-1} as follows. If the metamaterial is described with a single permittivity tensor $\epsilon' = \epsilon'(\omega, \mathbf{k})$ (Landau–Lifshitz formulation), the magnetic flux density is given by

$$\mathbf{B} = \frac{i\mu_0 \mathbf{k} \times \mathbf{J}_{\text{ext}}}{k^2 - \frac{\omega^2}{c^2}\epsilon'_\perp}, \tag{A3}$$

analogously to (9a). Substituting (24) and (A3) into (6b), we have

$$\frac{\mu_0}{2V}\int_V \mathbf{r} \times \mathbf{j}\, \mathrm{d}^3 r = (1 - \mu^{-1})\frac{i\mu_0 \mathbf{k} \times \mathbf{J}_{\text{ext}}}{k^2 - \frac{\omega^2}{c^2}\epsilon'_\perp}. \tag{A4}$$

Choosing a source with $\mathbf{k} \times \mathbf{J}_{\text{ext}}$ in the $\hat{\mathbf{z}}$-direction,

$$1 - \mu^{-1} = \frac{1}{J_{\text{ext}}} \frac{k^2 - \frac{\omega^2}{c^2}\epsilon'_\perp}{2ikV} \hat{\mathbf{z}} \cdot \int_V \mathbf{r} \times \mathbf{j}\, \mathrm{d}^3 r. \tag{A5}$$

The source J_{ext} can be chosen to be analytic in the upper half-plane. It can also be chosen zero-free. The function $\epsilon'_\perp$ is analytic in the upper half-plane, provided the metamaterial is made of causal constituents [19]. Clearly the microscopic current $\mathbf{j}$ is analytic in the upper half-plane, since it is causally related to the source. It therefore follows that μ^{-1} is analytic in the upper half-plane.

With the analyticity and the asymptotic behavior, Kramers–Kronig relations (18) for μ^{-1} can finally be stated.

[1] T. Koschny, P. Markos, D. R. Smith, and C. M. Soukoulis, Phys. Rev. E **68**, 065602 (2003).
[2] M. G. Silveirinha, Phys. Rev. B **83**, 165119 (2011).
[3] A. L. Efros, Phys. Rev. E **70**, 048602 (2004).
[4] M. G. Silveirinha, Phys. Rev. B **75**, 115104 (2007); in *Metamaterials Handbook: Theory and phenomena of metamaterials*, edited by F. Capolino (CRC Press, London, 2009) Chap. 10.
[5] A. Alù, Phys. Rev. B **84**, 075153 (2011).
[6] L. P. Pitaevskii, Int. J. Quant. Chem. **112**, 2998 (2012).
[7] A. D. Yaghjian, A. Alù, and M. G. Silveirinha, Photonics and Nanostructures - Fundamentals and Applications **11**, 374 (2013).
[8] L. D. Landau, E. M. Lifshitz, and L. P. Pitaevskii, *Electrodynamics of continuous media* (Pergamon Press, Oxford, 1984).
[9] P. C. Martin, Phys. Rev. **161**, 143 (1967).
[10] V. A. Markel, Phys. Rev. E **78**, 026608 (2008).
[11] V. M. Agranovich and V. L. Ginzburg, *Crystal optics with spatial dispersion, and excitons* (Springer Verlag, Berlin, 1984).
[12] C. A. Dirdal, H. O. Hågenvik, H. A. Haave, and J. Skaar, arXiv:1701.01708 (2017).
[13] J. B. Pendry, A. J. Holden, D. J. Robbins, and W. J. Stewart, IEEE Trans. Microwave Theory and Tech. **47**, 2075 (1999).
[14] A. C. Rose-Innes and E. H. Rhoderick, *Introduction to superconductivity* (Pergamon Press, 1978).
[15] T. P. Orlando and K. A. Delin, *Foundations of applied superconductivity* (Addison-Wesley, 1991).
[16] A. P. Vinogradov, Physics-Uspekhi **45**, 331 (2002).
[17] M. A. Ordal, L. L. Long, R. J. Bell, S. E. Bell, R. R. Bell, R. W. Alexander, and C. A. Ward, Appl. Opt. **22**, 1099 (1983).
[18] O. V. Dolgov, D. A. Kirzhnits, and E. G. Maksimov, Rev. Mod. Phys. **53**, 81 (1981).
[19] A. Alù, A. D. Yaghjian, R. A. Shore, and M. G. Silveirinha, Phys. Rev. B **84**, 054305 (2011).